UNIVERSIDADE FEDERAL DO PAMPA
DOUTORADO EM CIÊNCIAS FISIOLÓGICAS

CARLOS IGNACIO DE LA FUENTE CANCINO

ON SURFACE ELECTROMYOGRAPHY INTERPRETATIONS: UNCOVERING ELECTRICAL PATTERNS IN TOPOGRAPHICAL MAPS, MOTOR UNIT DECOMPOSITION, AND RESPONSES TO ACUTE AND CUMULATIVE FATIGUE

Uruguaiana
2023

UNIVERSIDADE FEDERAL DO PAMPA
DOUTORADO EM CIÊNCIAS FISIOLÓGICAS

CARLOS IGNACIO DE LA FUENTE CANCINO

SOBRE INTERPRETAÇÕES DE ELETROMIOGRAFIA DE SUPERFÍCIE: DESCOBRINDO PADRÕES ELÉTRICOS EM MAPAS TOPOGRÁFICOS, DECOMPOSIÇÃO DE UNIDADES MOTORAS E RESPOSTAS À FADIGA AGUDA E ACUMULADA

Uruguaiana
2023

CARLOS IGNACIO DE LA FUENTE CANCINO

ON SURFACE ELECTROMYOGRAPHY INTERPRETATIONS: UNCOVERING ELECTRICAL PATTERNS IN TOPOGRAPHICAL MAPS, MOTOR UNIT DECOMPOSITION, AND RESPONSES TO ACUTE AND CUMULATIVE FATIGUE

Tese de Doutorado apresentada ao Programa de Pós-graduação Multicêntrico em Ciências Fisiológicas da Universidade Federal do Pampa, como requisito para obtenção do título de Doutor em Ciências Fisiológicas.

Orientador: Prof. Dr. Felipe Pivetta Carpes

Uruguaiana
2023

CARLOS IGNACIO DE LA FUENTE CANCINO

ON SURFACE ELECTROMYOGRAPHY INTERPRETATIONS: UNCOVERING ELECTRICAL PATTERNS IN TOPOGRAPHICAL MAPS, MOTOR UNIT DECOMPOSITION, AND RESPONSES TO ACUTE AND CUMULATIVE FATIGUE

Tese de Doutorado apresentada ao Programa de Pós-graduação Multicêntrico em Ciências Fisiológicas da Universidade Federal do Pampa, como requisito para obtenção do título de Doutor em Ciências Fisiológicas.

Área de concentração: Ciências Fisiológicas

Tese de doutorado para ser defendida em 22 de Setembro de 2023.

Banca examinadora:

_____

Prof. Dr. Felipe Pivetta Carpes
Orientador
UNIPAMPA / RS / Brasil

_____

Prof. Dr. Fernando Diefenthaeler
UFSC / RS / Brasil

_____

Profa. Dra. Andresa Mara de Castro Germano
TUC / Saxony / Alemanha

_____

Prof. Dr. Conrado Torres Laett
INTO / RJ / Brasil

SUMMARY

ACKNOWLEDGEMENTS

I would like to thank the professors from the Programa de Pós-Graduação Multicêntrico em Ciências Fisiológicas da UNIPAMPA for encouraging critical thinking, discussion, honesty, and exploring unfamiliar areas for physiology, like data science and biomedical engineering. Particularly, I want to thank my supervisor, Prof. Felipe P Carpes. who encouraged me to study in Brazil and challenged me during the program, despite my Ph.D. period being severely affected by the COVID pandemic restrictions. Finally, I am very grateful to the Brazilian Federal Universities. Although it is not a perfect system and has issues to improve, the Brazilian Federal University system allowed me to study for a Doctorate grade only based on my capacities instead of my *wallet weight*. Also, I would like to thank Delsys, Inc., for providing me with a demo license to decompose surface electromyography signals for my last experiment.

Funding

During my Ph.D. program, I worked and studied simultaneously because it was the best option that aligned with my economically constrained circumstances and my academic desire to progress. This approach allowed me to self-fund my research and allowed me to combine the search for the answer in my research with my routine of work in the clinics and faculty. Additionally, three grants were obtained to complement the costs, which were the "Delsys Donation Initiative" granted by the De Luca Foundation and Delsys Inc. (2020), the "Interdisciplinary Grant of Health Sciences" from Pontificia Universidad Católica de Chile (2021), and "The International Affiliate Development Grant Program" from the International Society of Biomechanics, which helped me to visit the University of Calgary in 2023, along with funding from the Startup Ciencia grants in 2021 and 2022.

ABSTRACT

The study of individual or pooled motor units' activity by means of surface electromyography (sEMG) opens a window of opportunities to study human movement. However, sEMG requires adequate signal processing, and there are physiological and non-physiological factors that can bias the measurement and interpretation of sEMG signals. Examples include technical and methodological choices for signal processing and presentation, as well as physiological factors such as acute and cumulative muscle fatigue and orthopedic conditions such as persistent weakness after an Achilles tendon rupture. Therefore, the proper use of sEMG information relies not only on how the signal is acquired and processed but also on the physiological condition of the individuals. In this research, we aimed to determine sEMG signal segmentation, posttraumatic muscle weakness, and fatigue conditions influencing myoelectrical manifestations, sEMG maps, and motor unit decomposition obtained from sEMG measurements. The experiments conducted and reported here hypothesized that 1) methodological biases are introduced during typical signal processing procedures when analyzing electrical manifestations to estimate muscle fatigue and muscle activation maps, 2) sEMG maps and motor unit decomposition patterns can be appropriately used to identify acute and chronic muscle adaptation in conditions of inhibition similar to cumulative fatigue, and 3) cumulative muscle fatigue impairs neurophysiological characteristics (firing rate and motor unit recruitment) expressed in sEMG signals. Our main findings were that 1) signal processing methods to estimate fatigue and activation maps introduce biased electrical manifestations, 2) sEMG maps and motor unit decomposition are sensible to identify patterns in acute and chronic adaptations, and 3) increased firing rate and new motor unit recruitment are the most relevant changes in sEMG signals in response to cumulative fatigue. Furthermore, the results highlight the relevance of visualization techniques in the analysis of regional muscle activation (sEMG maps) and regional distribution and suggest the increase in firing rate as the most relevant marker of cumulative fatigue. We expect that our results can have an important impact on how to approach signal processing and define procedures to study different physiological conditions throughout the use of sEMG.

Keywords: Muscle Activation, Exercise, Injury, Signal processing, Data Science.

RESUMO

O estudo da atividade de unidades motoras individuais ou agrupadas por meio da eletromiografia de superfície (sEMG) abre uma janela de oportunidades para estudar o movimento humano. No entanto, a sEMG requer o processamento adequado do sinal, e existem fatores fisiológicos e não fisiológicos que podem enviesar a medição e interpretação de sinais de sEMG. Exemplos incluem escolhas técnicas e metodológicas para o processamento e apresentação do sinal, bem como fatores fisiológicos, como fadiga muscular aguda e cumulativa e condições ortopédicas, como fraqueza persistente após uma ruptura do tendão de Aquiles. Portanto, o uso adequado da sEMG depende não apenas de como o sinal é adquirido e processado, mas também da condição fisiológica dos indivíduos. Nesta pesquisa, nosso objetivo foi determinar como segmentacao da sinal de sEMG, debilidade muscular postraumatica e fadiga influenciam manifestacoes myoeletricas, mapas de sEMG e decomposicao de unidades motoras obtidas de medições de sEMG. Os experimentos realizados e relatados aqui basearam nas hipóteses de que 1) vieses metodológicos são introduzidos durante procedimentos típicos de processamento de sinal para analisar manifestações elétricas de fadiga muscular e mapas de ativação muscular, 2) mapas de sEMG e padrões de decomposição de unidades motoras podem ser usados de forma para identificar adaptações agudas e crônicas em condições de fadiga acumulada, e 3) a fadiga muscular acumulada prejudica características neurofisiológicas (taxa de disparo e recrutamento de unidades motoras) expressas nos sinais de sEMG. Nossas principais descobertas foram que 1) os métodos de processamento de sinal para estimar fadiga e mapas de ativação introduzem vieses na análise de manifestações elétricas, 2) mapas de sEMG e decomposição de unidades motoras são sensíveis para identificar padrões em adaptações agudas e crônicas, e 3) aumento da taxa de disparo e recrutamento de novas unidades motoras são as mudanças mais relevantes nos sinais de sEMG em resposta à fadiga acumulada. Além disso, os resultados destacam a relevância das técnicas de visualização na análise da ativação muscular regional (mapas de sEMG) e distribuição regional, e sugerem o aumento da taxa de disparo como o marcador mais relevante de fadiga cumulativa. Esperamos que nossos resultados possam ter um impacto importante em como abordar o processamento de sinais e definir procedimentos para o estudo de diferentes condições fisiológicas por meio do uso da sEMG.

Palavras-chave: Ativação Muscular, Exercício, Lesão, Processamento de Sinais, Ciência de dados.

LIST OF ABBREVIATIONS

Ag: Silver

AgCl: Silver Chloride

ANOVA: analysis of variance

AT: Achilles Tendon

ATP: Adenosine triphosphate

ATRG: Achilles Tendon Rupture Group

ATRS: Achilles Tendon Rupture Score

AMPA: aminomethylphosphonic acid

BMI: body mass index

Ca^{++}: Calcium

Cl-: Clorum

CG: Control Group

CoV: Coeficient of Variance

DBSCAN: Density-Based Spatial Clustering of Application with Noise

DHPR: Dihydropyridine receptor

d.u.: Dimensionless units

EMG: Electromyography

ES: Effect Size

FFT: Fast Fourier Transform

GABA: γ-Aminobutyric acid

GM: Gastrocnemius Medialis

HD-sEMG: High-density surface electromyography

IRB: Institutional Review Board

LoC: Location of Center

LoCx: Location of Center in x direction

LoCy: Location of Center y direction

MATLAB: Matrix laboratory software

MG: Medial Gastrocnemius

Mg: Magnesium

MU: Motor Unit

MUAPT: Motor Units Action Potential Trains

MVIC: Maximal Voluntary Isometric Contraction

No: Number

NMDA: N-metrhyl-D-aspartate receptor

PCA: Principal component analysis

PPS: Pulses per Second

Qx: Surgery

RMS: Root Mean Square

RyR: Ryanodine recpetor

R^2: Determinant coefficient

sEMG: Surface electromyography

SENIAM: Surface electromyography for the non-invasive assessment of muscles

SOM: Self-organized maps

SPSS: Statistical Package for the Social Sciences software

STFT: Short-Time Fourier Transform

tSNE: t-distributed stochastic neighbor embedding

TKO: Taeger Keirger energy operator

US: Ultrasonography

UMAP: Manifold Approximation and Projection

V: Voltage

LIST OF FIGURES

LIST OF TABLES

1 CHAPTER ONE – INTRODUCTION

In this thesis, results of different experiments conducted to determine how methodological choices in signal processing and physiological conditions may influence the outcomes of surface electromyography (sEMG) measurements are reported. The development of this thesis was done mostly during the coronavirus pandemic. In the beginning (2020 to 2022), such public health conditions had a major impact on the planned experiments. For this reason, the study was first dedicated to understanding the influence of methodological choices in processing sEMG signals on the final outcomes. Despite the difficulties, this approach brought interesting and promising results, which were published in recognized journals. In due course of the project, it was possible to develop experimental studies in which physiological conditions that disturb the neuromuscular system were considered. Again, we found results that instigate an applied discussion on how to handle and present outcomes of the sEMG analysis to understand human movement.

The content of this thesis is organized into 10 chapters. Following this chapter, **Chapter 1, Chapter 2** present the theoretical background for this study, including the statement of the research problem, the aims, and the hypotheses. **Chapter 3** is composed of a manuscript related to methodological aspects in analyzing electrical manifestations of fatigue using sEMG signals. **Chapter 4** is a manuscript related to the methodology for assessing sEMG using muscle activation maps. **Chapter 5** is a manuscript on the applicability of muscle activation map patterns to assess the neuromuscular activity in a condition of chronic muscle weakness. **Chapter 6** is a manuscript related to the applicability of muscle motor unit decomposition to quantify and discuss outcomes of muscle activation. **Chapter 7** is a manuscript on determining the motor unit behavior during muscle contractions in response to cumulative fatigue. **Chapter 8** includes a general discussion of the findings across the different studies. **Chapter 9** discusses the limitations of the experiments composing this thesis. Finally, **Chapter 10** includes a general conclusion of the thesis. Additional sections at the end of the document include the list of references, ethical approvals, and generic codes for signal processing approaches developed in the studies.

2 CHAPTER TWO – BACKGROUND AND STATEMENT OF THE PROBLEM

2.1 Electromyography signal generation

Electromyography is a technique that measures the electrical activity emanating from the depolarization of several plasmatic membranes surrounding the muscle fibers in skeletal muscle (Basmajian and de Luca 1985). In physiological terms, the electromyographic signal is the summation of trains of action potential from active motor units during a muscle contraction (Basmajian and de Luca 1985); see anatomic and physiologic model section of Figure 1. Therefore, muscle activation can be monitored using sEMG (Ladegaard et al., 2002).

sEMG devices allow the non-invasive voltage collection from active motor units (Ladegaard et al., 2002). The electromyography signals involve the voltage sum of different motor units, where the convolution between motor unit basis and firing rate of each active motor unit is the best model to explain the sEMG signal generation (Figure 1, see physiologic model section). In other words, the sEMG signal is the sum of voltage generated by different activated motor units across time. In addition to the resting action potentials, the electromyography signal has electrical noise associated with current traveling through surrounding tissues and electrical phenomena generated by electronic elements (Raez et al., 2006). The noise is summed to the convolution model, obtaining the final output of physiology information merged with noise (Figure 1, see instrumentation section). Therefore, the sEMG signal can be considered an interfered signal due to its different voltage sources and superposed waves, including cancelation (opposed waves).

Consequently, the sEMG signal is a window to study human movement under physiology or pathological conditions, reflecting any human activity at any stage of life postpartum. Unfortunately, several factors can interfere with sEMG interpretations. Although we can get a good sEMG acquisition, factors like signal processing parameters, visualization methods to refer to activations, inhibitory physiology mechanisms like muscle fatigue, action potential regulation (Figure 2), or no physiological conditions like signal processing assumptions might distort the true information. Identification and possible solutions to these assumptions are the main motivation and focus of this thesis.

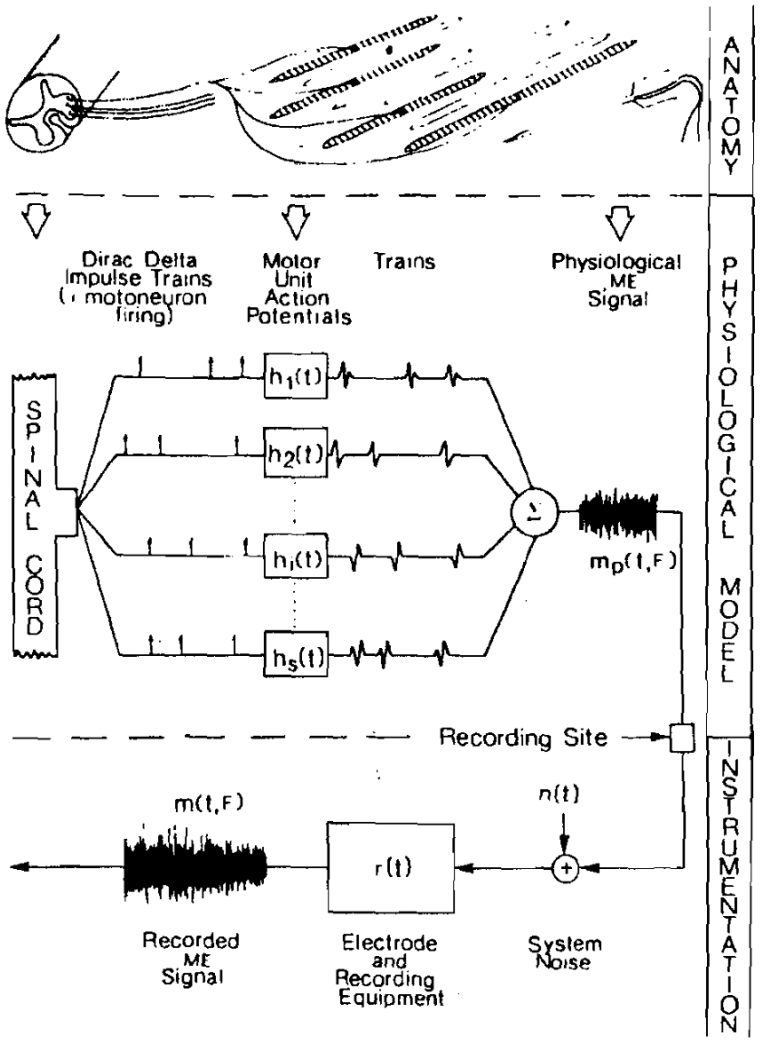

Figure 1. A generative model of the sEMG signal (Basmajian et al., 1985).

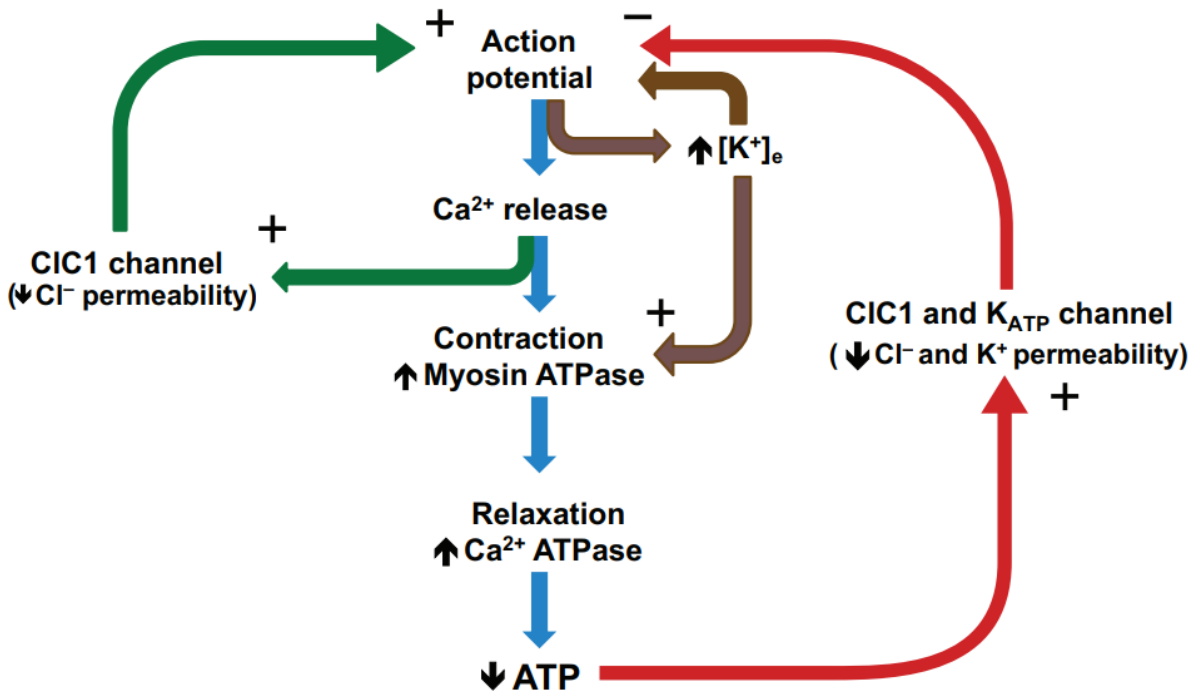

Figure 2. Regulation of membrane excitability during muscle contraction. Blue arrows indicate the physiological muscle contraction. The action potentials allow the release of Ca^{++} from the sarcoplasmic reticulum to activate the contractile proteins, resulting in force generation (protein displacement hypothesis of muscle contraction by ATP hydrolysis). Relaxation is associated with the pumping of Ca^{++} back into the sarcoplasmic reticulum by the Ca^{++} ATPase. Brown arrows indicate that repetitive action potentials result in a large K+ efflux and eventually increased [K+]e reduces action potential amplitude. Green arrows indicate that the increase in $[Ca2^{+}]_i$ during contraction is involved in the closing of ClC1, possibly through the activation of protein kinase C. The subsequent decrease in Cl2 permeability improves action potential amplitude, thus counteracting the K^+ -depressing effect. The events depicted by the brown and green arrows are expected to predominate at the onset of exercise and as long as there is no metabolic stress. Red arrows indicate what happens when ATP use exceeds the production rate, causing a decrease in ATP concentration; the resulting metabolic stress then triggers the fatigue mechanism, including activation of ClC1 and KATP channels. Activation of these channels will cause very large decreases in action potential amplitude and as a consequence, the sarcoplasmic

reticulum releases less Ca^{++} and less force is generated in order to preserve ATP (MacIntosh et al., 2012).

2.2 Surface electromyography techniques

The depolarization of α-motor unit arises from trains of potential motor units of the central nervous system, and the sum of the electrical activity of muscles results in the electromyography or myoelectrical signal (Cifrek et al. 2009; De Luca 1979). These signals can be acquired invasively or non-invasively, which constitutes an essential development in studying cumulated fatigue and muscle activation (Farina et al. 2003). Among the possible techniques to study electromyography are bipolar (sEMG) and high-density surface electromyography (HD-sEMG).

The bipolar sEMG technique is a non-invasive method to record the electrical activity of muscles during muscular contractions (Merletti et al., 2019). In this technique, pairs of electrodes are placed on the surface of the skin directly above the muscle of interest in a bipolar configuration (two electrodes and a reference). These surface electrodes detect the sum of voltage produced by motor units within the muscle fibers as they activate during muscle contractions (Basmajian et al., 1985). The distance between electrodes is not trivial because this determines the conductor volume and crosstalks (Campanini et al., 2022). sEMG electrodes allow us to measure the amplitude, frequency, and duration of the muscle activation by measuring signal features. As a non-invasive and easily applicable method, sEMG has become a valuable tool in understanding motor control and function (Campanini et al., 2022).

The HD-sEMG allows the investigation of muscle activity, including spatial resolution with multiple voltage sources, different from traditional bipolar sEMG, which collects only one voltage signal (Campanini et al., 2022). This technique places a grid or array of multiple-spaced electrodes on the skin above the muscle of interest (Campanini et al., 2022). By capturing signals from multiple locations, HD-sEMG provides detailed information about the spatial distribution and activation patterns of muscles (Campanini et al., 2022). This technique is especially valuable for topography activation distribution, motor unit decomposition, or conduction velocity.

In the context of HD-sEMG technique, one of the most relevant applications is motor unit decomposition. The motor unit decomposition uses the HD-sEMG acquisition and follows the inverse steps of sEMG signal generation (Figure 1). Here, the motor unit basis and firing rate can be obtained. The most relevant methods are the Bayesian and blind source separation models. These are two distinct approaches used for motor unit decomposition. Bayesian models employ probabilistic inference to estimate the underlying sources of the observed HD-sEMG signals (Nawab et al., 2010). These models leverage prior knowledge about the statistical properties of the sources and the mixing process, making them effective in resolving spatially overlapping muscle activities and providing source separation (Nawab et al., 2010). By incorporating prior information, Bayesian models can enhance motor unit recognition (Nawab et al., 2010).

On the other hand, blind source separation models use statistical algorithms to extract independent sources to identify motor unit basis (Negro et al., 2016). These models assume the observed HD-sEMG signals are linear convoluted mixtures of underlying muscle activities (Negro et al., 2016). While blind source separation techniques can efficiently separate the sources, they may face challenges in disentangling the complex spatial patterns of muscle activations, especially when muscle activities significantly overlap.

In summary, both Bayesian and blind source separation models have strengths and limitations in the context of HD-sEMG analysis. Bayesian models excel in incorporating prior knowledge and providing robust source separation, while blind source separation techniques offer a data-driven approach but may struggle with spatially overlapping muscle activities. The choice between these approaches depends on the specific research question, the level of available prior information, the desired accuracy in identifying individual muscle contributions during motor tasks, and, in our case, the availability of the equipment.

2.3 Electrical manifestations of surface electromyography

The ability to measure electrical modifications in the sEMG or myoelectric signal has been traditionally described in the literature (Table 1). The most common application has been the study of fatigue through quantitative indicators known as electrical manifestations of fatigue (Ament et al., 1993; E. Martinez-Valdes et al., 2016). The primary descriptors among these

indicators are the median, mean, and peak frequencies. These descriptors are obtained from the time and frequency domain (Ament et al., 1993; Raez et al., 2006; Angelova et al., 2018; Cifrek et al., 2009). These descriptors can be used for different applications and not exclusively for fatigue.

In the context of fatigue, the main descriptor is the median frequency due to findings related to its lower sensitivity to noise compared to peak and mean frequencies (Shair et al., 2017); see Table 1. One of its foundations relies on the possibility of obtaining these indicators through a Fourier transformation when there are stationary signal periods (Angelova et al., 2018) and when the signal extension is appropriate based on repetitive statistical parameters over time. This supports the need to obtain instantaneous parameters of the changes in myoelectric signal characteristics when sEMG is used (Zhang et al., 2010).

The most common expected behavior of muscular fatigability over time shows a shift towards lower frequencies (spectral compression), accompanied by a decrease in muscular conduction velocity (due to a more acidic environment) and possibly an increase in indicators in the time domain (due to changes in the morphology of action potentials) (Xie et al., 2006; Zhang et al., 2010; Martinez-Valdes et al., 2016; Fujisawa et al., 2017), see Figure 3. The median frequency divides the spectrum in half as a measure of central tendency. The mean frequency is the arithmetic average of the frequencies in the spectrum, and the peak frequency represents the fundamental frequency of the frequency spectrum of an electrical signal (Cifrek et al., 2009).

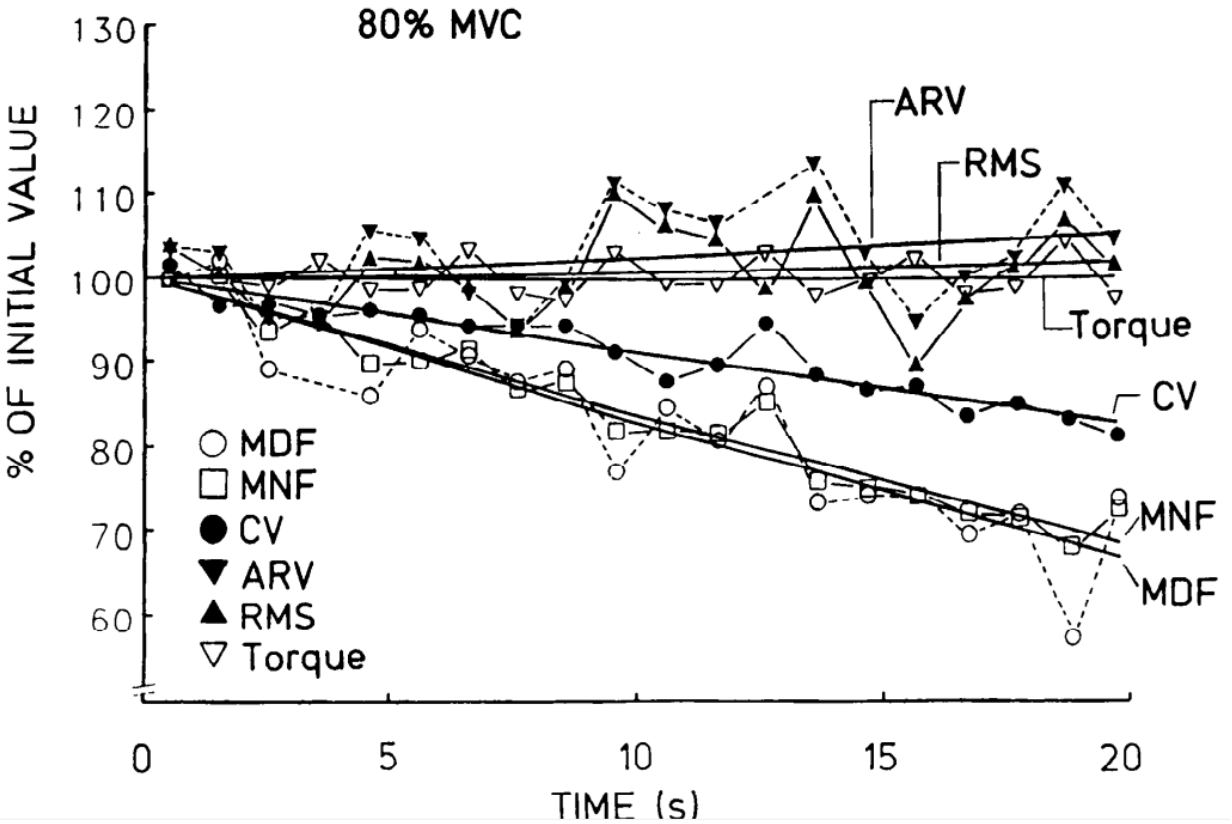

Figure 3. Myoelectric manifestations of muscular fatigue (Merletti, Knaflitz, and De Luca 1990)**.** ARV = average rectified value. RMS = root mean square. CV = conduction velocity. MNF = mean frequency. MDF = median frequency. MVC = maximal voluntary contraction. % = percentage.

Based on the observed changes regarding the leftward shift in the frequency spectrum and median and mean frequencies during dynamic contractions (Dimitrov et al., 2006; Angelova et al., 2018) as electrical manifestations of fatigue (Table 1), these descriptors have been questioned in sensitive and reliability in muscular fatigue (Dimitrov et al., 2006). In the same way, muscle activation using sEMG descriptors has been questioned (Vigotsky et al., 2017). Hence, it is imperative to consider appropriate sEMG methods prior to applying them. Due to that, this thesis starts with methodological assumptions of sEMG analysis.

Table 1. Electrical manifestations of sEMG described in the literature (Shair et al., 2017).

Electrical manifestation of fatigue	
Time domain	**Frequency domain**
Integral EMG	Mean frequency
Root mean square	Median frequency
Mean Absolute Value	Peak frequency
Modified mean absolute value type 1	Mean power
Simple integral square	Total power
Variace of EMG	Spectral moments
V-order	Instantaneous frequency variance
Log detector	Averaged instantaneous frequency
Waveform length	Dimitrov spectral fatigue index
Average amplitude change	
Difference absolute standard	
Deviation value	
Zero crossing	
Myopulse percentage rate	
Willison amplitude	
Slope sign change	
Mean absolute value slope	
Multiple hamming windows	
Multiple trapezoidal windows	
Histogram of EMG	
Autoregressive coefficient	
Cepstral coefficient	

2.4 Bias in surface electromyography processing

In signal processing, bias refers to a systematic error or deviation in the processed digital signal that consistently causes it to differ from the true or expected value (different meaning used from the statistical concept of Expected value [x] of a distribution, which can correspond to a mean in a normal distribution). This deviation can arise due to several factors, such as measurement inaccuracies, signal acquisition or processing system imperfections, or inappropriate assumptions made during the signal analysis or treatment. Bias can significantly impact the accuracy and validity of the final results, leading to erroneous conclusions or interpretations. Because of that, it is essential to identify and mitigate bias in signal processing to

ensure the validity (measure that the instrument really measures) of the analyzed data and to achieve more accurate and meaningful insights from the processed signals. Calibration, normalization, and removal of known sources of bias are employed to minimize the effects of bias and enhance the quality of signal processing outcomes. But also, conceptual mistakes or underestimated procedures would affect the final results.

From a statistical point of view, bias can also be defined as deviation from a true value (ground truth) and directly affects error types I and II, validity, accuracy, and reliability. Error type I relates to an erroneous assignation, and error type II relates to not identifying a condition even when it exists. Also, it can be described as a systematic (repetitive error action) error.

In the case of the sEMG signal (time series), factors like signal processing parameters, models, and visualization methods to refer to activations might distort the true information, making it difficult to understand special conditions like inhibition under physiological or non-physiological conditions like fatigue or posttraumatic muscle weakness, respectively. These distortions can cause both statistical type errors. In this thesis, bias will be understood as any signal treatment method that causes non-physiological divergence from the true or expected value.

2.5 Muscle activation and topographical maps as muscle activation descriptors

Under physiological conditions, muscle activation results from action potentials from different motor units propagating down to motoneuron, which activates its branches to reach the muscle fibers in an α-motor unit. Then, when the postsynaptic membrane of a muscle fiber is depolarized, the depolarization propagates in both directions along with the muscle fiber. The membrane depolarization, accompanied by a movement of ions, generates an action potential with an electromagnetic field in the vicinity of the muscle fibers projected outside of the skin, acting in the deeper tissues as low-pass filtering (Cifrek et al., 2009; De Luca et al., 1979).

The muscle activation term in muscle contraction measured by sEMG classically refers to the period (delta of time) when the muscle contracts with sufficient intensity (amplitude) to cause a useful (from synergies to primary motor effector) mechanical effect for a determined task (voluntary or involuntary) being triggered and controlled by the nervous system. Two relevant properties can be quantitatively measured: the timing and intensity (amplitude) of a sEMG signal. The first and most classical technique to define timing was the mean and standard deviation

technique (Soderberg et al., 1984). However, there are better techniques like the use of the Taeger Keiger energy operator (TKO) (Solnik et al., 2010) or wavelets techniques (De la Fuente et al., 2018). The amplitude of a sEMG signal can be classically measured through the root mean square (RMS), mean absolute value or the peak of the rectified signal (Vigotsky et al., 2017). However, better modern techniques like single-value decomposition can also be used (Gallina et al., 2018).

sEMG maps are visual representations that depict the spatial distribution of electrical muscle activity recorded through sEMG sensors (Merletti et al., 2019). These maps use colors or intensity gradients to illustrate the varying muscle activation levels across different regions of the muscle or muscle group being studied (Merletti et al., 2019). sEMG maps are valuable tools in surface HD-sEMG studies, providing researchers and clinicians with detailed insights into muscle activation and coordination patterns during various tasks and movements (Merletti et al., 2019). By visualizing the distribution of electrical signals on the skin, sEMG maps help understand muscle recruitment strategies, muscle synergies, and potential imbalances, contributing to the evaluation of neuromuscular function (Merletti et al., 2019).

2.6 Neurophysiology of posttraumatic muscle weakness: An inhibitory neuromuscular model

Following a traumatic joint injury (that includes joint surrounding tissues like muscles), the immediate inability to completely contract a muscle can be attributed, in part, to acute central inhibitory mechanisms originating from peripheral damage (Figure 4). These mechanisms involve afferent signals, which subsequently lead to the downregulation of α-motor units (Rice et al., 2010). This response is a reflex response against structural injury and joint edema (Hart et al., 2010). However, long-term persistent posttraumatic muscle weakness triggers a similar inhibitory neural circuitry (Figure 5). But, sustained muscle weakness does not necessarily require long-term structural, edema or innervating nerve damage to be under persistent muscle weakness status (Lepley a et al., 2021). Here, both central inhibition and posttraumatic muscle weakness interact and underlie on neural adaptations that finish in a persistent downregulate α-motoneurons state (Hart et al., 2010).

Although inhibition can be caused by posttraumatic persistent muscle weakness, muscle fatigue can also cause it, sharing a similar neurophysiological inhibitory mechanism that involves pre-synaptic inhibition via Ia, Ib, II, III, and IV afference neurons level on α-motoneurons activation (McPherson et al., 2023); see Figure 6-B, which shows the inhibitory mechanism during muscle fatigue. In this sense, posttraumatic muscle weakness caused by Achilles tendon ruptures on medial gastrocnemius (as the posttraumatic event) would serve as a muscle model capable of being explored through sEMG methods (De la Fuente et al., 2021).

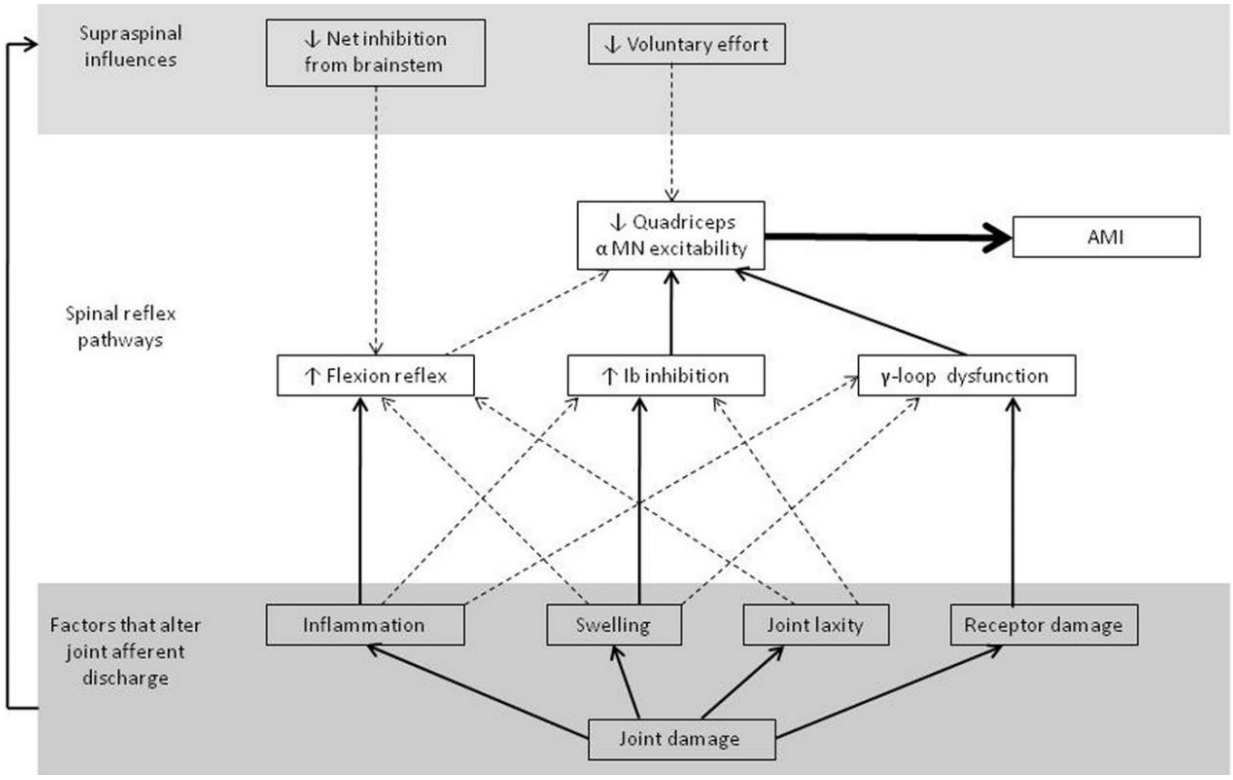

Figure 4. Acute inhibitory mechanisms model related to proprioceptive damage (Hart et al., 2010)**.** AMI = arthrogenic muscular inhibition.

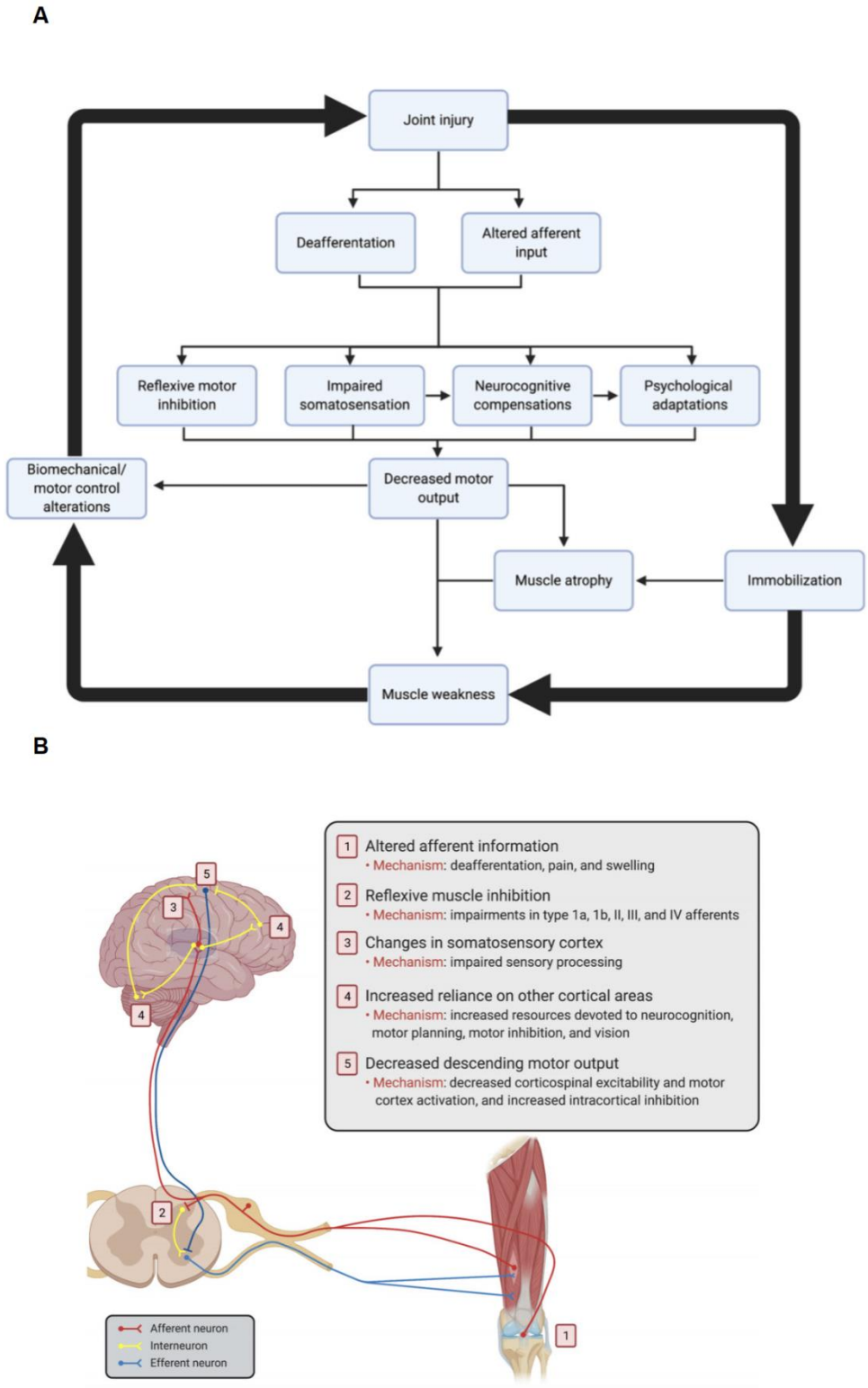

Figure 5. Persistent muscle weakness neurophysiology inhibition mechanism. A Persistent muscle weakness path. B Persistent muscle weakness effects (Lepley et al., 2021).

2.7 Muscle fatigue

Fatigue is a primary consequence of sports practice and exercise. Muscle fatigue (from now on called fatigue) is characterized by a task-dependent decrease in the maximal force capacity (Enoka et al., 2008). Fatigue excludes the incapacity to maintain a force level by the central nervous origin or motor endplate, known as central fatigue and neuromuscular junction fatigue (Cifrek et al., 2009). Their acute effects are transient and result from a metabolic, structural, and energetic chain of events due to insufficient oxygen and nutrient supply from the bloodstream at the muscular level with electrical changes from the nervous system (Basmajian et al., 1985). Acute fatigue impairs reactive motor responses (Larson et al., 2018), increases electromechanical delay (Smith et al., 2017), and stimulates alterations in muscle synergies (Cowley et al., 2014).

In the presence of acute fatigue, a metabolic process affects the muscle concentration of $[H^+]$ and their clearance due to alterations in the blood supply; due to deficits of oxygen, nutrient supply, and metabolites clearance (Cifrek et al. 2009; Gandevia 2001), see Figure 6 and 7. Finally, the conduction velocity of fiber muscle is affected, altering the behavior of motor neurons, while there is a reduction in the ability of the muscle to generate force or power (Cifrek et al., 2009; De Luca et al., 1979). When fatigue is reversible, a brief rest of ~3-5 min can restore the blood supply and metabolite clearance, reverting the ischemic reflex. Because of that, the maximal voluntary force is possible to recover quickly. This phenomenon is known as acute muscle fatigue (Carroll et al., 2017; Gandevia 2001). However, a non-complete recovery of pre-fatiguing levels may be observed and occurring due to excitation-contraction coupling (Allman et al., 2001). Thus, changes in the internal acid-base balance due to a higher accumulation of $[H^+]$ reduces the speed of action potential generation. Consequently, the muscular conduction velocity and the morphology of the action potentials from motor units that generate the myoelectric signal are affected (Raez et al., 2006), see Figure 7. Thus, a shift toward low frequencies in the frequency spectrum can be observed when the sEMG signal is transformed into the frequency domain, i.e. Fourier Transform. This is known as "spectral compression" (Zhang et al., 2010).

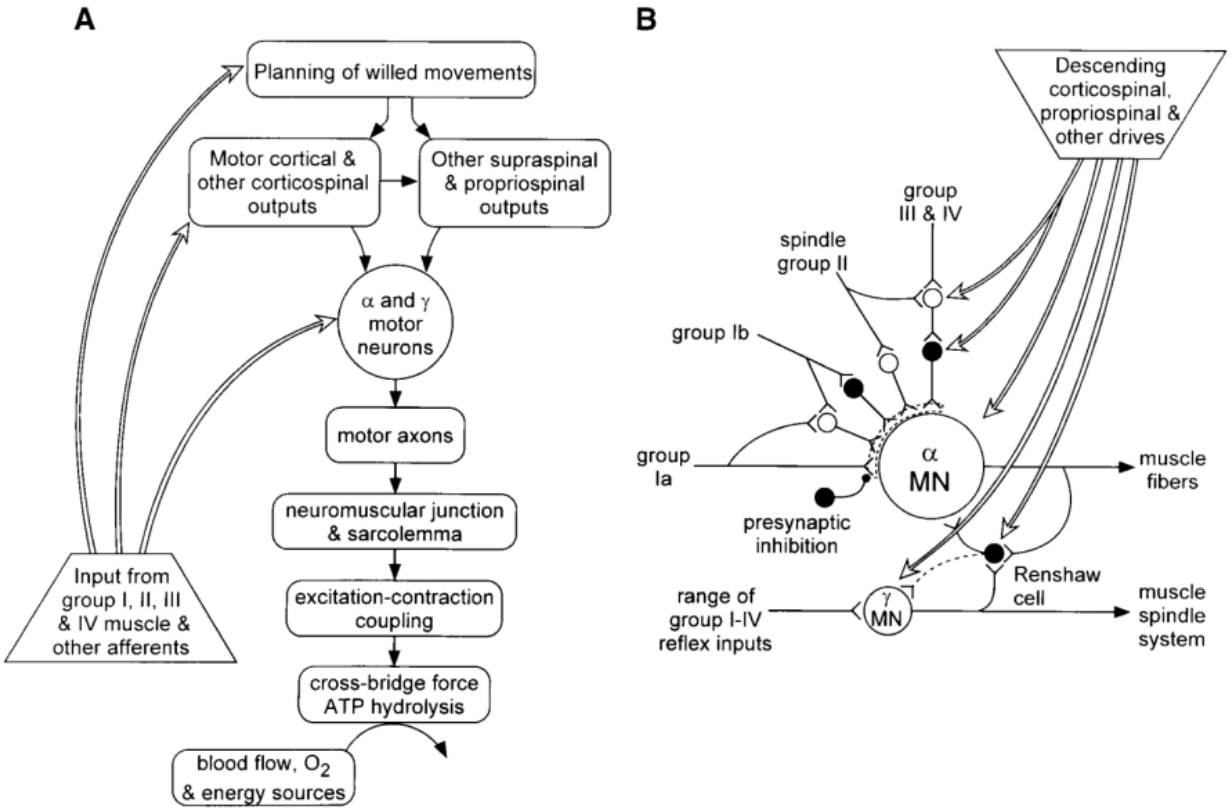

Figure 6. Muscle weakness by causes. (A) Peripheral (metabolic) cause. (B) Presynaptic inhibition during muscle fatigue (Gandevia 2001).

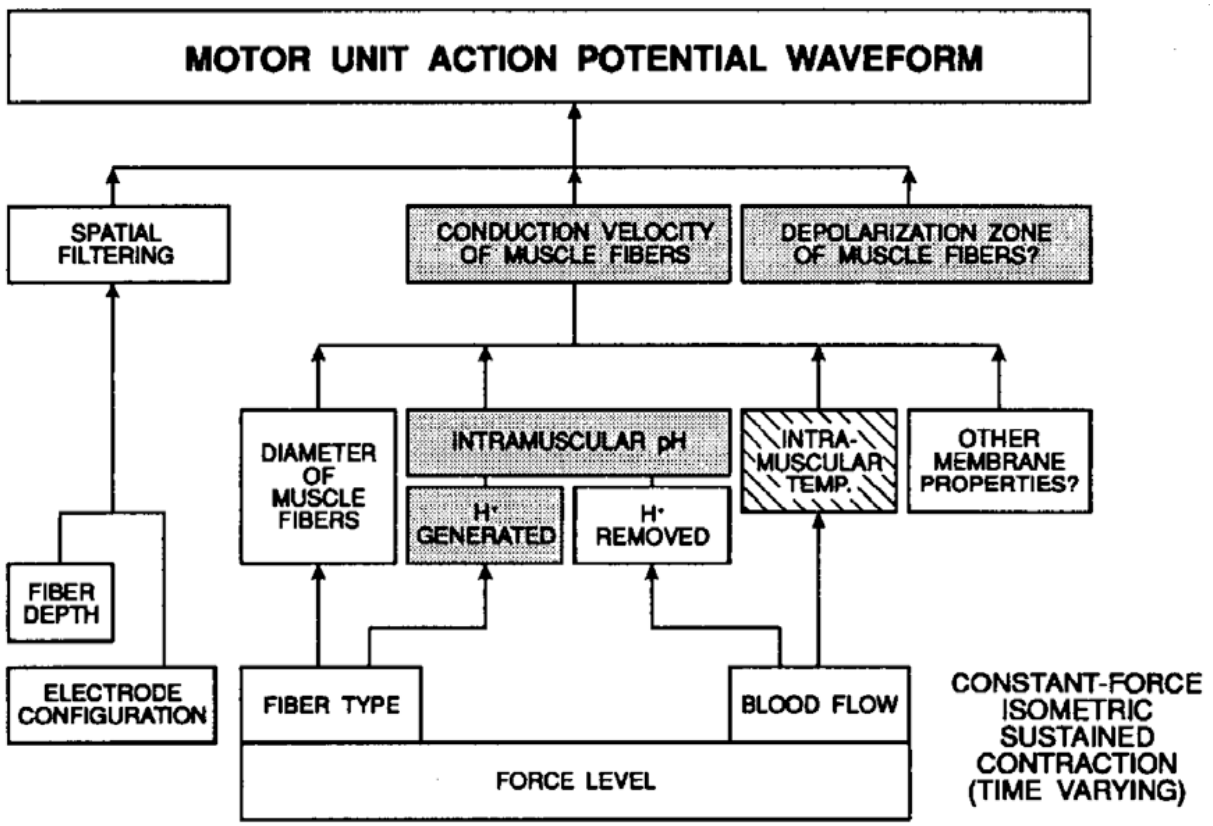

Figure 7. Factors that can affect the morphology of MUAP during muscle contraction. The gray boxes show the main factors in isometric contractions eliciting around 30% of maximal voluntary contraction. Temperature is indicated with shading to illustrate its minor weight compared to other factors at the same level (De Luca et al., 1979).

Under acute fatigue, the force is reduced by pre-synaptic afferences (Figure 6). α-motoneurons may be inhibited by changing the firing rate and muscle spindle "disfacilitation." Then, the deficit of local blood O_2 triggers the ischemic reflex, which acts on small-diameter muscle afferences (group III and IV), impairing the motor unit responses transitorily during the task (Gandevia 2001), see Figure 6. As was mentioned for posttraumatic persistent muscle weakness, both fatigue and inhibition share a similar neurophysiological inhibition mechanism that involves pre-synaptic inhibition via Ia, Ib, II, III, and IV afference neurons level on α-motoneurons activation, which ends in the downregulation of α-motoneurons (McPherson et al., 2023).

2.8 Cumulative muscle fatigue

Cumulative fatigue is a motor condition observed after a repeated bout of exercise or load, which may cause a decrease in the maximal capacity of force and require days to recover (Jones et al., 2017; Machado et al., 2018; Priego-Quesada et al., 2019). This process may have a wide implication on human movement, including impaired inter-limb coordination, creating a scenario where a worse motor response may occur, increasing muscle/joint overload and the risk of suffering an injury (Jones et al., 2017; Machado et al., 2018). Combinations of exercise intensity and duration may result in the repetitive peak of load on muscles, causing musculoskeletal dysfunction, not only in sports activities but also affecting working and daily life activities (Sjøgaard et al., 1998; Søgaard et al., 2017). Although most studies in the past focused on isometric muscular fatigue, the main challenge relies on understanding dynamic cumulative conditions, including bouts of fatigue across different days. However, the neuromuscular effects of cumulative fatigue on muscle force and neuromuscular behaviors, which result from repeated sessions of exercise, are still debatable (Machado et al., 2018).

While a condition of acute fatigue elicits transient neural (Stock et al., 2012), mechanical, and cellular adaptations (McHugh 2003), cumulative fatigue may also involve tissue damage, inflammation, and oxidative stress (Twist et al., 2005). The impairment in force due to cumulative fatigue would last from hours to days until full recovery (Jones et al., 2017; Machado et al., 2018; Priego-Quesada et al., 2019). However, evidence of cumulative fatigue is not consistent and seems to depend on several factors. For example, some studies aimed to address cumulative fatigue but ended up discussing overreaching (Lacome et al., 2018) or considered low intensity efforts (Sarker et al., 2020). In this sense, four hypotheses help to explain the effects of cumulative fatigue: 1) the glycogen depletion hypothesis, 2) the muscle damage hypothesis, 3) the inflammation hypothesis, and 4) the oxidative stress hypothesis (Cheng, Jude, and Lanner 2020).

The glycogen depletion hypothesis relates to a low level of muscle glycogen available (Snyder 1998) and insufficient recovery nutrition (Alghannam et al., 2018). The other hypotheses involve the disruption of muscle fibers. It particularly relates to damages in the membrane and

sarcomeres with the release of [Ca^{++}] by the retinaculum (Proske et al., 2001), but also a higher intracellular [Ca^{++}] via stretch-activated channels and increasing the permeability of the membrane to extracellular [Ca^{++}] (Kano et al., 2012). The metabolic stress of [Ca^{++}] has toxic effects on the plasmatic membrane, contributing to muscle damage, signaling, and regeneration via apoptosis and necrosis (Horn et al., 2018; Kano et al., 2012; Schanne et al., 1979). Similar effects appear during cumulative fatigue associated with inflammation and the increased production of reactive oxygen species (Machado et al., 2018). The loss of [Ca^{++}] homeostasis leads to coagulative necrosis, irreversible injury, and cellular death (Farber 1990; Schanne et al., 1979). Therefore, cumulative fatigue may be composed of central causes, where a progressive reduction in voluntary activation would occur in the central nervous system, or peripheral causes, which would involve distal changes in the neuromuscular junction (Gandevia 2001) and likely motor unit thresholds.

Unfortunately, repetitive loads on muscle can increase fiber permeability, particularly to [Ca^{++}], which can cause damage to the membrane (MacIntosh et al., 2012). Due to that, during fatigue, [Ca^{++}] release at the peripheral level may cause damage to the muscle fibers membrane (MacIntosh et al., 2012), see Figure 8. This is a fundamental change during acute and possibly cumulative fatigue. Regarding that, the main kwon physiological regulation to produce force is the control of the contractile actin and myosin proteins by [Ca^{++}] and myosin light chain phosphorylation, regulation of membrane excitability through [K^{+}] and [Cl^{-2}] channels, and the regulation of [Ca^{++}] in the sarcoplasmic retinaculum. The regulations involve the excitation-contraction coupling of proteins using ATP and Na+/K+-ATPase at the surface and transverse tubule membranes. The excitation-coupling contraction event sequence needs an action potential generated at the neuromuscular junction, which propagates along the membrane to reach the transverse tubules that connect with the sarcoplasmic retinaculum (Figure 8-A). The voltage sensor DHPR detects the associated depolarization and opens the RyR channel to release [Ca^{++}] into the sarcoplasm. [Ca^{++}] diffuses throughout the cell and binds to several ligands, including troponin and calmodulin. The binding of [Ca^{++}] to troponin moves the tropomyosin away from the myosin-binding site on actin, permitting cross-bridge cycling, which uses the phosphorylation of ATP converting biochemical to mechanical energy (Figure 8-B). Removal of [Ca^{++}] from the cytoplasm by Ca^{++} ATPase results in the recovery of tropomyosin to its blocked position and then the relaxation occurs (Calderón et al., 2014; MacIntosh et al., 2012).

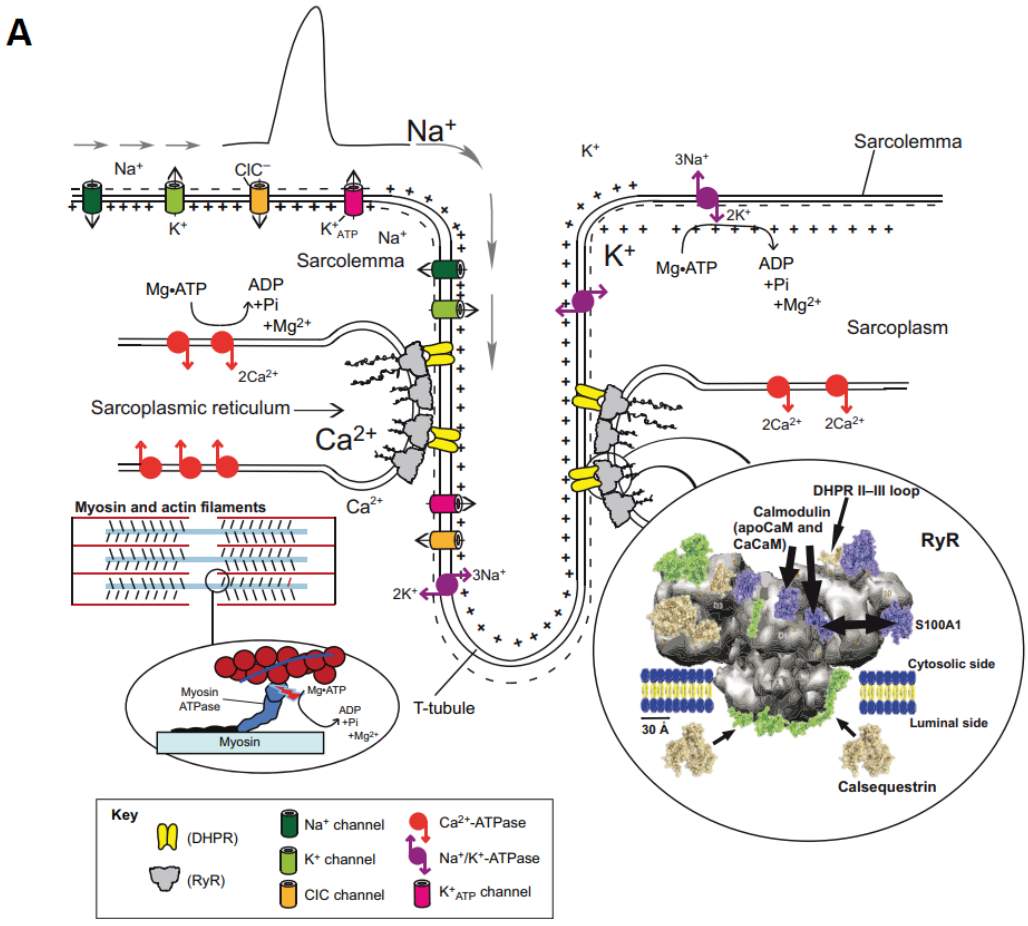
A
Na+
ClC−
K+
K+ATP
Na+
Sarcolemma
Mg•ATP
ADP
+Pi
+Mg2+
2Ca2+
Sarcoplasmic reticulum
Ca2+
Ca2+
Myosin and actin filaments
2K+
3Na+
T-tubule
Myosin ATPase
Mg•ATP
ADP
+Pi
+Mg2+
Myosin
K+
3Na+
2K+
Mg•ATP
ADP
+Pi
+Mg2+
Sarcolemma
Sarcoplasm
2Ca2+
2Ca2+
DHPR II–III loop
Calmodulin
(apoCaM and
CaCaM)
RyR
S100A1
Cytosolic side
Luminal side
30 Å
Calsequestrin
Key
(DHPR)
(RyR)
Na+ channel
K+ channel
ClC channel
Ca2+-ATPase
Na+/K+-ATPase
K+ATP channel

B

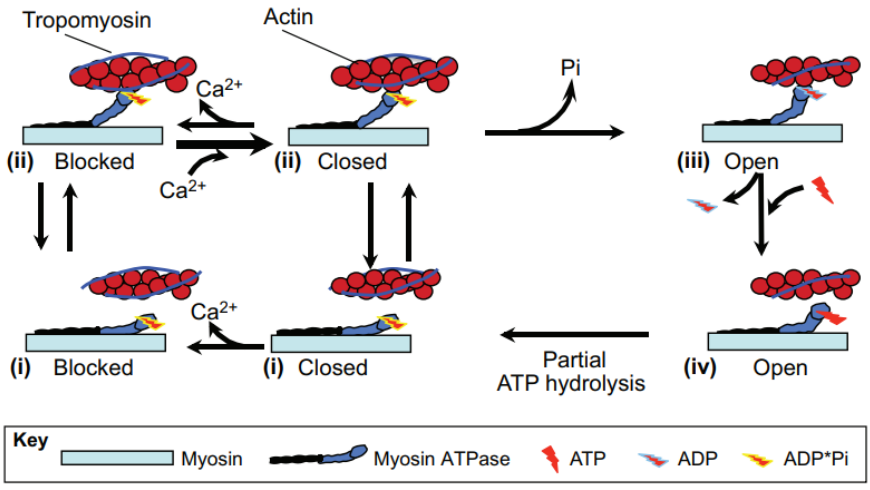
Tropomyosin
Actin
Ca2+
Ca2+
Pi
(ii) Blocked
(ii) Closed
(iii) Open
Ca2+
(i) Blocked
(i) Closed
Partial
ATP hydrolysis
(iv) Open
Key
Myosin
Myosin ATPase
ATP
ADP
ADP*Pi

Figure 8. Excitation–contraction coupling. (A) Action potential propagation during muscle contraction. (B) filament displacement contraction hypothesis. (MacIntosh et al., 2012).

2.9 Action potential of Motor Unit under single-session of fatigue

Neurophysiological characteristics of motor units, i.e. firing rate and motor units recruitment, permit the measurement of how the central nervous system regulates muscle force production during fatigue (Contessa et al., 2009; Farina et al., 2014; Farina et al., 2015). Previously, it was determined there is a correlation between force decrease and motor unit behavior (Contessa et al., 2009). Motor units under intra-session with intermittent repetitive contractions in an invasive set-up have shown that low- and high-threshold motor units under fatiguing contraction could not be individually controlled by a central drive. But can be influenced by motoneurons adaptation and afferent feedback from the active muscle (Carpentier et al., 2001). Under fatigue, motor units have electrical shape changes during intermittent repetitive fatigue (Carpentier et al., 2001), see Figure 9-Cc123 below. These changes clearly increase the pea-to-peak amplitude of the action potential of the motor units, which can explain why bipolar sEMG increases their amplitude (see Figure 9). But also, it is clearly appreciated the addition of new motor neurons at the end of the contractions to maintain the same initial force level (see Figure 9-ABC, please see at the beginning, there are two motor units, and at the end, there are three motor units). The behavior can suggest how the nervous system modified its motor units strategies to maintain the initial force requirement, demonstrating that electromyographical changes occur prior to the incapacity to maintain the force in time (mechanical failure). However, several factors can introduce bias to the sEMG signals and their interpretations.

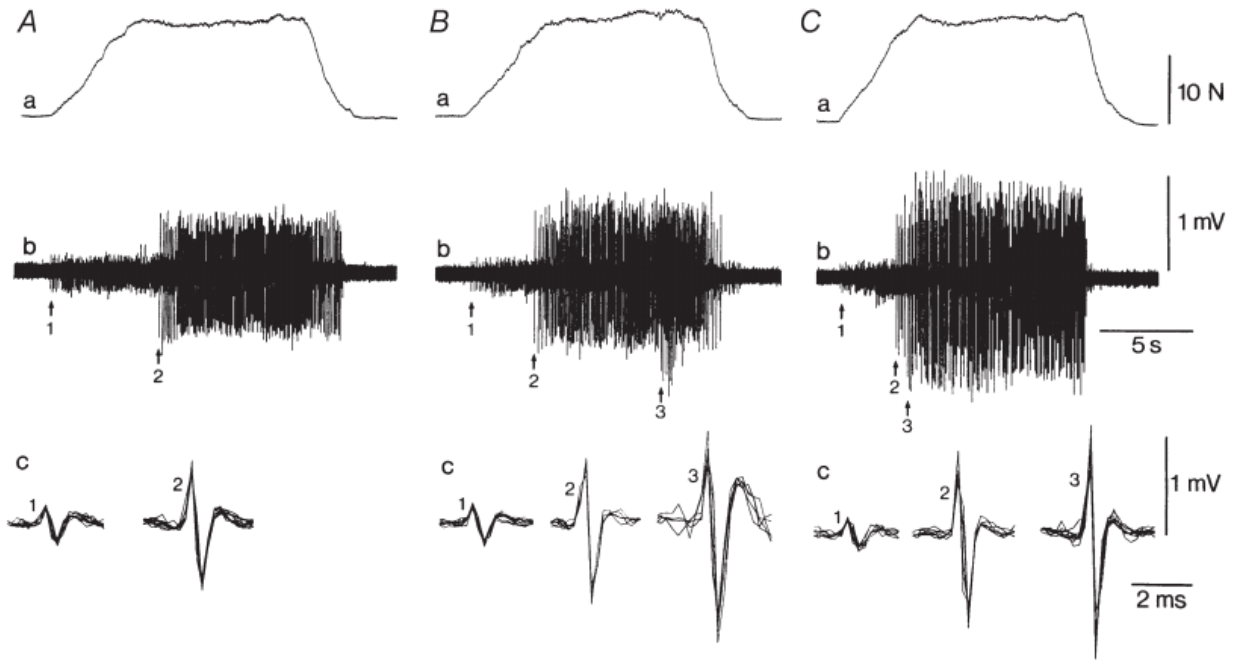

Figure 9. Motor unit shape changes during single-session fatigue. A,B,and C forces. b. Intramuscular sEMG signals. c intramuscular motor unit wave basis (Carpentier et al., 2001).

2.10 Eccentric component into dynamic contractions cause fiber muscle damage

Eccentric muscle contractions cause mechanical damage to the muscle fibers (Yamaguchi et al., 2020), see Figure 10. The damage is not directly linked to the level of force generated; instead, it is related to the length of the muscle (Allen et al., 2018). Membrane and sarcomeres damage, releasing [Ca^{++}] from the retinaculum (Proske et al., 2001), but also the intracellular [Ca^{++}] increases via stretch-activated channels, which increases the permeability of the membrane to extracellular Ca^{++}, triggering fiber apoptosis (Kano et al., 2012) (Figure 10). Therefore, dynamic exercising with eccentric components is not trivial because eccentric contractions may interact with cumulate fatigue effects. Also, their location is near to myotendinous junctions (Figure 10).

The [Ca^{++}] accumulation in the cytosol had toxic effects on the plasmatic membrane, leading to muscle damage, signaling, and regeneration via apoptosis and necrosis (Horn et al., 2018; Kano et al., 2012; Schanne et al., 1979). The loss of [Ca^{++}] homeostasis in the cell is

accompanied by coagulative necrosis at the final stage; the events leading to the coagulative necrosis cause irreversible injury and cell death, loss of the plasma membrane's ability to maintain a gradient of [Ca^{++}], an influx and accumulation of [Ca^{++}] in the cell, and the morphologic appearance of coagulative necrosis (Farber 1990; Schanne et al., 1979). Particularly, eccentric actions lead to more continuous high levels of intracellular [Ca^{++}] via stretch-activated channels than other muscle contractions (Hody et al., 2019; Kano et al., 2012).

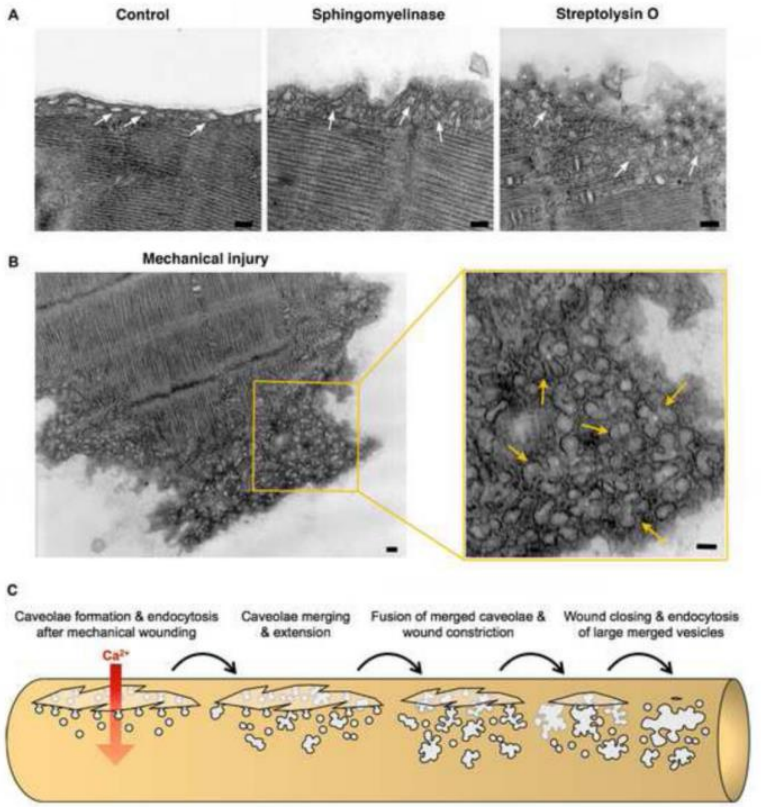

Figure 10. Plasmatic membrane damage (Andrews et al., 2014).

2.11 Use of reduction dimension techniques to explore activation patterns

sEMG is important to understand muscle fatigue and activation but involves a big dimension of the dataset because it needs high sampling frequency and time to represent the physiological phenomena. Understanding how to use sEMG parameters tunning to estimate

fatigue for dynamic muscle contractions and its visualization would require reduction dimensions techniques for redundant information. Often, researchers increase the number of features (dimensions) since they do not know the best ones beforehand. Also, when one acquires time series, features depend on many or all the time samples, and this dependency is unknown.

Nowadays, sEMG data sets have multiple features, bringing more information to users. However, at the same time, the raw data is noisy and may have a significant amount of redundant information (Huang et al., 2019; Pandian et al., 2020). Hence, transforming the original data from a high-dimensional space to a lower-dimensional while preserving many of the essential features is the objective of the dimensionality reduction techniques (Huang et al., 2019). More precisely, dimensionality reduction techniques find an approximation of a raw data matrix $X \in \mathbb{C}^{n \times d}$ into $X \in \mathbb{C}^{n \times r}$ where n is the number of samples, d is the number of features, and $r \ll d$ is the dimension of the low-dimensional space (Pandian et al., 2020; Siva 2020). There are two main approaches to reducing dimensionality (Géron 2019):

1) By Projection: These techniques project each high-dimensional data point onto a suitable lower-dimensional subspace such that distances between points are approximately preserved (Huang et al., 2019; Pandian et al., 2020; Siva 2020). Principal Components Analysis (PCA) is an example of this class of techniques.

2) By Manifold Learning: These techniques are commonly called Manifold learning, and they rely on the manifold hypothesis or assumption, which holds for most real-world high-dimensional datasets. Under this hypothesis, the data is modeled by a manifold on which the high-dimensional data lie. The dimension of this manifold is much smaller than the dimension of the original space (Huang et al., 2019; Pandian et al., 2020; Siva 2020). Uniform Manifold Approximation and Projection (UMAP) is an example of this class of techniques (McInnes et al., 2018).

Examples of dimensionality reduction techniques include feature selection, variance threshold, ranking, correlation, Eigen-problem reduction, and non-linear reduction. In the feature selection method, the most straightforward dimensionality reduction approach, a subset of good features are selected, and the remaining features are discarded based on predefined criteria. The variance threshold method is a feature selection approach where features are dropped when their corresponding variance is below a given threshold (Pandian et al., 2020). The feature ranking

method assigns a rank to each variable based on a scoring function. A low score means it is less valuable to the outcome. Hence, features are sorted in decreasing scoring order. The least ranked features are removed, and the accuracy of the model is calculated again. This process is repeated until the accuracy of the model is significantly lost. This approach is only effective in supervised learning and is effective with a low number of features. The correlation method searches for similarities between pairs of or multiple features. If the correlation coefficient is above a given threshold, one of the features can be dropped since they carry similar information. The Eigen-problem methods decompose the data along the axes of maximum variance and then keep the necessary components to explain a high level of the total variance. Finally, non-linear dimensionality reduction techniques transform the data based on the minimization of a non-linear cost function. Examples of non-linear techniques are Isomap, self-organized maps (SOMs), t-Distributed Stochastic Neighbor Embedding (tSNE), and Uniform Manifold Approximation and Projection (UMAP) (McInnes et al., 2018). The nonlinear nature of many datasets has shifted the community towards the use of nonlinear dimensionality reduction techniques. Table 2 summarizes the cost function used by some of these methods.

Table 2. Classical dimensionality reduction algorithm (Huang et al., 2019).

Algorithm	Linear	Supervise	Objective function	Parameters
PCA	Yes	No	$J(U) = U^T \sum U - \alpha (U^T U - 1)$	α is an eigenvalue of the covariance matrix and U contains de orthogonal projection of xi vectors resulting in un projections.
Isomap	No	Yes	$J(X) = \sum_{i=1}^{n} \sum_{j=1}^{n} d_G(i,j) - \|y_i - y_j\|$	$d_G(i,j)$ is a geodesic distance from i to j.
SOM	No	No	$d_j(X) = \sum_{i=1}^{n} (x_i - w_{ji})^2$	w_{ji} denotes the weight vector.

PCA = principal components analysis.
SOM = Self-organizing map.

PCA is probably the most popular dimensionality reduction algorithm. The method works by projecting the data on the space span by the eigenvectors with the largest eigenvalues. A predefined criterion gives the number of eigenvectors that are kept. Two or three principal components are kept if one wishes to visualize the data. Another criterion is to keep the necessary number of components to explain 95% of the data variance. Some drawbacks and assumptions of PCA are:

- Input variables are assumed to be independent of one another. This is not necessarily true (uncorrelated), and other algorithms like independent component analysis try to resolve this assumption better.

- PCA assumes that the principal components are a linear combination of the original features. If this is not true, PCA will not give sensible results.

- The eigenvectors of the PCA have contributions from all input variables. This makes their interpretation difficult since a large feature value cannot be attributed to a few (ideally a single) input values.

PCA attempts to find the largest variance through orthogonal projection (U). U matrix contains Un vectors as orthogonal projections of X, which is the raw data matrix $\mathbf{X} \in \mathbb{C}^{\mathbf{n} \times \mathbf{d}}$. PCA maximizes the objective function $\mathbf{J(U)} = \mathbf{U^T} \sum \mathbf{U} - \boldsymbol{\alpha} (\mathbf{U^T U} - \mathbf{1})$, where $\mathbf{U^T U} = \mathbf{1}$, $\boldsymbol{\Sigma}$ is the covariance matrix, and $\boldsymbol{\alpha}$ is an eigenvalue of the covariance matrix $\boldsymbol{\Sigma}$ (Huang, Wu, and Ye 2019). The direction of the first principal component $\mathbf{u_1}$ is the direction of the maximum variance $\mathbf{u_2}$ is the second principal component, which is orthogonal to $\mathbf{u_1}$, and have the second direction with the higher variance. This process is repeated until find the r-dimensional approximation of the raw matrix $\mathbf{X} \in \mathbb{C}^{\mathbf{n\,x\,d}}$ into $\mathbf{X} \in \mathbb{C}^{\mathbf{n\,x\,r}}$ where $\mathbf{n}$ is the number of samples, $\mathbf{d}$ is the number of features, and d > $\mathbf{r}$. PCA assumes that the data is zero-mean and the fitted subspace is a linear projection (Huang, Wu, and Ye 2019).

Another algorithm is the UMAP algorithm. A high-dimensional dataset X can be transformed into a low-dimensional dataset using UMAP. UMAP creates a fuzzy topological structure using the gradient of the binary cross-entropy as the loss function where the weights are the existence probability of the 0-simplex (the lowest dimensional connection) or 1-simplex, which is a topographic representation of the connection or not-connection between neighbors (McInnes et al., 2018). The weight between neighbors is modeled as $w = e^{\frac{-d(x_i - x_j) - \rho_i}{\sigma_i}}$, with ρ_i the distance between the i-th data point and its first nearest neighbor (Oskolkov 2019). The binary cross-entropy is given by $\sum_{je \in E} \left[w_h(e) \log \frac{W_h(e)}{W_l(e)} + (1 - w_h(e)) \log(\frac{1 - W_h(e)}{1 - W_l(e)}) \right]$. In this expression, it may be understood that the first term provides attractive forces to ensure connectivity between the points whenever a large weight is associated with the existence of the simplex. In contrast, it may be understood that the second term provides repulsive forces, generating connectivity whenever a small weight is associated with the non-existence of simplex since it minimizes. $W_l(e)$ (McInnes et al., 2018). To embed the intrinsic structure of the data belonging to a high-dimensional space into a low-dimensional space, UMAP optimizes the distance of probabilities using $Q(d_{ij}) = (1 + a(y_i - y_j)^{2b})^{-1}$, by finding a and b coefficients from the non-linear least square fitting to the piecewise function with "min_dist" hyperparameter: $Q(d_{ij}) \approx \begin{cases} 1 & \text{if } y_i - y_j \leq \text{min\_dist} \\ e^{-(y_i - y_j)} & \text{if } y_i - y_j > \text{min\_dist} \end{cases}$. Besides, the connectivity of the algorithm also defines the number of nearest neighbors as $k = 2^{\sum_i p_{ij}}$. In general terms, the algorithm projects a

fuzzy topological set of high dimensions equivalent to a low-dimensional space. In other words, the algorithms assign almost the same low-dimensional coordinates for all points close to each other into the low-dimensional space to construct a topological representation of the high-dimensional data (Ali et al., 2019; McInnes et al., 2018).

2.12 Use of clustering techniques to identify data similarities

Data clustering techniques are unsupervised machine learning methods used to segment a dataset into distinct groups or clusters based on similarity criteria. The goal of clustering is to group data points that are more similar to each other within the same cluster and dissimilar to those in other clusters. There are various clustering algorithms, each with its approach to defining similarity and forming clusters. Two common clustering methods are K-means and hierarchical clustering. K-means partitions the data into K clusters (see annexes codes for more details), where each data point belongs to the cluster with the nearest mean. When the median is used, the algorithm is known as k-medoids. Hierarchical clustering builds a tree-like structure of clusters, allowing the user to choose the number of clusters. Clustering techniques find applications in diverse fields, such as image segmentation, customer segmentation, anomaly detection, and pattern recognition, aiding in understanding the underlying structure datasets.

2.13 Problem statement

As the former items of this thesis tried to demonstrate, there are physiological (muscle fatigue), pathological (posttraumatic muscle weakness), and non-physiological (sEMG signal segmentation) factors that can modify the interpretation of sEMG methods (myoelectrical manifestations, sEMG maps, and motor unit decomposition) obtained from sEMG measurements. For example, muscle fatigue and inhibition are the most common physiological mechanisms that interfere with muscle activation and human performance, and the clarity between acute and cumulative fatigue, as well as the influence of physiological conditions related to neuromuscular impairments such as persistent weakness, remains unclear. Nevertheless, the methodological choices (like windowing and overlapping) associated with the processing of electromyography signals can also interfere with outcomes interpretations and interact with physiological factors. Due to all the above, we identified three main research questions that drove this research:

1. Does methodological bias in electrical manifestations influence the estimation of cumulative muscle fatigue? For example, the choice of data analysis methods, fatigue estimation, and sEMG activation maps.
2. How do sEMG maps and motor unit decomposition behave for conditions similar to fatigue (inhibition and persistent weakness)? For example, to understand whether a condition of posttraumatic persistent muscle weakness modulates outcomes of muscle activation in a way that the methodological choice to describe the signal may hide or highlight outcomes.
3. How does cumulative muscle fatigue affect neurophysiological characteristics of muscle contraction (firing rate and motor unit recruitment)? For example, to identify how the outcomes of sEMG analysis are influenced by the condition of cumulative fatigue.

2.14 Justification

Although sEMG patterns are well described in the literature concerning general conditions of movement, when it comes to fatigue effects, studies present a high variability even when tests are performed under similar experimental conditions (Marco et al., 2017). Due to that and our previous statements, methodological assumptions based on whether bias in electrical manifestations influences the estimation of cumulative muscle fatigue support our first research question.

In the past, neurophysiological characteristics of motor units, i.e., firing rate and motor unit recruitment, have shown a correlation with force impairments (Contessa et al., 2009). Because of that, after exploring our first question and based on the last developments with HD-sEMG, questions on whether sEMG maps or motor unit decomposition techniques would be appropriate. Therefore, it supports our second research question regarding myoelectrical differences in models that highlighted inhibition and persistent weakness conditions as one fatigue characteristic.

Finally, the study of motor unit decomposition permits the discussion of the mechanisms of fatigue considering large populations of motor units that can be collected (Negro et al., 2016). This relatively new technique helps to address not only traditional aspects of muscle contraction (Table 1), but also allow exploring recruitment mechanism considering the different types of recruitment threshold. Muscle damage derived from cumulative fatigue can cause substantial changes at the single motor unit level, resulting in altered recruitment thresholds, discharge rates, motor unit conduction velocities, and synchronization. The alterations can last up to one week, with preferential damage to the high-threshold motor unit (Semmler 2014). Therefore, our third question addresses the cumulative fatigue impact on different aspects of motor control and the neuromuscular adaptations at the different levels of the central nervous system. Notably, there is also a lack of knowledge about how the motor unit firing rate and motor unit recruitment behaves during cumulative fatigue (Contessa et al., 2009; Farina et al., 2014; Farina et al., 2015).

Table 3 describes the organization of the research questions and the corresponding manuscripts in which the results are presented.

2.15 Aims and Hypotheses

2.15.1 General Aim

To determine sEMG signal segmentation, posttraumatic muscle weakness, and fatigue conditions influencing myoelectrical manifestations, sEMG maps, and motor unit decomposition obtained from surface electromyography measurements.

2.15.2 Specific Aims

To identify windowing and overlap bias in the analysis of electrical manifestations to estimate muscle fatigue and sEMG activation maps.

To determine the behavior of sEMG maps and motor unit decomposition for inhibition conditions caused by posttraumatic persistent muscle weakness.

To determine the motor unit behavior in cumulative fatigue resulting from dynamic muscle contractions.

2.15.3 Hypotheses

We hypothesize that windowing and overlap bias affect (can increase and decrease) the electrical manifestations to estimate muscle fatigue and muscle activation maps.

We hypothesize that sEMG maps and motor unit decomposition identify changes sEMG maps (increase and decrease activation) and motor unit decomposition (increase or decrease motor unit recruitment and firing rate) for conditions similar to fatigue (inhibition and persistent weakness).

We hypothesize that three bouts of fatiguing exercise (cumulative muscle fatigue) trigger neurophysiological adaptations (an increase in firing rate and motor unit recruitment) to control submaximal isometric contractions.

2.15.4 Manuscripts layout (Table 3):

Table 3. Thesis criteria. Research question, Fatigue or activation setup condition, sample, period of intervention or testing, sEMG kind, and answered topic.

Criteria / Manuscript number (#):	**# 1**	**# 2**	**# 3**	**# 4**	**# 5**
By research question:					
Research Question 1	■	■			
Research Question 2			■	■	
Research Question 3					■
By fatigue or activation setup condition:					
Fatigue contraction on setup	■	■			■
Activation contraction on setup			■	■	
By sample condition:					
Physiology condition	■	■			■
Posttraumatic muscle weakness condition			■	■	
By Period of Intervention or testing:					
Single session (acute fatigue)	■		■	■	
Repeated sessions (cumulative fatigue)		■			■
By sEMG kind:					
Bipolar sEMG signals	■				
HD-sEMG		■	■	■	■
By answered topic:					
Electrical manifestation bias in acute fatigue	■				
sEMG maps bias in cumulative fatigue		■			
sEMG maps in a presynaptic inhibition model			■		
Acute responses using MU decomposition				■	
Cumulative fatigue using MU decomposition					■

3 CHAPTER THREE – UNDERSTANDING THE EFFECT OF WINDOW LENGTH AND OVERLAP FOR ASSESSING sEMG IN DYNAMIC FATIGUING CONTRACTIONS: A NON-LINEAR DIMENSIONALITY REDUCTION AND CLUSTERING

Published as:

De la Fuente, C., Martinez-Valdes, E., Priego-Quesada, J. I., Weinstein, A., Valencia, O., Kunzler, M. R., Alvarez-Ruf, J., & Carpes, F. P. (2021). Understanding the effect of window length and overlap for assessing sEMG in dynamic fatiguing contractions: A non-linear dimensionality reduction and clustering. Journal of Biomechanics, 125, 110598. https://doi.org/10.1016/j.jbiomech.2021.110598

ABSTRACT

The Short-Time Fourier transform (STFT) is a helpful tool for identifying muscle fatigue with clinical and sports applications. However, the choice of STFT parameters may affect the estimation of myoelectrical manifestations of fatigue. Here, we determine the effect of window length and overlap selections on the frequency slope and the coefficient of variation from sEMG spectrum features in fatiguing contractions. We also determine whether STFT parameters affect the relationship between frequency slopes and task failure. Eighty-eight healthy adult men performed one-leg heel-rise until exhaustion. A factorial design with a window length of 50, 100, 250, 500, and 1000 ms with 0, 25, 50, 75, and 90% of overlap was used. The frequency slope was non-linearly fitted as a task failure function, followed by a dimensionality reduction and clustering analysis. The STFT parameters elicited five patterns. A small window length produced a higher slope frequency for the peak frequency (p<0.001). The contrary was found for the mean and median frequency (p<0.001). A larger window length elicited a higher slope frequency for the mean and peak frequencies. The largest frequency slope and dispersion were found for a window length of 50 ms without overlap using peak frequency. A combination of 250 ms with 50% of overlap reduced the dispersion both for peak, median, and mean frequency, but decreased the slope frequency. Therefore, the selection of STFT parameters during dynamic contractions should be accompanied by a mechanical measure of the task failure, and its parameters should be adjusted according to the experiment's requirements.

Keywords: electromyography; methods; muscle activation; Fourier; gastrocnemius medialis; fatigue.

3.1 Introduction

Muscle fatigue is characterized by reducing the maximal capacity to generate force or power output (Vøllestad 1997). It can be assessed by reductions in maximal force or time until task failure (Enoka et al., 2008). Although these assessments provide information when fatigue is installed, evaluating changes in muscle's electrophysiological properties extracted from electromyography time-series helps identify fatigue or non-fatigue status (Merletti et al., 1990). The myoelectric manifestations of muscle fatigue are indirectly related to reduced motor unit firing rate (Mettler et al., 2016) and a concomitant decrease in muscle fiber conduction velocity (Rampichini et al., 2020). This information can be obtained by analyzing different spectral Short-Time Fourier Transform (STFT) patterns (Karthick et al., 2016).

The variation in the sEMG spectrum as a function of time can be estimated by applying the Fourier transform to signal segments. The STFT is a sequence of Fourier transform (Cifrek et al., 2009; Jeon et al., 2020). The STFT provides time-localized frequency information on how the frequency components of a signal vary over time. The signal segments, also known as window length, affect the time and frequency resolution of the STFT. An increase in the widow length increases the frequency resolution and decreases the time resolution. Meanwhile, a decrease in the window length decreases the frequency resolution and increases the time resolution (Jeon et al., 2020). Therefore, the STFT is widely used for frequency tracking over time (K. Zhang et al. 2020), and it is of particular interest in assessing biological signals and supporting decisions between fatigue or no-fatigue status (Cifrek et al., 2009; Rampichini et al., 2020). The relatively low computational cost allows the easy implementation of detection algorithms, i.e., features extraction is used to detect several conditions using machine learning algorithms (Wang et al., 2018).

The features median, mean, and peak frequencies extracted from the electromyography periodogram are commonly used to quantify the myoelectric manifestations of muscle fatigue (Merletti et al., 1990; Cifrek et al., 2009; Cifrek et al., 2000; Shair et al., 2017; Rampichini et al., 2020). These descriptors estimate the changes in the sum of motor units action potential trains (MUAPT) in response to fatigue when the spectrum shifts towards lower frequencies (Cifrek et al., 2009; Cifrek et al., 2000; Rampichini et al., 2020; Martinez-Valdes et al., 2016; Eken et al.,

2019). Applying regressions methods to the myoelectric manifestations of muscle fatigue frequency parameters over time allows determining the frequency slope during a muscle contraction (rate of change of frequency in time) (Merletti et al., 1990). More negative slopes represent a larger left shifting of the spectrum (also known as compression of the spectrum), which is associated with higher muscle fatigue status (Merletti et al., 1990; Cifrek et al., 2009; Cifrek et al., 2000; Eken et al., 2019; Ament et al., 1993). However, this approach has limitations due to the low sensitivity for the motor unit's discharge rate (Rampichini et al., 2020), sEMG amplitude cancelation (Cifrek et al., 2009; Rampichini et al., 2020), frequency leakage (Tan et al., 2019), and time-frequency resolution problems. The STFT time-frequency resolution limitations can be overcome by using more modern methods such as wavelets (Cifrek et al., 2009; Costa et al., 2010; Waly et al., 1996). However, physiological information is available in the periodograms to be used for muscle fatigue (Costa et al., 2010). Previous studies using bipolar and HD-sEMG recordings found high variability in the chosen window length for analysis of isometric and dynamic contractions (Cifrek et al., 2009; Cifrek et al., 2000; Ament et al., 1993; Guzmán-Venegas et al., 2015; Zhu et al., 2017; Jordanić et al., 2017; Jordanic et al., 2016; Hill et al., 2018; Angelova et al., 2018; Hegyi et al., 2019; Falla et al., 2017; do Espírito Santo et al., 2018; Watanabe et al., 2018; Hawkes et al., 2018). Most of these studies did not provide details about the windows overlap (Hill et al., 2018; do Espírito Santo et al., 2018; Lark et al., 2019; Hawkes et al., 2018). Furthermore, the effects of window length and overlap have mainly been studied for isometric contractions (Zhang et al., 2010; Xie et al., 2006), but its effects remain unclear for dynamic muscle contractions. The recognition of adequate parameters is essential to avoid bias (Waly et al., 1996; Jordanic et al., 2016). Most importantly, these parameters must accurately predict failure during dynamic fatiguing tasks (Cifrek et al., 2009). However, an improper selection of window length and overlap might worsen the sensitivity of sEMG parameters to assess fatigue during dynamic contractions.

Continuous wavelet transform and STFT can provide similar muscle fatigue estimations, but considerably higher variability is found for STFT outcomes (Costa et al., 2010). Hence, we hypothesized that only a subset of the STFT parameters allows for estimating muscle fatigue robustly. Recently, the dimensionality reduction technique is known as UMAP, combined with density-based spatial clustering of applications with noise (DBSCAN) technique, has been successfully used to find latent information of raw data (McInnes et al., 2018). For this reason,

we considered that these same techniques are helpful in understanding the effect of STFT on the estimation of muscle fatigue. Also, considering that the gastrocnemius medialis muscle is highly susceptible to fatigue during dynamic contractions (Ament et al., 1993), we selected this muscle as an appropriate model to investigate the effects of the STFT parameters on sEMG outcomes in response to muscle fatigue. In summary, we aimed to determine the effects of STFT window length and overlap parameters on the frequency slope and coefficient of variation from median, mean, and peak frequencies from sEMG data from the gastrocnemius medialis recorded during a fatiguing protocol until task failure. We also determine which clusters of STFT parameters affect the relationship between the frequency slope and task failure.

3.2 Material and Methods

3.2.1. Study design

The study had two factors (window length and overlap) and five levels for window length (50, 100, 250, 500, and 1000 ms) and overlap (0, 25, 50, 75, and 90%). The sample included 88 healthy untrained men of age 22 ± 2 years, height 172.4 ± 2.5 cm, and body mass 71 ± 6 kg. The eligible participants were male adults, university students, ages between 18 and 25 years old, and not enrolled in regular physical activity. They were self-reported as healthy, without a life history of injury to the lower extremities, no history of cardiovascular or metabolic alterations, no skin allergy, chronic pain, or cognitive impairments. Participants were requested to avoid alcohol intake and perform any physical exercise and keep their regular daily routine 48 h before the experiment. Any participant was excluded if they reported alcohol intake, physical exercise, or sleep alteration on the night before the experiment. This study was approved by the local institutional ethics committee IRB 032019. All participants signed an informed consent form, agreeing to participate in the study.

3.2.2. Sample size

A sample size of 80 participants was *a priori* estimated considering a difference for factorial ANOVA with two factors (window length and overlap) and five levels for each one,

using the F-test family distribution, an alpha error of 5%, the statistical power of 80% (four times the alpha error). We considered that the sEMG differences could require a small (0.01) to medium effect size (0.06) due to intrinsical variability and decided for an arbitrary η^2 of 0.025. Furthermore, eight additional participants were included to anticipate possible losses (10% of estimation). The sample size estimation was performed using G*Power software version 3.1.9.2. (Kiel University, Germany).

3.2.3. Fatigue protocol

Participants performed the one-leg heel-rise test on a plane surface until exhaustion (Figure 11). During the test, they were allowed to touch two fingers over the wall to help keep the balance (De la Fuente et al., 2018). Each participant was familiarized with the task one week before data collection. For data collection, after performing a 10 min warm-up pedaling at 60 rpm on a cycle ergometer (535U, SportsArt, USA) without external load, the participants performed the one-leg heel-rise test. They continuously lifted their heels as high as possible at a rhythm of 45 bpm following auditory feedback provided by a metronome (Google, USA). Task failure was defined as the point where participants could no longer lift their heel. Constant visual supervision and verbal encouragement were given to each participant to control the heel's lift. The criteria to finish the test were the drop of the cadence or the exhaustion of volunteers, defined as the incapacity to lift the heel from the floor.

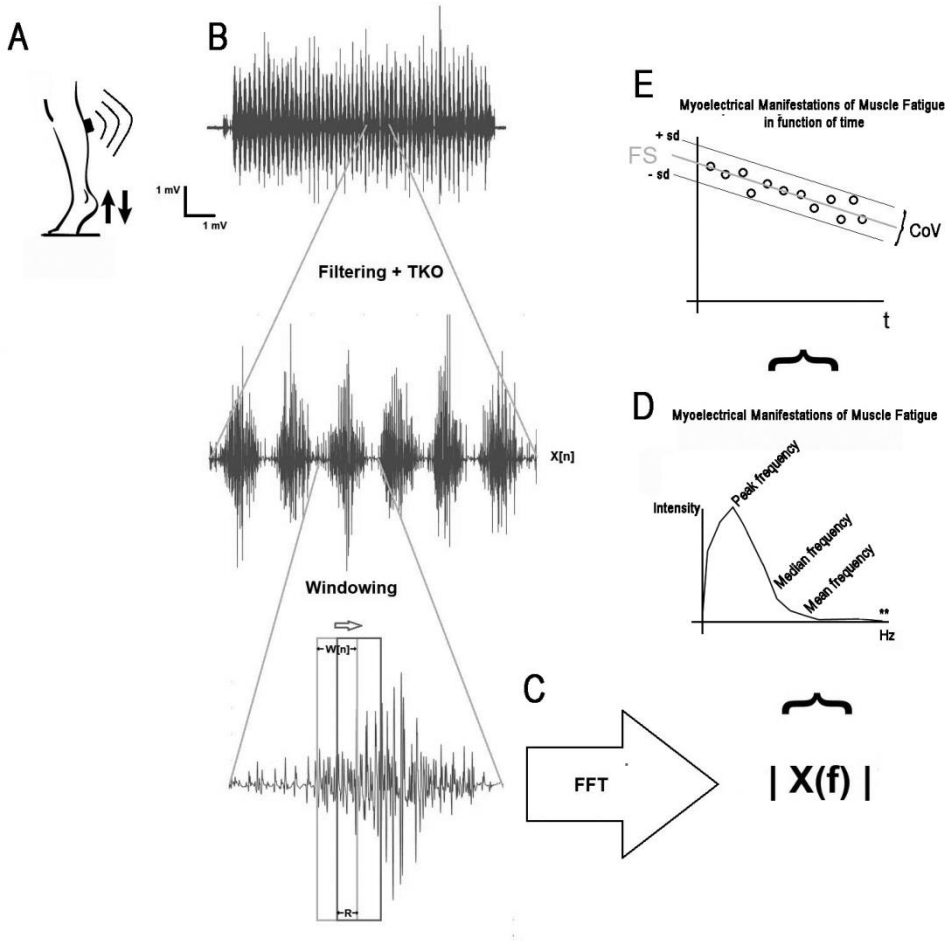

Figure 11. Experiment design. A. The figure shows the heel-rise test until task failure, where the time series of the electromyography signal (x [n]) is wirelessly transmitted, collected to be zero mean-centered, and filtered. B. Then, each burst is identified using the TKO. On each burst, a window manipulation of the length and the overlap (R) of the window (w [n]) is performed. C. From each segmented signal, the Fast Fourier Transform (FFT) is applied, and the magnitude is obtained. D. From each segmented signal, the frequency features mean, median, and peak can be extracted from spectrum, ** notice that if the sampling frequency increases the median and mean frequencies displace towards right frequencies (right-skewed distribution). E. Finally, the frequency slope (FS) is extracted from linear regression, and the dispersion of data measured as the coefficient of variance (CoV) also is obtained. sd = standard deviation.

3.2.4. Data acquisition and processing

Muscle activation was recorded continuously during the performance of the one-leg heel-rise test by a wireless sEMG sensor placed on the skin over the gastrocnemius medialis (Delsys inc., USA). The skin was shaved and cleaned with alcohol before the electrode placement according to SENIAM guidelines (Hermens et al., 2000). The sEMG signals were acquired using a Trigno™ electromyography amplifier (Delsys Inc., Boston, USA) with an Avanti sensor (Delsys Inc., Boston, USA) with an inter-electrode distance of 10 mm (De Luca et al., 2012). Data were collected with a 16-bit analog-digital converter card (Vicon Motion Systems, Oxford, UK) and sampled at 4 kHz, analog bandpass filtered (20±5–450±50 Hz), CMRR > 80 dB, resolution of 168 nV/bit, basal noise of < 0.75 μV, with hardware amplification of 1000 V/V. All data were recorded using the software Nexus 2.0 (Vicon Motion Systems, Oxford, UK).

3.2.5. Data processing and analysis

The sEMG signals were zero mean-centered, zero-padded to equal the length of the window used. They were filtered by a zero-lag fourth-order bandpass Butterworth filter with a bandpass between 20 and 450 Hz. The Teager-Kaiser energy operator threshold-based method was used to detect the individual sEMG muscle contraction bursts during the heel test (Solnik et al. 2010), see Figure 11. This operator is defined as $\Psi[x[n]] = x[n]^2 - x[n+1]x[n-1]$, where de $x[n]$ is a time series at sample n. Rest sEMG signals used for the Kaiser energy operator threshold-based were extracted while standing and analyzed for 500 ms.

The STFT provides time-localized frequency information when frequency components of a signal vary over time (Jeon et al., 2020; Karthick et al., 2016). The discrete-time form of the STFT was defined as $X_{(m,\omega)} = \sum_{n=-\infty}^{\infty} x[n]\, w[n - mR]\; e^{-j\omega n}$. The STFT was evaluated at sample time m, $x[n]$ was each sEMG burst time-series at sample time n, $w[n]$ was a rectangular window function, and R was the hop size that determines the amount of overlap. The window length used were 50, 100, 250, 500, and 1000 ms. The overlap, R, was 0, 25, 50, 75, and 90% (Figure 11). Although there are many options for selecting the shape of the window function, we

used a rectangular one as a fixed and controlled experimental factor. The effect of the window type on myoelectric manifestations of fatigue is outside the scope of our study, and these limitations have been addressed in a previous publication (Tan et al., 2019). Finally, as $X_{(m,\omega)}$ is a complex quantity, the assessment of fatigue was performed using the STFT's magnitude $|X_{(m,\omega)}|$ (Karthick et al., 2016). As a result, a Fourier transformation was determined for each contraction burst, which allowed the extraction of median, mean, and peak frequencies (frequency features) from each spectrum varying the length of $w[n]$ and R, see Figure 9.

The three frequency features combined with the five window lengths and the five overlaps resulted in 75 time series containing a variation of the median, mean, and peak frequencies obtained from each sEMG burst (Figure 11). We applied a linear regression to estimate the rate of change in frequency (Hz s^{-1}) during the motor task (Horita et al., 1987; Priego-Quesada et al., 2019), see Figure 11. From the same 75 time series, the coefficient of variation, defined as the ratio between standard deviation and mean and expressed as a percentage, was obtained for each frequency feature.

To find the window length and overlap that minimizes the over- and sub-estimation (outliers) of the coefficient of variation and frequency slope, we estimated the centroid of the plane formed by the ratio between the frequency slopes and the coefficient of variation. This ratio reflects the capability to estimate the variation of a frequency feature over time normalized by its dispersion. The centroid was the sum of the dot product between the ratio of the frequency slope/ coefficient of variation and the factor level (1, 2, 3, 4, or 5), divided by the total sum of the ratio of the frequency slope/ coefficient of variation, expressed as the number of window and overlap (Jordanic et al., 2016).

Finally, to understand the sensitivity to the task failure for all combinations of window length and overlap, we obtained curve patterns from the relationship between the frequency slope and the number of heel rise repetitions until task failure. These patterns were fitted using the non-linear least squared method with the model $y = a\,e^{bx} + c\,e^{dx}$, where y is the frequency slope for each combination of window length, overlap, and frequency features (a total of 75 models), x is the number of repetitions until task failure for each participant, and *a*, *b*, *c*, and *d* are model parameters (Merletti et al., 1990). Hence, one curve was fitted for each combination of window length, overlap, and frequency features. Therefore, if a heterogeneous curve pattern for all

combinations exists, there will be only one pattern. In contrast, if different patterns exist, different combinations would produce different patterns from the same sample.

All computations were performed using Matlab 2020a (Matworks Inc., USA) and its signal processing toolbox, including the functions fft, next2power, filtfit, and butter. We also used basic math functions like image, surf, abs, linspace, median, fix, size, find, sum, polyfit, std, mean, repmat, and exp. The non-linear fitting was made through the curve fitting tool available on the app Matlab screen to perform the non-linear model previously described.

3.2.6. Non-linear dimensionality reduction and clustering

We performed a non-linear dimensionality reduction to capture the latent data characteristics using the UMAP algorithm (McInnes et al., 2018). It determined the pattern from the relationship between the frequency slope and the heel-rise repetitions until failure for all parameters, features, and participants. The UMAP approximates a high-dimensional dataset (all relationships between the slope and the number of heel rise repetitions until failure) by a low-dimensional dataset (a projection of the raw data from a Riemannian manifold to a space of the Real numbers, which we could easily refers as the UMAP domain) by creating a fuzzy topological structure using the gradient of the binary cross-entropy as the loss function. The weights are the probability of the existence of 0-simplex (lowest dimensional connection) or 1-simplex, which is a topographic representation of the connection between neighbors (McInnes et al., 2018). The weight between neighbors was modeled as $w = e^{-d(x_i - x_j) - \rho_i / \sigma}$, being ρ_i the distance from i-th data points to its first nearest neighbor (Oskolkov 2019). The binary cross-entropy was modeled as $\sum_{je \in E} \left[w_h(e) \log \left(\frac{W_h(e)}{W_l(e)} \right) + (1 - w_h(e)) \log \left(\frac{1 - W_h(e)}{1 - W_l(e)} \right) \right]$. The input to UMAP was the set of 75 patterns, each one represented by the fitted curve evaluated for x between 1 and 88, that is a time series that involved a dimension of 88 heel rises until task failure. The algorithm reduced these 75 curves of dimension 88 into 75 points of dimension 3 into the UMAP domain. The parameters used for the UMAP algorithm were: Euclidean metric, number of neighbors set to 7, learning rate set to 1, local connectivity set to 1, repulsion strength set to 1, and minimal distance equal 0.5 (Meehan et al., 2020).

DBSCAN was used after the dimensionality reduction steps described in the above paragraph. Each DBSCAN cluster represents a set of STFT parameters that produces a similar muscle fatigue model performed in the UMAP domain grouping dataset based on the density of the space. Then, we determined the clusters or families of parameters related to its capacity to identify muscle fatigue and labeled the families of the pattern (clusters). The parameter for DBSCAN was an epsilon set to 5. Finally, the mean of the data was used to summarize the behavior for each cluster. The estimations were obtained using the Matlab software 2020a (Mathworks, Inc., USA).

3.2.7. Outcomes

The study outcomes were the frequency slope (Hz s^{-1}) and the coefficient of variability (%) for the 75 possible combinations of STFT parameters, the number of heel-rise repetitions to failure, the clusters of STFT parameters (label of the cluster), and the patterns obtained from the relationship between the frequency slope and task failure (Hz s^{-1} no. of repetitions^{-1}).

3.2.8. Statistic analysis

Results are described as mean, standard deviation, percentage, proportions, and coefficients. The Shapiro-Wilk test confirmed the normality of data distribution. Homoscedasticity and sphericity assumptions were confirmed using the Bartlett and Mauchly tests, respectively. To determine the within and between groups effects and interactions, we conducted a two-way ANOVA with five levels for window length (50, 100, 250, 500, and 1000 ms), and five levels for overlap (0, 25, 50, 75, and 90%) with a Tukey post-hoc test, considering a significance level set at .05. The proportion between myoelectric manifestations for each cluster was obtained using an adjusted-χ^2 test with confidence of 99%, 10 K samples for Monte Carlo simulation, and 0.5 references of the proportions. To compare proportions, we used the Pearson's-χ^2 test for a contingency table of 3 x 5. All data were analyzed considering a significance level set at .05 using the trial SPSS software (IBM, USA).

3.3. Results

Window length showed a main effect on the frequency slope and the coefficient of variation ($p < 0.001$, Figure 12). The multiple comparisons showed that the smaller window lengths (50, 100, and 250 ms) elicited larger frequency slopes for peak frequency ($p < 0.001$) while larger window lengths (1000 and 500 ms) elicited larger frequency slopes in the median frequency ($p < 0.001$). Similarly, the largest window length (1000 ms) elicited larger frequency slopes for mean frequency ($p < 0.001$). The multiple comparisons showed that the smaller window length (50 and 100 ms) elicited a small coefficient of variation for peak frequency ($p < 0.001$). The larger window lengths (500 and 1000 ms) elicited a smaller coefficient of variation in the median frequency ($p < 0.001$). The smaller window lengths (50, 100, and 250 ms) elicited a smaller coefficient of variance for mean frequency ($p < 0.001$).

Overlap showed a main effect for the coefficient of variation ($p < 0.001$, Figure 12), but no effect was found for the frequency slope ($p = 0.1584$). The multiple comparisons showed that the smaller overlap (0%) elicited a smaller coefficient of variation for peak frequency ($p < 0.001$). The overlap of 25% elicited a small coefficient of variation for peak frequency ($p < 0.001$). The smaller overlap (0%) elicited a smaller coefficient of variation for mean frequency ($p < 0.001$). Interaction between window length and overlap was found for the coefficient of variation ($p < 0.001$) and frequency slope ($p < 0.001$).

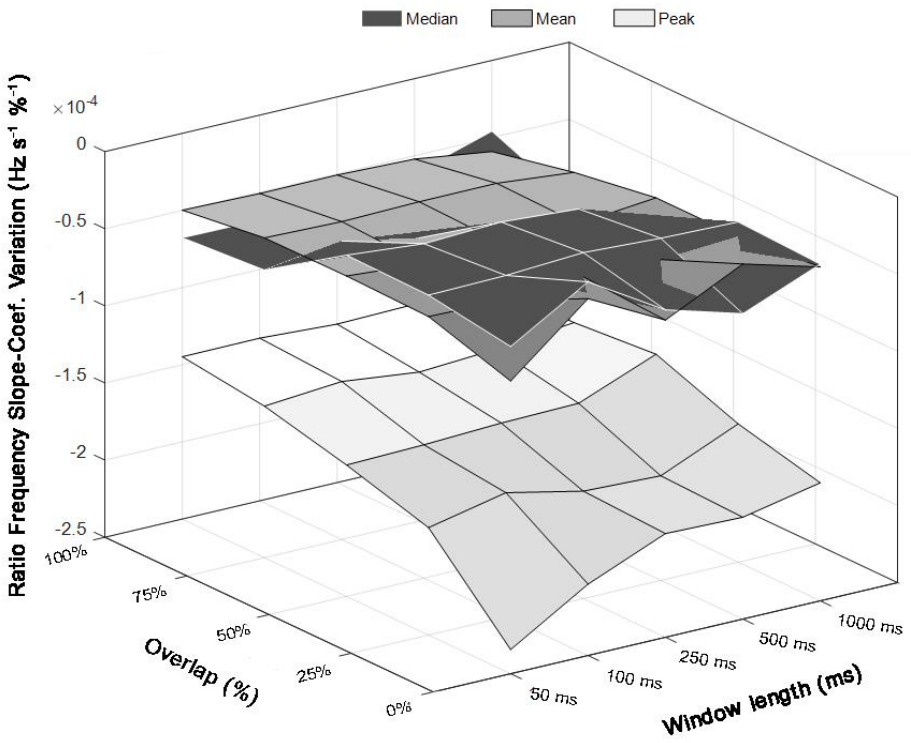

Figure 12. STFT parameters behavior during the heel-rise test. The figure shows how the frequency slope obtained by linear regression and normalized respect for its dispersion behaves regarding the window length and overlap for the mean, median, and peak frequency. Main effects for window length ($p < 0.0001$), overlap ($p < 0.0001$), and interaction between have existed ($p < 0.0001$). The lowest value was found for the combination of 50 ms and overlap of 0% using the peak frequency, and the centroid for the three planes is located at 250 ms with 50% of overlap. For the same motor task performed until exhaustion, different manifestations of muscle fatigue depending on STFT parameters existed.

A 50 ms window length without overlap (0%) resulted in the minimal value for the plane ‘frequency slope - coefficient of variation’ (Figure 12). A 250 ms window length and a 50% overlap were the nearest parameters to the location of the centroids for the plane ‘frequency slope - coefficient of variation’ (Table 4).

Task failure occurred after 39.6 ± 13.3 heel-rise repetitions (median 45; range 18 to 63 repetitions). The *R*-squares for the relationship between the frequency slope and the number of heel rise repetitions until failure are summarized in Table 5. There were 5 clusters of STFT parameters detected by DBSCAN in the UMAP domain (Figure 13 and Table 5). The bigger cluster that includes higher slope frequencies was found for the fifth cluster (Figure 11 and Table 5). The frequency features corresponding to each cluster are described in Table 6. The relationship between the frequency slope and task failure patterns is summarized in Figure 13.

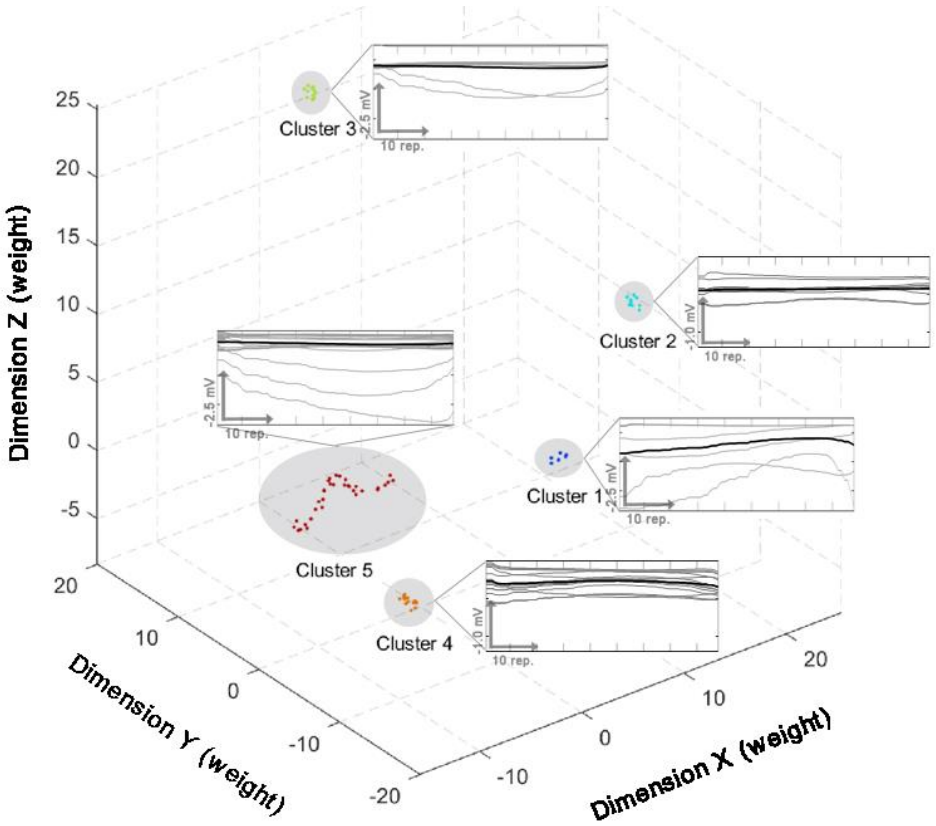

Figure 13. Non-linear dimensionality reduction and clustering for the relationship between slope frequency and task failure (number of maximal heel rises obtained by the sample). The figure shows the projection of the UMAP algorithm into a tridimensional domain measured in weights. The dots indicate the projected families of STFT parameters, and the gray ellipsoid shadow delimits the recognized cluster by DBSCAN algorithm. Each dot cluster is expanded, showing the pattern of sensitivity to task failure as graphs; the black line of these graphs illustrates the cluster's mean pattern.

Table 4. Centroids localization in the coefficient of variation – slope frequency plane.

	(Windows coordinate, Overlap coordinate)
Median frequency	(3.39, 3.03)
Mean frequency	(3.09, 2.96)
Peak frequency	(2.79, 2.92)

Table 5. Proportions of window and overlap combinations found in the 5 clusters and their goodness-of-fit statistics.

Cluster	**Cluster 1**	**Cluster 2**	**Cluster 3**	**Cluster 4**	**Cluster 5**
Median frequency	28% (7/25)	36% (9/25)	36% (9/25)	0% (0/25)	0% (0/25)
Mean frequency	0% (0/25)	0% (0/25)	12% (3/25)	52% (13/25)	36% (9/25)
Peak frequency	0% (0/25)	0% (0/25)	0% (0/25)	0% (0/25)	100% (25/25)
Total	**9.3% (7/75)**	**12% (9/75)**	**16% (12/75)**	**17.3% (13/75)**	**45.3% (34/75)**
Adjusted- χ^2	**p<0.001**	**p<0.001**	**p<0.001**	**p<0.001**	**p<0.001**
Person- χ^2 : p<0.001					
Goodness-of-fit:	**Cluster 1**	**Cluster 2**	**Cluster 3**	**Cluster 4**	**Cluster 5**
R-square	0.57 ± 0.28	0.51 ± 0.25	0.36 ± 0.22	0.38 ± 0.25	0.46 ± 0.24

Table 6. Family parameters.

	Median frequency				
	50 ms	100 ms	250 ms	500 ms	1000 ms
90%	3	3	3	3	3
75%	3	3	3	3	3
50%	2	2	2	2	2
25%	1	1	2	2	2
0%	1	1	1	1	1
	Mean frequency				
	50 ms	100 ms	250 ms	500 ms	1000 ms
90%	5	5	5	5	5
75%	4	5	5	5	5
50%	4	4	4	4	4
25%	4	4	4	4	4
0%	3	3	3	4	4
	Peak frequency				
	50 ms	100 ms	250 ms	500 ms	1000 ms
90%	5	5	5	5	5
75%	5	5	5	5	5
50%	5	5	5	5	5
25%	5	5	5	5	5
0%	5	5	5	5	5

3.4. Discussion

We showed that STFT parameters selection affects the frequency slope of myoelectrical manifestations of fatigue estimated from the median, mean, and peak frequencies recorded from gastrocnemius medialis. This, in turn, affects the sensitivity of muscle fatigue estimation. The window length and overlap directly influenced the relationship between slope frequency and task failure, distorting different myoelectrical manifestations of muscle fatigue depending on the parameters selected for the STFT.

The endurance capacity varied among the participants, most likely due to different levels of neuromuscular adaptations to fatigue between the individuals (Walton et al., 2002). An early or delayed task failure may depend on participant tolerance to fatigue. This helps to understand the different sensitivity patterns for the relationship between slope frequency and

task failure. In particular, the fitted series in each cluster with different frequency slopes and dispersion demonstrates how the STFT parameters change the frequency manifestation of muscle fatigue. For instance, some clusters show a higher electrical frequency slope for an earlier task failure, such as cluster 1 shows. This cluster appears to be physiologically consistent with individuals with poor tolerance to fatigue (higher electrical frequency slope for an earlier task failure) and with an individual with better tolerance to fatigue (negative frequency slope but lower for a delayed task failure). But, the pattern was not observed in all clusters. For example, cluster 5 showed a lower frequency slope for an earlier task failure in comparison with delayed task failure, but this cluster achieved the highest slope frequencies between the clusters. This suggests that STFT parameters may introduce non-linear distortion in the electrical manifestation of fatigue.

Here, we found that a window length of 50 ms with 0% overlap of the peak frequency resulted in a higher frequency slope. However, it is essential to consider that a small window length elicits a high risk of overestimating muscle fatigue when the peak frequency is used. In contrast, large-length windows had the opposing effect. This confusion may result from noise (outliers) that increase the dispersion and affect the regression outcomes. Hence, we recommended treating the outliers before applying the regression, especially for the peak frequency. If it is decided to use the mean and median frequencies extracted from raw signals highly sampled, a decision of the band for analysis should be considered because the mean and median are sensitive to a right displacement in a right-skewness distribution of frequencies losing sensitivity to muscle fatigue. STFT parameters may easily influence frequency slopes, but it is worth mentioning that the frequency slope per se does not reflect the entire fatigue process (L. Wang et al., 2018; Ament et al., 1993; Horita et al., 1987; González-Izal et al., 2010). Frequency slopes mainly reflect the global electrophysiological processes accompanying the generation of fatigue, which depends on central and peripheral motor unit properties. However, these properties may be hidden by synthetic assumptions, such as we showed here affect the frequency slope. Moreover, non-physiological phenomena from the target muscle, such as cross-talk and volume conduction, may also influence the frequency slope (Farina et al., 2014). Therefore, the use of the frequency slope as an index of fatigue requires caution.

Fourier methods have been validated to analyze sEMG signals when slow changes exist in the time domain (Farina et al., 2014; Srhoj-Egekher et al., 2011). Nevertheless, some complexities related to muscle fatigue, such as motor unit action potential changes in

morphology, amplitude and/or spatial distribution, can influence spectral analysis (Martinez-Valdes et al., 2020). Indeed, these complexities can affect both time and spectrum domain characteristics (Rampichini et al., 2020), which may lead to misinterpretation of the physiological phenomenon due to fixed resolution problems (Cifrek et al., 2009; Srhoj-Egekher et al., 2011; Singh et al., 2017). In these cases, wavelets are suggested by its adaptative time-frequency resolution (Costa et al., 2010). However, Fourier decomposition methods generating a set of a small number of bands derived from empirical decomposition mode have been proposed as a better method for non-linear behavior than STFT or wavelet method (Singh et al., 2017). Nevertheless, more in-depth work is required to understand and develop better techniques that might help dynamic muscle fatigue.

When we compared window lengths of 50 ms, 100 ms, and 250 ms, the largest slopes were found when the peak frequency was considered. In contrast, the mean and median frequencies generated the highest frequency slope, with windows of 500 ms and 1000 ms. This suggests a negative covariance between the frequency components and the number of heel-rise repetitions, explaining the largest negative frequency slope obtained after the linear regression analysis (Cifrek et al., 2009). An improper parameter definition may result in statistical bias. For instance, the statistical type I error is induced when contractions are not performed to fatigue, and a negative frequency slope is found (Krzywinski et al., 2013). On the other hand, considering that the median and mean frequencies show small frequency slopes, this could be associated with an underestimation, resulting in a higher probability of statistical type II error (Krzywinski et al., 2013).

The largest dispersion found for the peak frequency agrees with a previous report (Srhoj-Egekher et al., 2011) and expressed a large spread of data concerning the mean and median frequencies. This behavior also means that the sum of squares is large. Therefore, to avoid the statistical type II error when the peak frequency is used, a larger number of samples is needed compared to the mean and median frequencies (Krzywinski et al., 2013). Peak frequency may be affected by a small number of samples despite its better capacity to generate a more negative frequency slope, as found herein.

Larger overlaps increased the dispersion of data for peak and mean frequencies. Median and peak frequencies showed similar behavior, except for the 0% overlap showing the highest dispersion. As we discussed for selecting window length, we need to be careful with the sample size to avoid statistical type II error due to increased data dispersion (Krzywinski et al., 2013). Finally, the centroid method used here tends to smooth small or large values in

the intensity-dispersion plane, acting as a low-pass filter. However, this does not guarantee the best sensitivity to predict task failure, and therefore, a more conservative selection of parameters could be considered (250 ms with 50% overlap).

We acknowledge the limitation of windowing and overlapping being set only in a forward manner. Another limitation was our incapacity to consider metabolic markers of peripheral fatigue to estimate fatigue intensity and correlate them with different stationary parameters from the sEMG signals.

3.5. Conclusion

In conclusion, 50 ms without overlap using peak frequency provides the highest frequency slope but generates a large dispersion of data. Instead, 250 ms with 50% of overlap for the mean, median, and peak frequency reduces the data dispersion but decreases the frequency slope during dynamic contractions. Therefore, we recommend that the selection of STFT parameters during dynamic contractions be accompanied by a mechanical measure of task failure. The parameters should be adjusted according to the experiment's requirements.

4 CHAPTER FOUR – BIASED INSTANTANEOUS REGIONAL MUSCLE ACTIVATION MAPS: EMBEDDED FUZZY TOPOLOGY AND IMAGE FEATURES ANALYSIS

Published as:

De la Fuente, C., Weinstein, A., Neira, A., Valencia, O., Cruz-Montecinos, C., Silvestre, R., Pincheira, P. A., Palma, F., & Carpes, F. P. (2022). Biased instantaneous regional muscle activation maps: Embedded fuzzy topology and image feature analysis. Frontiers in Bioengineering and Biotechnology, 10, 934041.
https://doi.org/10.3389/fbioe.2022.934041

ABSTRACT

The instantaneous spatial representation of the electrical propagation produced by the muscle contraction may introduce bias in the sEMG activation maps. Here, we described the effect of instantaneous spatial representation (sEMG segmentation) on embedded fuzzy topological polyhedrons and image features extracted from sEMG activation maps. We analyzed 73,008 topographic sEMG activation maps from seven healthy participants (age 21.4 ± 1.5 years and body mass 74.5 ± 8.5 kg) who performed submaximal isometric plantar flexions with 64 surface electrodes placed over the Medial Gastrocnemius muscle. Windows lengths of 50, 100, 150, 250, 500, and 1000 ms and overlap of 0, 25, 50, 75, and 90% to change the sEMG map generation were tested in a factorial design (grid search). Shannon entropy and volume of global embedded tri-dimensional geometries (polyhedron projections), and Shannon entropy, location of the center (LoC), and image moments of maps were analyzed. The polyhedron volume increased when the overlap was <25% and >75%. Entropy decreases when overlap was <25% and >75%, and when window length was <100 ms and >500 ms. The LoC in the x-axis, entropy, and the histogram moments of maps showed effects for overlap ($p<0.001$), while LoC in the y-axis and entropy showed effects for both overlap and window length ($p<0.001$). In conclusion, the instantaneous sEMG maps are first affected by outer parameters of overlap followed by the length of the window. Thus, choosing window length and overlap parameters can introduce bias in sEMG activation maps, resulting in distorted regional muscle activation.

Keywords: sEMG, data science, dimension reduction, HD-sEMG.

4.1 Introduction

Physical therapists, biomechanists, and engineers regularly infer (quantitative or qualitative interpretation) neuromuscular adaptations from sEMG activation maps (Merletti et al., 2020; Vieira et al., 2011; Campanini et al., 2020). sEMG activation map represents the discrete distribution of the voltage propagation elicited from the train sum of motor unit action potentials (MUAPs) collected from an array of electrodes on the skin (Merletti et al., 2020; Botter et al., 2015; Guzmán-Venegas et al., 2015; Jordanić et al., 2017; Merletti et al., 2019; Vigotsky et al., 2017; Ghaderi et al., 2017). Thus, multiple electrodes allow for obtaining sEMG activation maps that can be interpreted as images (Jordanić et al., 2017; Merletti et al, 2019), similar to brain activation (Beniczky and Schomer 2020) or uterus electromyogram (Xu et al. 2022). Each map pixel corresponds to the voltage acquired by each electrode. Thus, the map can be defined by $\mathrm{I_{i,j,t}} = \sqrt{\frac{1}{\mathrm{N-1}} \sum_{\mathrm{k=1}}^{\mathrm{N}} (\mathrm{sEMG[nT]_{i,j}\, w[n - mR])_k^2}}$. The $\mathrm{I_{i,j,t}}$ is the pixel intensity that represents the magnitude of the muscle activity located at (i,j), t is the number of maps obtained after windowing, $\mathrm{sEMG[nT]_{i,j}}$ is the sEMG signal located in the array, w[n] is window or epoch, N is the length of the w[n], and R is the hop size that determines the amount of overlap.

Traditionally, sEMG activation maps quantification involves feature extraction, where the location of the center (LoC or barycenter) and Shannon entropy are the most used (Guzmán-Venegas et al, 2015). The LoC is defined by $\mathrm{LoC} = \frac{\sum_{\mathrm{i,j}} \mathrm{I_{i,j}} \begin{bmatrix} \mathrm{i} \\ \mathrm{j} \end{bmatrix}}{\sum_{\mathrm{i,j}} \mathrm{I_{i,j}}}$ (Jordanic et al. 2016; Pincheira et al. 2020). Meanwhile, the entropy that explores homogeneity is defined by $\mathrm{E} = -\sum_{\mathrm{k=1}}^{\mathrm{N}} \mathrm{p(k)^2 \log_2 p(k)^2}$. The $\mathrm{p(k)^2}$ is the probability of the square of the root mean square value at electrode k (Farina et al., 2008). In addition, image moments (expected value, variance, skewness, and kurtosis) also can describe image changes in the spatial time domain.

On the other hand, several conditions might introduce undesired dispersion and noise. Therefore, capturing latent map data might be convenient for understanding how synthetic distortions are introduced. The latent data, which retains lower-dimension information that explains higher-dimension data, has been optimized through the Uniform Manifold Approximation and Projection (UMAP) algorithm (Ali et al., 2019; McInnes et al, 2018; Oskolkov 2019). UMAP projects a fuzzy topological set of high dimensions equivalent to

low-dimensional data (Ali et al., 2019; McInnes et al, 2018). The approximation is possible by creating fuzzy topological projections with binary cross-entropy and projections (McInnes, Healy, and Melville 2018). The binary cross-entropy is modeled by $\sum_{je \in E}\left[w_h(e)\ \log\frac{W_h(e)}{W_l(e)} + (1 - w_h(e))\ \log(\frac{1-W_h(e)}{1-W_l(e)})\right]$, while the weight between neighbors is modeled by $w = e^{-d(x_i - x_j) - \rho_i / \sigma}$. The ρ_i is the distance from the *i*-th data points to its first nearest neighbor (Oskolkov 2019). The first term ensures fuzzy connectivity (simplex or node connections). In contrast, the second term not permitting the creation of simplexes (McInnes, Healy, and Melville 2018). Hence, UMAP might allow the topological representation of different sEMG maps (high dimensions) resulting from N and R parameters.

Previously, sEMG segmentation influenced the electrical manifestation of fatigue conclusions (De la Fuente et al., 2021). Since sEMG activation maps depend inherently on the segmentation, it is expected alterations in the sEMG activation map. However, there is still large variability in choosing windows length, i.e., 50 ms, 100 ms, 150 ms, 250 ms, 500 ms, or 1000 ms (Botter et al, 2015; Falla et al., 2017; Hegyi et al., 2019; Martinez-Valdes et al., 2018; Vinti et al., 2018; Watanabe et al., 2018; Guzmán-Venegas et al., 2015; Zhu et al., 2017; Jordanić et al., 2017; Jordanic et al., 2016), and truncation methods (non-overlapping (Falla et al., 2017; Guzmán-Venegas, Biotti et al, 2015; Jordanić et al., 2017)). Therefore, understanding how segmentation may distort regional muscle activation is still a concern. Here, we aimed to describe the effect of instantaneous spatial representation (sEMG segmentation) on embedded fuzzy topological polyhedrons and image features extracted from the sEMG activation maps obtained with HD-sEMG on healthy participants performing a submaximal isometric contraction of Medial Gastrocnemius.

4.2 **Materials and Methods**

4.2.1 Study design

We conducted a factorial experiment to test 30 signal processing conditions (Figure 14). The sample included 73,008 sEMG activation maps obtained from seven healthy participants (aged 21.4 ± 1.5 years, body mass 74.5 ± 8.5 kg, height 1.77 ± 0.01 m, and body

mass index 20.9 ± 2.2 kg/m^2) who performed a submaximal isometric plantar flexion with the ankle at neutral position (60% with the ankle in a 90º position) in a controlled lab set-up (Figure 14). Here, we considered the Medial Gastrocnemius muscle as a good muscle model due to its interest in clinics and biomechanics as well as in previous studies addressing the sEMG segmentation (De la Fuente et al., 2021; Theisen et al., 2016). The Bioethics Committee of the Andes University (Santiago, Chile) approved this study (# INV-IN201701), which was developed according to the principles of the Declaration of Helsinki. All participants signed a consent term agreeing to participate in this study.

4.2.2. Data

Seventy-three thousand eight sEMG activation maps were included in the study (data are available in the supplementary material). They were the result of 39 experiments of a total of 42 (6 trials x 7 participants). Three experiments were excluded due to artifacts. These 39 experiments contained 10,240 samples x 64 channels. The 73,008 sEMG activation maps resulted in combining 1,872 maps and 39 experiments. The 1,872 maps resulted from 30 conditions, that is, window lengths (50, 100, 150, 250, 500, and 1000 ms) combined with an overlap (0%, 25%, 50%, 75%, and 90%) without repetition. This combination resulted in 100, 136, 199, 423, and 1014 maps (Pincheira et al. 2021).

4.2.3 Experimental set-up

Participants were lying prone on a bench with their hip, knee, and ankle in a neutral joint position. The ankle of the participants was tightly strapped into a customized rigid structure (Figure 14). Then, they were asked to perform three maximal voluntary isometric contractions against a force transducer placed at metatarsal head level (Revere Transducers®, 9363-B10-500-20T1R, USA). Each attempt lasted five seconds, with a three-minute rest period between repetitions (period of non-contraction to recover basal muscle energy conditions). Immediately, the participants were asked to perform the submaximal voluntary contraction. The contractions were sustained for 20 s, and the duration of the

ascending/descending ramps was 6s and 8s for the hold phase. The participants received real-time visual feedback displaying a trapezoid target (Figure 14). The participants completed six trials.

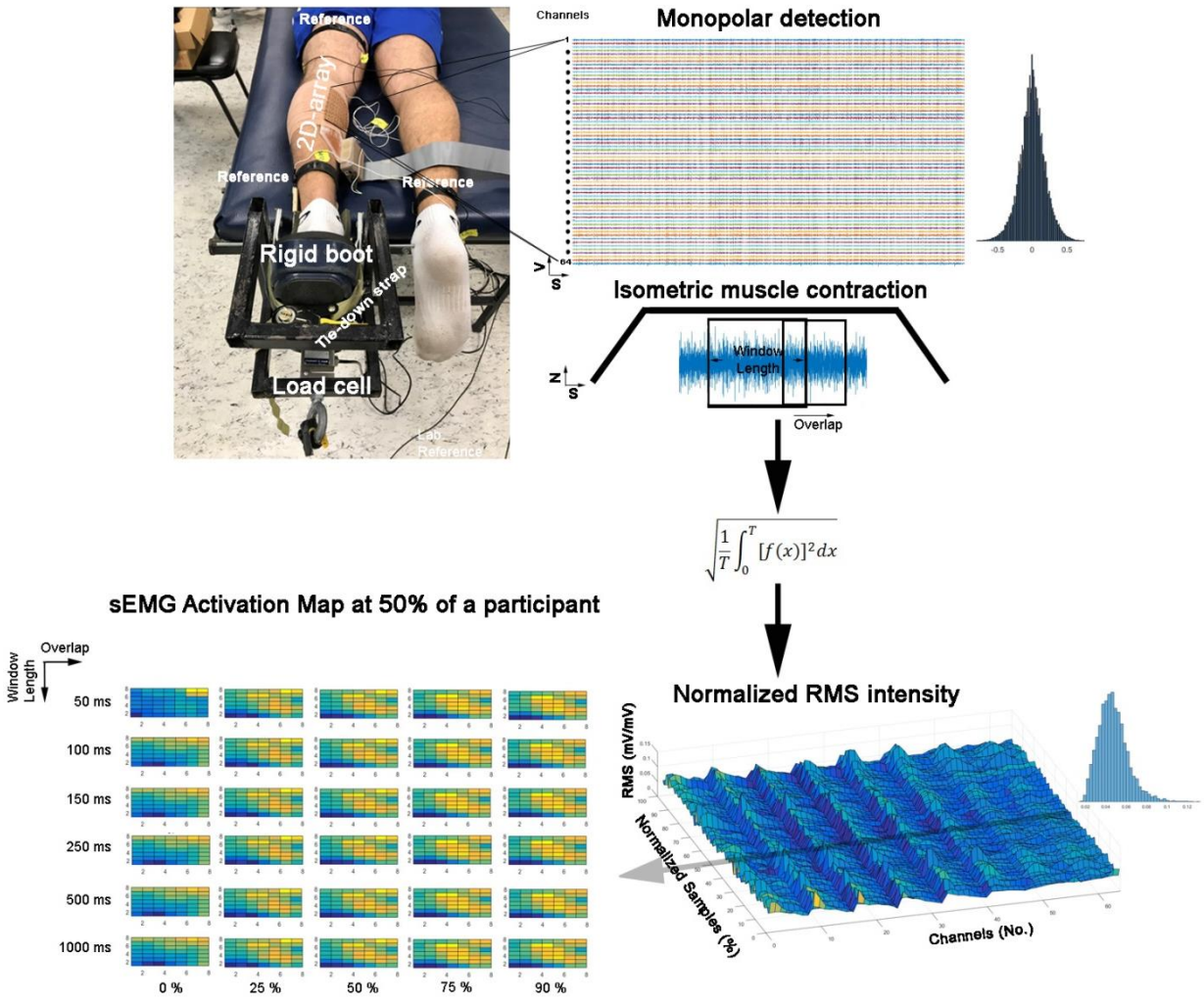

Figure 14. Experiment set-up and instantaneous surface Electromyographic map generation flow. Colors represent the instantaneous potential amplitude distribution (yellow indicates more intensity, and blue is the lower intensity).

4.2.4 Electrode location and data acquisition

Prior to data acquisition, the skin was shaved, abrased (Everi: Spes Medica s.r.l, Battipagglia, Italy), and cleaned with alcohol to diminish the skin impedance. Then, a semi-disposable adhesive with 64 electrodes organized in 8 rows and 8 columns of 1 mm diameter and an inter-electrode distance of 10 mm was attached (GR10MM0808, OT Bioelettronica, Torino, Italy)(Pincheira et al., 2021). The electrode spaces were filled with a conductive cream (Spes Medica s.r.l., Italy) (Pincheira et al., 2021).

The electrode was placed over the most prominent region of the Medial Gastrocnemius, and the muscle belly was determined by palpation during a resisted plantar flexion. Then, the electrode was aligned in the cephalocaudal axis with respect to the line formed between the medial femoral condyle and malleolus. For the mediolateral axis, the electrode was aligned with respect to the medial contour of the medial gastrocnemius muscle. The superomedial electrode corner was fixed at 30% of the distance of the cephalocaudal axis, as was described previously (Pincheira et al., 2021).

Sixty-four monopolar sEMG signals were collected from electrodes, amplified with a gain of 200, and digitized at a sampling frequency of 2048 Hz with a 12-bit resolution and 3dB bandwidth 10–500 Hz (sEMG-USB2: OTBiolettronica, Turin, Italy). The reference electrodes were positioned according to Pincheira et al. (Pincheira et al., 2021) over the contralateral ankle and superior to the electrode near the popliteal fossa (Pincheira et al., 2021). Two additional reference electrodes were placed on the tibial tuberosity and the fibula to improve the sEMG signal-to-noise ratio. Once the quality of the signals was assured, the electrodes were firmly secured with an elastic adhesive bandage (Figure 14).

Correct electrode placement was confirmed by assessing sEMG signals online for low baseline noise levels and possible artifacts, cortocircuit, or bad contact during visual inspection during brief plantar-flexion contractions (Pincheira et al., 2021). The signal was evaluated at rest (without contraction) and under contraction (Pincheira et al., 2021). Non-saturated signal and out-of-power line interference were appreciated during the acquisition (Pincheira et al., 2021). Nevertheless, three experiments were excluded during the offline signal processing after observing in the time and frequency domain. The domains showed increased noise.

4.2.5 Pre-processing

The sEMG signals were mean-centered to zero and segmented at the force plateau signal. Then, the signals were filtered by a zero-lag second-order Butterworth with a Bandpass of 20 to 400 Hz. Outlier channels were manually identified and confirmed using the Z-score. A mean with 1 pixel of radio was assigned for outlier pixels (<0.01% was assigned) from channels with confirmed higher Z-scores. Afterward, the sEMG signals were convolved with a rectangular window. Our convolved sEMG signals were arranged in a matrix 8x8, and the maps were normalized to the maximum value of the whole matrixes during the plateau (Figure 14).

4.2.6 Window length and overlap (intervention)

The window lengths were chosen based on previous reports (Falla et al., 2017; Guzmán-Venegas et al., 2015; Hegyi et al., 2019; Jordanic et al., 2016; Jordanić et al., 2017; Martinez-Valdes et al., 2018; Watanabe et al., 2018; Zhu et al., 2017). The overlap parameters were 0, 25, 50, 75, and 90% resulting in 30 different combinations between window length and overlap were $\{(50,0), (50,25), \dots, (1000,75), (1000,90)\}$ to introduce variability to the sEMG activation maps to study its effects.

4.2.7 UMAP and feature image extraction

The sEMG activation maps of each condition of all participants were concatenated [73,008 x 64] and introduced to UMAP algorithm version 1.4.1 (Meehan et al., 2020). The global structure of high-dimensional data (64 dimensions) was embedded into three-dimensional data (McInnes 2018; McInnes et al., 2018). The number of neighbors was 10, the min distance was 0.7, the number of components was three dimensions, the metric was Euclidean, the number of epochs was 200, the learning rate was 1, local connectivity was 1, repulsion strength was 1, the spread was 1, the fuzzy set operation was 1, and the negative sample rate was 5. After assessing the level of connectivity and homogeneity of the structures, we created a 3d polyhedron (finite elements) to obtain their volume and Shannon entropy. In

addition, we extracted the image features from sEMG activation maps; LoC, Shannon entropy, and image moment (expected value –moment 1-, variance –moment 2-, skewness –moment 3-, and kurtosis –moment 4-) (Brown et al., 2011).

4.2.8 Variables

The following continuous variables were determined; 1) Volume of the fuzzy topological structure obtained from the embedded data set and normalized to a maximum value, 2) Entropy of the fuzzy topological structure from the embedded data set obtained as Shannon entropy (Farina et al., 2008), 3) LoC obtained from the sEMG activation map in both x and y coordinates (Jordanić et al., 2017), 4) Shannon entropy obtained from the sEMG activation maps (Farina et al., 2008), 5) Moment-1 of maps obtained from sEMG activation map as expected value (Brown et al., 2011), 6) Moment-2 of maps obtained from the sEMG activation map as variance (Brown et al., 2011), 7) Moment-3 of maps obtained from the sEMG activation map as skewness (Brown et al., 2011), and 8) Moment-4 of maps obtained from the sEMG activation map as kurtosis (Brown et al., 2011).

4.2.9 Data Analysis

The sEMG activation maps were described as expected values and variance. Normality and homoscedasticity assumptions were checked prior to the image analysis feature using a two-way ANOVA 2x5x6 (2 factors: window length and overlap, 6 levels of the length of windows: 50 ms, 100 ms, 150 ms, 250 ms, 500 ms, and 1000 ms, and 5 levels of sliding: 0%, 25%, 50%, 75%, and 90%) for main effects. Effect sizes were described as the square sum of effect divided by the total sum of squares to show the explained variance (small: $\eta^2 <$ 0.04 (< 4%), medium: between 0.04 (4%) and 0.64 (64%), and large: > 0.64 (64%) (Ferguson 2009)). The Tukey–Kramer test was used to find differences between groups. The K-medoids algorithm was applied to explore the differences between factors. The number of clusters with K-medoids was evaluated as the sum of the ratio between the sum of within Euclidean distance and Euclidean distance of each point with their medoid found. Then, the elbow method before convergence was chosen. The alpha error was equal to 0.05 for all statistics.

The volume and entropy behavior were studied by a non-linear least square method, and Fuzzy sEMG polyhedrons were described in the UMAP space. The zero crossing of the fitted curve was described. All calculus was made through Matlab software (MathWorks, Inc., USA).

4.3 Results

The polyhedron volume increased when the overlap was <25% and >75%. Entropy decreased when the overlap was <25% and >75%, and when window length was <100 ms and >500 ms. The polyhedron volume R^2 was 73.5% and 16.9% for overlap and windows length, respectively. The polyhedron entropy R^2 was 90.1% and <1% for overlap and windows length, respectively. The polyhedron zero crossing for volume in overlap was at 25%, and between 75% and 90%. The polyhedron zero crossing for entropy in overlap was between 25% and 50%, and between 75% and 90%. Non-zero crossings were found for windows length. Figure 15 summarizes the volume and entropy behavior of embedded sEMG activation maps.

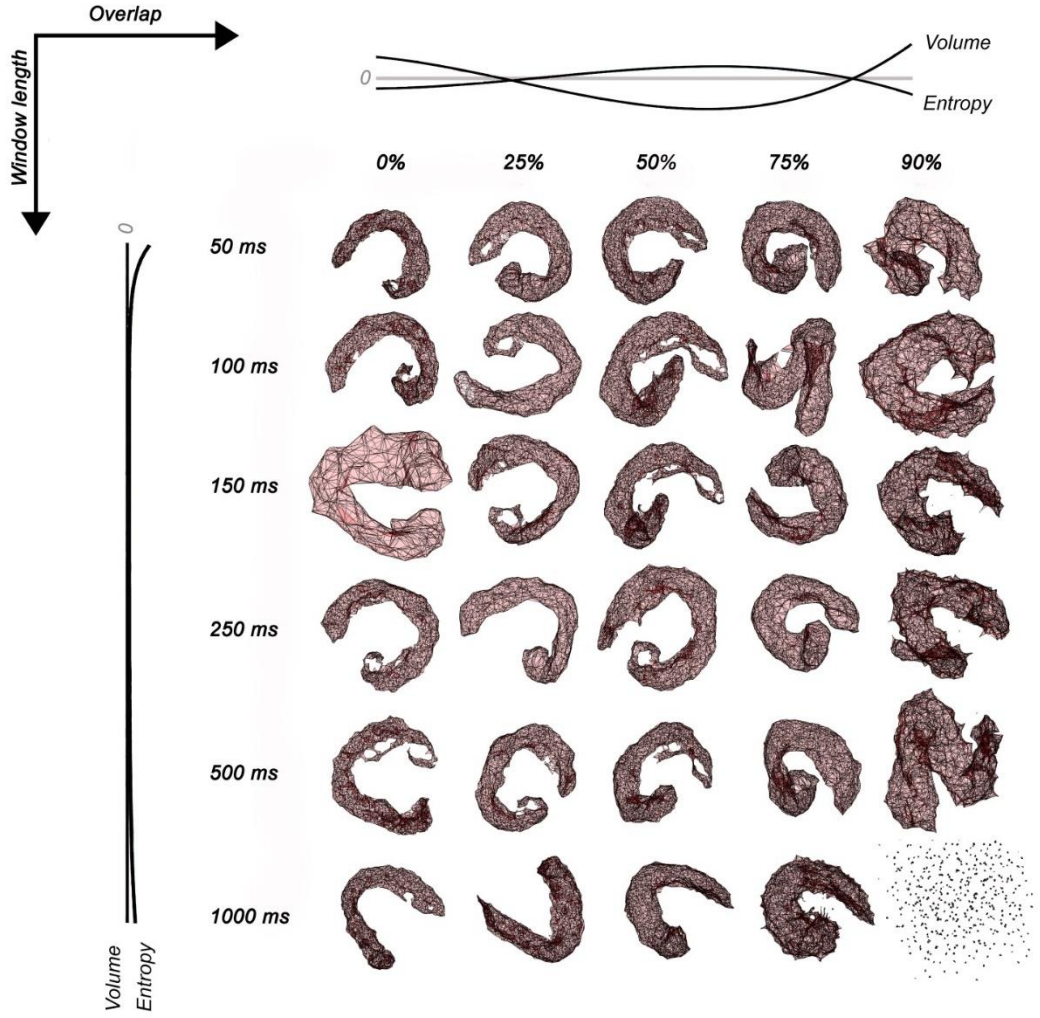

Figure 15. sEMG maps embedded in three dimensions for 30 conditions of signal processing varying window length (50 ms, 100 ms, 150 ms, 250 ms, 500 ms, and 1000 ms) and overlap (0, 25, 50, 75, and 90%). The normalized no-linear fitting for Shannon Entropy and Volume of sEMG polyhedrons are also shown in dark lines.

Map LoC_x (Table 7) showed a main effect both overlap ($p < 0.001$, $\eta^2 = 0.998$, large effect size) and window length ($\eta 2 < 0.04$, small effect size), and there was interaction ($p < 0.001$, $\eta^2 < 0.04$, small effect size). Overlap showed differences between all multiple comparisons ($p < 0.001$). Window length showed multicomparison differences between 50 ms and all widow lengths ($p < 0.001$). Data were grouped into 5 clusters with centroids: 3.2 mm, 7.7 mm, 16.4 mm, 24.1 mm, and 32.8 mm. Map LoC_y (Table 7) showed only a main effect for overlap ($p < 0.001$, $\eta^2 = 0.998$, large effect size). There were multiple comparison differences

between all overlaps ($p < 0.001$), and data were grouped into 6 clusters with centroids: 3.5 mm, 8.2 mm, 17.6 mm, 25.9 mm, 34.5 mm, and 35.9 mm.

Map entropy (Table 7) showed a main effect both overlap ($p < 0.001$, $\eta^2 = 0.998$, large effect size) and window length ($p < 0.001$, $\eta^2 < 0.04$, small effect size) and there was interaction ($p < 0.001$, $\eta^2 < 0.04$, small effect size). There were multiple comparison differences between 50 ms and all widow lengths ($p < 0.001$). Data were grouped into 5 clusters with centroids: 1.8 d.u., 2.4 d.u., 2.9 d.u., 3.0 d.u., and 4.3 d.u..

Map moment-1 (Table 7) showed a main effect for window length ($p < 0.001$, $\eta^2 < 0.04$, small effect size). There were differences between 50 ms and 1000 ms ($p = 0.036$), 50 ms and 150 ms ($p = 0.004$), 50 ms and 250 ms ($p = 0.001$), 50 ms and 500 ms ($p = 0.001$), and 50 ms and 1000 ms ($p < 0.004$). Data were grouped into 5 clusters with centroids: 0.06 d.u., 0.09 d.u., 0.13 d.u., 0.18 d.u., and 0.24 d.u.. Map moment-2 (Table 7) showed a main effect for window length ($p < 0.001$, $\eta^2 < 0.04$, small effect size). There were differences between 50 ms and all window lengths ($p < 0.001$). Data were grouped into 1 cluster. Map moment-3 (Table 7) showed a main effect for window length ($p < 0.001$, $\eta^2 < 0.04$, small effect size). There were differences between 50 ms and all window lengths ($p < 0.001$), 100 ms and 150 ms ($p = 0.005$), and 100 ms and the rest of the window lengths ($p < 0.001$). Data were grouped into 1 cluster. Map moment-4 (Table 7) showed a main effect for window length ($p < 0.001$, $\eta^2 < 0.04$, small effect size). There were differences between 50 ms and the rest of window lengths ($p < 0.001$), 100 ms and 250 ms ($p = 0.006$), and 100 ms 500 ms ($p < 0.001$), and 100 ms and 1000 ms ($p < 0.001$), and 150 ms and 1000 ms ($p = 0.017$). Data were grouped into 1 cluster.

Table 7. Topographical sEMG maps outcomes.

	50 ms	100 ms	150 ms	250 ms	500 ms	1000 ms
LoCx, m.m.						
0%	33 (0.013)	33 (0.013)	33 (0.010)	33 (0.010)	33 (0.010)	33 (0.010)
25%	24 (0.007)	24 (0.006)	24 (0.005)	24 (0.005)	24 (0.005)	24 (0.005)
50%	16 (0.003)	16 (0.003)	16 (0.002)	16 (0.002)	16 (0.002)	16 (0.002)
75%	08 (7.4e-4)	08 (5.7e-4)	08 (5.4e-4)	08 (5.2e-4)	08 (5.2e-4)	08 (5.1e-4)
90%	03 (1.2e-4)	03 (9.7e-5)	03 (9.2e-5)	03 (8.9e-5)	03 (8.7e-5)	03 (8.7e-5)
LoCy, m.m.						
0%	35 (0.012)	35 (0.010)	35 (0.010)	35 (0.010)	35 (0.009)	35 (0.009)
25%	26 (0.007)	26 (0.005)	26 (0.005)	26 (0.005)	26 (0.005)	26 (0.005)
50%	18 (0.003)	18 (0.003)	18 (0.002)	18 (0.002)	18 (0.002)	18 (0.002)
75%	08 (6.6e-4)	08 (5.5e-4)	08 (5.2e-4)	08 (5.0e-4)	08 (5.0e-4)	08 (4.9e-4)
90%	03 (1.2e-4)	03 (9.4e-5)	03 (8.9e-5)	03 (8.6e-5)	03 (8.5e-5)	03 (8.4e-5)
Entropy, d.u.						
0%	3.11 (0.012)	3.11 (0.012)	3.12 (0.012)	3.11 (0.012)	3.11 (0.012)	3.11 (0.023)
25%	3.11 (0.012)	3.11 (0.012)	3.11 (0.012)	3.11 (0.012)	3.11 (0.012)	3.11 (0.012)
50%	3.11 (0.012)	3.11 (0.012)	3.11 (0.012)	3.11 (0.012)	3.11 (0.012)	3.11 (0.012)
75%	3.11 (0.009)	3.11 (0.009)	3.11 (0.009)	3.11 (0.009)	3.11 (0.009)	3.11 (0.009)
90%	2.97 (7.1e-4)	2.97 (7.1e-4)	2.97 (5.1e-4)	2.97 (4.8e-4)	2.98 (4.6e-4)	2.98 (4.7e-4)
Moment-1, d.u.						
0%	0.126 (0.004)	0.128 (0.004)	0.128 (0.004)	0.128 (0.004)	0.128 (0.004)	0.129 (0.004)
25%	0.126 (0.004)	0.128 (0.004)	0.128 (0.004)	0.128 (0.004)	0.128 (0.004)	0.129 (0.004)
50%	0.126 (0.004)	0.128 (0.004)	0.128 (0.004)	0.128 (0.004)	0.128 (0.004)	0.129 (0.004)
75%	0.126 (0.004)	0.128 (0.004)	0.128 (0.004)	0.128 (0.004)	0.128 (0.004)	0.129 (0.004)
90%	0.126 (0.004)	0.128 (0.004)	0.128 (0.004)	0.128 (0.004)	0.128 (0.004)	0.129 (0.004)
Moment-2 x 10^{-5}, d.u.						
0%	2.14 (8.84e-11)	1.04 (3.71e-11)	1.03 (3.45e-11)	1.03 (3.25e-11)	1.03 (3.20e-11)	1.03 (3.19e-11)
25%	1.89 (8.00e-11)	1.33 (4.77e-11)	1.33 (4.60e-11)	1.33 (4.43e-11)	1.33 (4.39e-11)	1.33 (4.38e-11)
50%	2.14 (8.84e-11)	1.28 (4.33e-11)	1.28 (3.91e-11)	1.28 (3.78e-11)	1.28 (3.73e-11)	1.28 (3.72e-11)
75%	2.24 (7.84e-11)	1.33 (3.99e-11)	1.33 (3.58e-11)	1.33 (3.44e-11)	1.33 (3.40e-11)	1.33 (3.39e-11)
90%	2.33 (7.95e-11)	1.33 (3.99e-11)	1.33 (3.57e-11)	1.33 (3.43e-11)	1.33 (3.39e-11)	1.33 (3.38e-11)
Moment-3, d.u.						
0%	-0.01 (0.41)	0.03 (0.42)	0.04 (0.41)	0.05 (0.41)	0.05 (0.41)	0.05 (0.41)
25%	-0.01(0.41)	0.03 (0.43)	0.05 (0.43)	0.05 (0.43)	0.06 (0.42)	0.06 (0.42)
50%	0.00 (0.42)	0.03 (0.42)	0.05 (0.41)	0.05 (0.42)	0.06 (0.41)	0.06 (0.41)
75%	0.00 (0.43)	0.03 (0.42)	0.05 (0.42)	0.05 (0.42)	0.06 (0.41)	0.06 (0.41)
90%	0.00 (0.43)	0.03 (0.42)	0.06 (0.42)	0.06 (0.41)	0.06 (0.41)	0.06 (0.41)
Moment-4, d.u.						
0%	2.47 (0.80)	2.52 (0.82)	2.52 (0.83)	2.53 (0.83)	2.54 (0.85)	2.55 (0.85)
25%	2.46 (0.82)	2.49 (0.79)	2.50 (0.82)	2.52 (0.83)	2.52 (0.83)	2.52 (0.83)
50%	2.48 (0.80)	2.51 (0.80)	2.52 (0.82)	2.53 (0.82)	2.54 (0.83)	2.54 (0.83)
75%	2.47 (0.79)	2.50 (0.79)	2.51 (0.81)	2.52 (0.81)	2.53 (0.82)	2.53 (0.81)
90%	2.47 (0.79)	2.50 (0.80)	2.51 (0.81)	2.52 (0.81)	2.53 (0.82)	2.53 (0.82)

d.u. = dimensionless unit.
Data are expressed as the expected value (E[x]) of the histogram and variance of the expected value ($E[x - E[x]]^2$).

4.4 Discussion

sEMG segmentation parameters (overlap and window length) of activation maps introduce bias, resulting in distorted regional muscle activation, compromising the map inferences. For example, we can conclude about regional sEMG activation with or without clear regional sEMG activation when there were not, e.g., the statistical error types (Akobeng 2016). The topological dimensional reduction and feature extraction of the sEMG maps confirmed it. Outer segmentation parameters tested here have caused the highest distortion in the activation maps; independently, no-overlap and small window length trends reduce the

activation map region, while large overlap and window length trends increase the activation map region. Thus, sEMG map generation can modify the spatial myoelectrical activity and should be carefully considered by their physiological and clinical repercussions, i.e., wrong rehabilitation or performance planning. Furthermore, many clinical and sport science studies did not fully consider it in the past, and there is high variability in the choice of segmentation parameters (Botter a et al, 2015; Guzmán-Venegas et al, 2015; Jordanić et al. 2017; Jordanic et al., 2016; Falla et al., 2017; Hegyi et al., 2019; Martinez-Valdes et al., 2018; Vinti et al., 2018; Watanabe et al., 2018; Zhu et al., 2017) as well as truncation use (Guzmán-Venegas et al, 2015; Jordanić et al., 2017; Falla et al., 2017; Stadler et al., 2007).

The high dimensional sEMG maps embedded into a low dimensional dataset were studied through their entropy and volume. These variables permitted an understanding of three regions of activation. Overlap showed an increased volume and decreased entropy at outer parameters (two regions) and increased entropy with low volume at central parameters (one region). Widow length showed decreased entropy at outer parameters (two regions) and higher entropy at central parameters (one region), while the volume trended to be constant. The entropy of sEMG polyhedrons quantified the geometrical heterogeneity of the embedding data (Franch et al., 2019), which represents the chance to order the fuzzy nodes projected from the RMS of MUAPs spatially distributed in our study. Thus, the decreased entropy shows a most regular geometry (homogeneity) due to decreased local connectivity (McInnes et al, 2018; Sánchez-Rico et al, 2019), which occurred with a large volume suggesting more distance between nodes (less similar RMS of MUAPs). Consequently, there was less chance to order the fuzzy nodes projected from the RMS of MUAPs. This last distorted muscle activation suggests two scenarios occurred in the outer parameters; an attenuated map for small overlap and windows length, where there was a more significant proportion of low RMS of MUAPs (blue pixels; please visualize the sEMG maps of Figure 14), and blurred map for large overlap and window length, where there was a more significant proportion of high RMS of MUAPs (yellow pixels; please visualize the sEMG maps of Figure 14).

On the other hand, an increased entropy shows a most irregular geometry (heterogeneity) due to increased local connectivity (McInnes et al, 2018; McInnes 2018; Sánchez-Rico et al, 2019), which occurred with a small volume suggesting a lower distance between nodes (more similar RMS of MUAPs). Central parameters with higher entropy and lower volume were found near 50% overlap, while for window length, higher entropy and lower volume were found between 100 ms and 500 ms. A case of the total loss of connectivity

was found for 1000 ms, and 90% of overlap in coherence with findings in genes studies using UMAP (Dorrity et al. 2020).

Regarding the extracted features from sEMG activation maps, the LoCx, LoCy, and entropy confirmed a main distorted effect of the overlap on maps. The clustering analysis permitted decomposing data in coherence with the multiple comparison results. For y-coordinates, six clusters were found, suggesting that overlap 0% had two centroids, meaning that there were two sub-groups of 50 ms. For x-coordinates and entropy, 5 clusters were found in coherence with overlapping. Regarding the window length, only the x-coordinate and entropy showed differences (small effect size). In consequence, the 50 ms without overlap generated the most dissimilar sEMG map. These findings agree with discontinuities that can be introduced by small window lengths and the artifacts caused without window sliding (Yip et al., 2017). This last issue is caused by the truncation ringing (Gibbs artifact), where small windowing abruptly magnifies intensity changes like a high pass filter (Stadler et al., 2007). Thus, overlapping and small windowing can be an essential source to create a synthetic bias on the sEMG activity, distorting the MUAPs visualization techniques (Vigotsky et al., 2017; Stadler et al. 2007).

Finally, the image moments changed the sEMG activation maps but with a small effect size. This change suggests a lower sensitivity of image moments to detect biased sEMG maps compared to UMAP, LoC, and entropy of map features. The main limitation of the current study was the sEMG available grid used, which is related to the level of spatial resolution of the sEMG intensity maps. The space aliasing was set according to our available electrode (inter-electrode distance of 10 mm). The standards acquisition of sEMG map indicates a relatively acceptable use of 10 mm and sampling frequency in space higher than 200 samples/m (Merletti et al, 2020; Merletti et al, 2019). Also, the maximal spatial sampling may be appreciated using 90% of the spatial power density distribution on the x-axis, y-axis, or both (Afsharipour et al, 2019). However, electrodes lower or equal to 8 mm would obtain better spatial resolution. Although there are many options for selecting the shape of the window function, we used a rectangular one as a fixed and controlled experimental factor. Here, the effect of the window type on myoelectric manifestations is outside the scope of our study, and these limitations have been addressed in a previous publication (Tan et al, 2019). The pinnate architecture of Medial Gastrocnemius limits our results only for this kind of muscle.

4.5 Conclusion

In conclusion, embedded sEMG maps and features of image extraction change the spatial muscle activation by segmentation parameters. The instantaneous sEMG maps were primarily affected by outer parameters of overlap, followed by the outer parameters of window length. Consequently, choosing window length and overlap parameters can introduce bias in sEMG activation maps, resulting in distorted regional muscle activation.

5 CHAPTER FIVE – DISTAL OVERACTIVATION OF GASTROCNEMIUS MEDIALIS IN PERSISTENT PLANTARFLEXION WEAKNESS FOLLOWING ACHILLES TENDON REPAIR

Published as:

De la Fuente, C., Martinez-Valdes, E., da Rocha, E. S., Geremia, J. M., Vaz, M. A., & Carpes, F. P. (2023). Distal overactivation of gastrocnemius medialis in persistent plantarflexion weakness following Achilles tendon repair. Journal of Biomechanics, 148, 111459. https://doi.org/10.1016/j.jbiomech.2023.111459

ABSTRACT

Structural alterations of the triceps surae and Achilles tendon (AT) can promote plantarflexion weakness one-year following an AT repair, influencing the activation strategies of the Gastrocnemius Medialis (GM) muscle. However, this is yet to be demonstrated. We aimed to determine whether patients with plantar flexion weakness one-year after AT repair show altered GM spatial activation. In this cross-sectional and case-control study, ten middle-aged men (age 34 ± 7 years old, and 12.9 ± 1.1 months post-surgery) with a high AT total rupture score who attended conventional physiotherapy for six months after surgery, and ten healthy control men (age 28 ± 9 years old), performed maximal and submaximal (40, 60 and 90%) voluntary isometric plantarflexion contractions on a dynamometer. The peak plantar flexor torque was determined by isokinetic dynamometry and the GM neuromuscular activation was measured with a linear surface-electromyography (sEMG) array. Overall, sEMG activation (averaged channels) increased when the muscle contraction levels increased for both groups. sEMG spatial analysis in AT repaired group showed an increased activation located distally at 85%-99%, 75%-97%, and 79%-97% of the electrode array length for 40%, 60%, and 90% of the maximal voluntary isometric contractions, respectively. In conclusion, patients with persistent plantar flexion weakness after AT rupture showed higher distal overactivation in GM.

Keywords: Strength, Muscle, Tendon tear, Triceps Surae, sEMG.

5.1 Introduction

Achilles tendon (AT) rupture develops in 11 to 37 cases per 100,000 inhabitants-year affecting mainly men (De la Fuente et al., 2021). The mechanical properties of the AT are not recovered even two years post-repair (Geremia et al., 2015), and patients show persistent plantar flexion weakness (De la Fuente et al., 2021; Finni et al., 2006), reduced concentric plantar flexion work during gait (Wenning et al., 2021), impaired heel-rise performance (Brorsson et al., 2017), compensatory knee and ankle movements during running (Jandacka et al., 2017), and unbalanced torque contribution between deep and superficial plantar flexors ((Finni et al., 2006).

The persistent weakness in these patients may result from structural adaptation, including a reduced Gastrocnemius Medialis (GM) fascicle length (Hullfish et al, 2019) and cross-sectional area (Zellers et al., 2019; Heikkinen et al., 2017), and a more lengthened tendon (Suydam et al., 2015; Stäudle et al., 2022). In addition, there are potential neural adaptations due to changes in motor unit firing properties compensating for increases in GM muscle fatty infiltration (Heikkinen et al., 2017), which trigger the ubiquitin-proteasome-mediated autophagy and proteolysis of the muscle fibers (Hamrick et al, 2016). Thus, impairments in GM activation can be observed (Hullfish et al, 2019).

GM activation following an AT rupture is debatable. Although AT rupture patients show GM hypotrophy and drastic changes in the myotendinous junction architecture (Stäudle et al., 2022) previous studies have not found altered activation during tasks demanding strong and fast contractions (Zellers et al., 2019; Peng et al., 2019), while others found lower normalized rates of electromyographic rise and lower rates of force development (Wang et al., 2013). In contrast, higher GM activation was found in AT rupture patients performing bilateral hopping (Oda et al., 2017) as well as during push-off in gait (Wenning et al., 2021), and in motor actions where the AT is lengthened (Suydam et al., 2015). In addition, the different normalization methods and parameters considering overall activation using bipolar configurations and not addressing the spatial distribution of the activation among the studies difficult the interpretation of sEMG patterns (Cronin et al., 2015).

The GM activation may present a physiological spatial distribution of the sEMG signal amplitude. Previously, it was discussed when a more distal activation was observed during isometric plantar flexion with an extended knee, but a more proximal redistribution was found with a flexed knee (Avancini et al., 2015). While performing heel-rises, larger distal

activation of the GM was observed for a more extended knee (Kinugasa et al, 2005), suggesting regional activation may play a role in force/moment generation. However, to the best of our knowledge, there is no information about the GM regional activation in AT patients with persistent plantarflexion weakness assessed using sEMG arrays.

Here, we determine whether patients with persistent plantar flexion weakness one year following AT repair show altered GM activation and spatial sEMG redistribution while performing plantar flexion at different contraction intensities. We hypothesized that AT patients with persistent plantar flexion weakness would show an altered activation pattern in GM during different levels of isometric plantarflexion compared with controls.

5.2 Materials and methods

5.2.1 Study Design

In this cross-sectional, case-control study, participants were middle-aged men recruited from the local community (metropolitan region of Santiago, Chile) one year after percutaneous AT repair, and a paired healthy control group. All participants provided written consent to participate in the study, which was approved by the ethics committee of the local institution (SM Clinic, IRB#032019) and developed following the declaration of Helsinki.

5.2.2 Participants

Non probabilistic sampling method by convenience was used. The experiments included ten middle-aged men with high Achilles tendon rupture score ATRS (Nilsson-Helander et al., 2007), Achilles Dresden repair, one-year after surgery, and submitted to conventional physiotherapy for six months, and ten healthy control men without AT rupture. To be included in the AT repaired group, participants should be i) men between 20 and 45 years old, ii) able to perform single heel-rise movements, iii) have competitive sports practice during weekends (weekend-warrior style), iv) had suffered an acute mid-substance Dresden repair (performed no more than ten days after rupture), iv) with a single lower limb tendon rupture, and vi) with evolution after surgical repair between 11 and 15 months. Participants in the control group were i) men aged between 20 and 45 years old, ii) with the capacity to perform single heel-rise movements, iii) with a history of recreational sports activity during the weekend, and iv) competitive sports practice during weekends (weekend-warrior style).

Participants from both groups could not have i) a history of tendinous injuries (other than the AT injury in the AT group), ii) history of autoimmune diseases, iii) a history of a traumatic lower leg injury, iv) orthopedic alteration of the lower leg, and v) steroid therapy dependence. Exclusion criteria involved the inability to perform the tests, pain or discomfort during measures or the days before, and volunteer absence. No participant was excluded from the study, and we had access to medical records to check that all criteria were met. For all participants, the preferred leg to kick a ball was considered for the assessments. AT patients had a rupture in the preferred leg to kick a ball.

5.2.3 Surgery and rehabilitation

The AT repair was performed using the percutaneous Dresden technique with FiberWire® Suture No. 2.0 (Arthrex Inc., Naples, Fl, USA). The patients followed a conventional rehabilitation program for the first three weeks after surgery, using a rigid boot restricting full weight-bearing but allowing active toe mobilization. At the end of the third-week post-surgery, the skin sutures were removed, and rehabilitation included dynamic plantarflexion exercises. From the fourth to the eighth weeks, patients focused on the active range of motion until zero-degree dorsiflexion and full weight-bearing using a rigid boot with heel edges. The treatment focused on plantarflexion strengthening and dorsal flexion range of motion from the eighth to the twelfth week (De la Fuente et al., 2021). Between the third and sixth months, patients focused on plyometric exercises and stretching, and after the sixth month, they could return to heavy work activities and sports (De la Fuente et al., 2021).

5.2.4 Strength testing

Plantar flexor strength was assessed by peak torque output on an isokinetic dynamometer Humac Norm (Computer Sports Medicine International, USA) sampling data at 100 Hz. We assessed the preferred leg in the healthy participants and the injured leg in the AT-repaired group. The foot of the testing leg was secured to the isokinetic footplate through straps and the medial malleolus of the ankle was aligned to the dynamometer's axis. In the days before the measurements, the participants performed submaximal trials in two sessions of 15 min each for familiarization with the dynamometer (plantarflexion using metatarsal region avoiding using the toes). On the testing day, the best of three measures for the peak

torque was used as the maximal voluntary isometric contraction (MVIC). After a 10 min rest, peak torque was determined for three submaximal plantar flexor contractions at 40%, 60%, and 90% of the MVIC peak torque, selected based on studies showing that single-leg standing, toe standing, and bilateral hopping require moderate to high levels of GM activation (Moritani et al, 1991). The submaximal contractions were ramped with 5 seconds of increase, 10 seconds of the plateau, and 5 seconds of decrease in torque. Real-time visual feedback of the signal torque was provided (Drazan et al, 2019). The ankle was in a neutral position in the sagittal plane, with the knee fully extended in a prone position (De la Fuente et al., 2021; Drazan et al, 2019). This posture was used to test the higher distal activation of the GM (Avancini et al., 2015). A 10 min rest period was allowed between the submaximal contractions, and the order of contraction intensity was randomized for each participant.

5.2.5 sEMG data collection

sEMG signals were recorded using a multi-channel linear sEMG sensor consisting of a linear array of sixteen Ag/AgCl electrodes of size 5 mm × 1 mm with 10 mm of inter-electrode distance (OT Bioelettronica, Torino, Italy). sEMG signals were acquired by a multi-channel sEMG amplifier (sEMG-USB2+, OT Bioelettronica, Torino, Italy) set in a single-differential derivation (Avancini et al., 2015). The common-mode rejection ratio was higher than 95 dB, the input impedance was higher than 10^{11} Ω, and the gain factor was 1000 to ensure an adequate signal-to-noise ratio without saturation. The total noise was lower than $1\mu V_{RMS}$, and the analog band-pass filter was set with a cut-off frequency between 10 and 500 Hz. An analog-digital converter of 12-bit sampled the sEMG signals at 2048 Hz. The reference electrode was located at the ankle medial malleolus level using a wet strap (Avancini et al., 2015). The reference circuitry that permitted the best signal acquisition combined a reference line of the patient connected to the dynamometer and the patient's table.

Before the data collection, we determined the location and orientation of the GM muscle fibers using linear ultrasonography (US) of 12 MHz (InnoSight®, Phillips, USA). The array positioning over the GM considered the distal end of the muscle's superficial aponeurosis, which was identified using ultrasound imaging and marked on the skin (Vieira et al., 2011). The array was attached proximally at the middle level of the popliteal fossa and orientated over GM when the examiner was able to see the more parallel fibers (Figure 16). To ensure good alignment of the electrode array to the muscle fibers, we rotated the array over the skin between -5º (clockwise) and +5º (anti-clockwise) to find the adequate parallel

orientation by doing a visual inspection of US images (Figure 16). The skin was shaved and cleaned with an abrasive paste and alcohol before the electrode placement. The electrodes were moistened with water, and the sensor was attached to the skin with hypoallergenic tape (Figure 16). The quality of the signals (electric interferences and contact problems) was visually inspected before data acquisition.

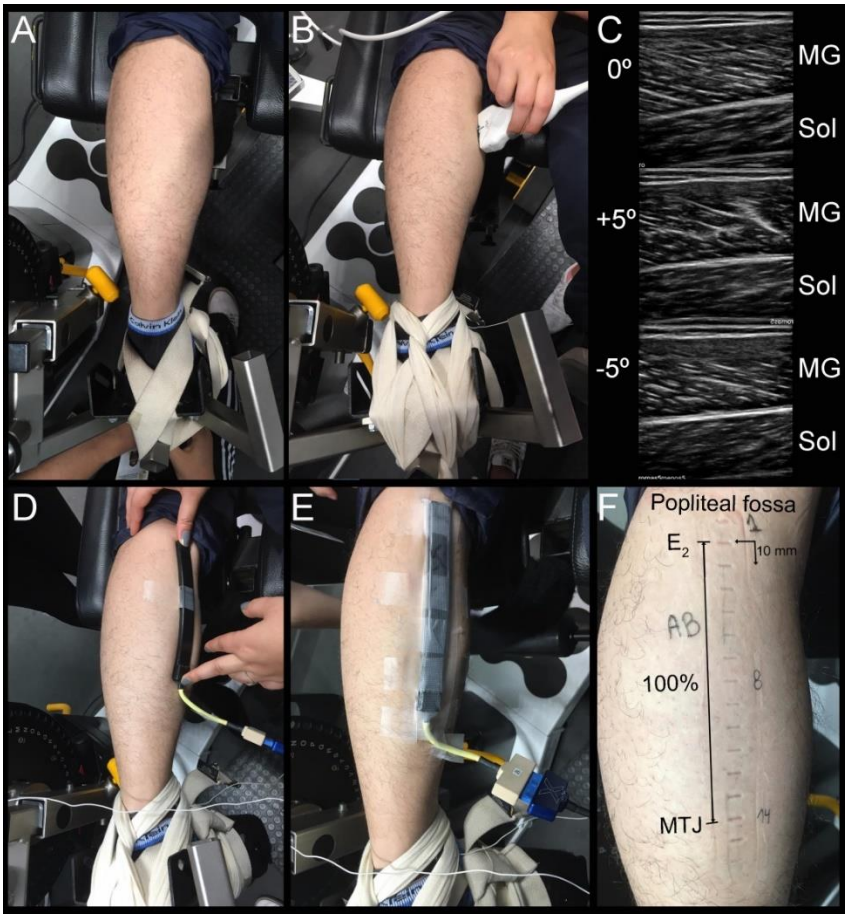

Figure 16. Set-up for data collection. A. Participant is positioned on the isokinetic dynamometer. B. Ultrasonography exploration for appropriate fiber alignment with the probe. C. Confirmation of the electrode positioning parallel to the fiber orientation assessed using ultrasonography (0º of probe rotation). D. Electrode linear array positioning. E. Attachment of the linear array. F. Spatial normalization and electrodes exclusion.

5.2.6 Time-domain sEMG parameters

All sEMG signals were zero-mean centered and filtered with a second-order band-pass digital Butterworth filter with a cut-off frequency between 10 Hz and 450 Hz. The first electrode was placed proximal to the tendon end, and the last electrode was placed proximal to the myotendinous junction, were excluded from the analysis. The remaining 14 electrodes were used for spatial normalization considering the array length (0% to 100%, where 100% length is the most distal part of the array, Figure 14F). Regarding the analysis, only the plateau phase of the muscle contraction task was considered. The overall sEMG amplitudes that represented GM activation were determined using the root mean square (RMS) of the merged sEMG signals (averaged channels) obtained from the averaged time series. The windowing was made with an epoch of 250 ms and 100 ms of overlap to obtain a matrix of $\{RMS_1^T \ldots RMS_n^T\}_{n*t}$ where n is samples and t is time. This matrix was normalized to the average sEMG basal activation of the array with an epoch of 100 ms during rest (the basal 100% was subtracted from the overall sEMG, obtaining data below 100% for better reading). Each time series of the matrix was interpolated, and the matrix was averaged to obtain a mean topographic group representation of the sEMG activation.

A differentiated topographic map between the repaired AT and control groups was obtained to determine GM's activation heterogeneity. Clustering was applied in the submaximal plantar flexion contractions at 40, 60, and 90% of the MVIC with the *k*-means algorithm. The *k*-means split the data in *k*-centroids based on the average distances between samples as a measure of similarity according to amplitude data (grouping samples). The centroids are originated randomly in the space of features until they converge in locations where the metrics of distance are minimized between the sample of one cluster and another. For this study, the *k*-number of clusters was defined based on the highest silhouette coefficient assessed from two up to twenty possible regional *k*-clusters. Hence, the *k*-centroids obtained from the sEMG activation map are described.

5.2.7 Outcomes

Outcomes were the peak plantar flexion torque, which represented the plantar flexor strength measured in Nm and Nm/kg, the sEMG activation of GM, which was obtained from the normalized merged sEMG signals and measured in $\mu V*\mu V^{-1}*100\%$, and the regional GM activation, which represented a normalized activation between the groups across a normalized length between subjects and measured in $\mu V*\mu V^{-1}*100\%$. Positive values indicate higher

activation in the repaired AT group, and negative values indicate higher activation in the control group. The regional thresholds of GM asymmetry activation represented a topographical region of heterogeneity activation, measured in percentage.

5.2.8 Statistical Analysis

Data were reported as topographic maps and mean ± standard deviation (normal distribution) or median [min-max] (non-parametric distribution) depending on its distribution and homoscedasticity. Data normality and homoscedasticity were checked with Shapiro-Wilk, and Levene's test, respectively. The sphericity principle of data was checked ($\varepsilon = 0.829$). Independent t-test compared groups for regional activations and normalized peak plantar flexion torque, while U-Mann Whitney compared groups for absolute peak plantar flexion torque. A two-way ANOVA for repeated measures (mixed) with factors group (control and AT repaired) and contraction intensity (40%, 60%, and 90%) with sphericity corrections for multiple comparisons was used to identify the independence or not between factors (group and contraction intensity). No interaction was found and the overall sEMG activation was compared between the contractions intensities using a repeated measures ANOVA ($p<0.05$) with Bonferroni post-hoc. Effect sizes (ES) from multiple comparison of one-way ANOVA were estimated as the ratio between mean difference and the square root of whithin mean sum of square (pooled standard). All statistical test were set with an alpha of 5%. The statistical analyses were performed using SPSS 26.0 (IBM, USA).

5.3 Results

The participants included in the AT rupture group were 10 males of age 34 ± 7 years old, height 171.8 ± 5.8 cm, body mass 80 ± 10 kg, body mass index 27.3 ± 2.8 kg/m^2, ATRS 92.5 ± 11.8 pts., and evolution time of 12.9 ± 1.1 months after surgery, all of them submitted to conventional physiotherapy for six months. The healthy control group included 10 males without AT rupture and aged 28 ± 9 years old, height 171.8 ± 5.8 cm, body mass 81 ± 12 kg, body mass index 27.5 ± 3.7 kg/m^2, and ATRS 100 ± 0 pts. There were no differences in age, height, body mass index, and calf circumference between the groups (Table 8).

Plantar flexion torque differences between groups were larger than the minimal detectable change of 12.4-13.0 Nm (Al-Urzi et al., 2016), which confirmed the persistent plantar flexion weakness in the repaired AT patients. Repaired AT patients showed lower absolute (18% lower, $p = 0.015$; $d = 0.107$) and normalized (21% lower, $p = 0.035$; $d = 0.121$) plantar flexion torque (136.3 [106-247] Nm; 1.62 ± 0.28 Nm/kg) than the control group (165.8 [115-155 Nm]; 2.06 ± 0.43 Nm/kg). See Table 8 for more details.

Table 8. Basal characteristics and outcomes of the participants of the study.

	ATRG n=10	**CG n=10**	**Δ**	***p*-value**
Basal characteristics				
Age, median [min - max], years	29.9 [21.0-54.0]	36.7 [20.0-53.0]	6.8	0.593
Height, median [min - max], m	1.72 ± 5.8	1.73 ± 6.1	0.01	0.962
Body mass, mean ± sd, kg	81.3 ± 12.0	83.1 ± 10.9	1.8	0.712
BMI, mean ± sd, kg/m^2	27.5 ± 3.7	27.3 ± 2.8	0.02	0.628
CC in right leg, mean ± sd, cm	39.8 ± 4.8	36.9 ± 2.6	0.0	0.904
CC in left leg, mean ± sd, cm	39.6 ± 5.6	36.8 ± 1.5	2.8†	-
ATRS, median [min - max], points	97 [63-100]	100 [100-100]	3	**0.005**
Persistent weakness				
Peak torque, median [min - max], Nm	136.3 [106-247]	165.8 [115-155]	29.5†	**0.035**
Peak torque, mean ± sd, Nm/kg	1.62 ± 0.28	2.06 ± 0.43	0.44†	**0.015**

† *Clinical importance estimated from the minimal detectable change of 12.4-13.0 Nm according to Al-Uzri et al. (2016),*(Al-Urzi et al., 2016) *of 0.6 cm for calf circumference according to Fong et al.(2009),*(Fong et al. 2010) *and 10 pts for ATRS according to De la Fuente et al. (2016).*(C. I. De la Fuente et al. 2016) *ATGR: Achilles' tendon repaired group; CG: Control group; BMI: Body mass index; CC: Calf circumference; sd: standard deviation.*

GM overall activation (Figure 17A) showed a main effect for group ($p = 0.039$, $\eta^2 = 0.215$) and contraction intensity ($p = 0.001$, $\eta^2 = 0.935$), without interaction between these factors ($p = 0.107$, $\eta^2 = 0.121$). Regarding the contraction intensity factor in the repaired AT group, one-way ANOVA ($p < 0.001$, $\eta^2 = 0.937$) showed higher GM overall activation at 90% of MVIC (84.3 ± 1.5 %) compared to 60% (42.2 ± 4.5 %, Δ = 42.1%, $p < 0.001$, ES = 0.154) and 40% of MVIC (23.1 ± 3.2 %, Δ = 61.2%, $p < 0.001$, ES = 0.224), while at 60% of MVIC (42.2 ± 4.5 %) was higher activation than at 40% of MVIC (23.1 ± 3.2 %, Δ = 19.1%, $p < 0.001$; ES = 0.070). Similar results were found in the control group, there was a higher GM overall activation at 90% of MVIC (71.2 ± 2.9 %) than 60% of MVIC (36.6 ± 2.5 %, Δ = 34.6 %, $p < 0.001$, ES = 0.127) and 40% of MVIC (20.9 ± 2.6 %, Δ = 50.3 %, $p < 0.001$, ES = 0.184), while at at 60% of MVIC (36.6 ± 2.5 %) was higher activation than at 40% of MVIC (20.9 ± 2.6 %, Δ = 15.7 %, $p < 0.001$; ES = 0.057). Figure 17-B describes the regional sEMG

activation distribution across the normalized length (0% to 100%) of the GM obtained in each group.

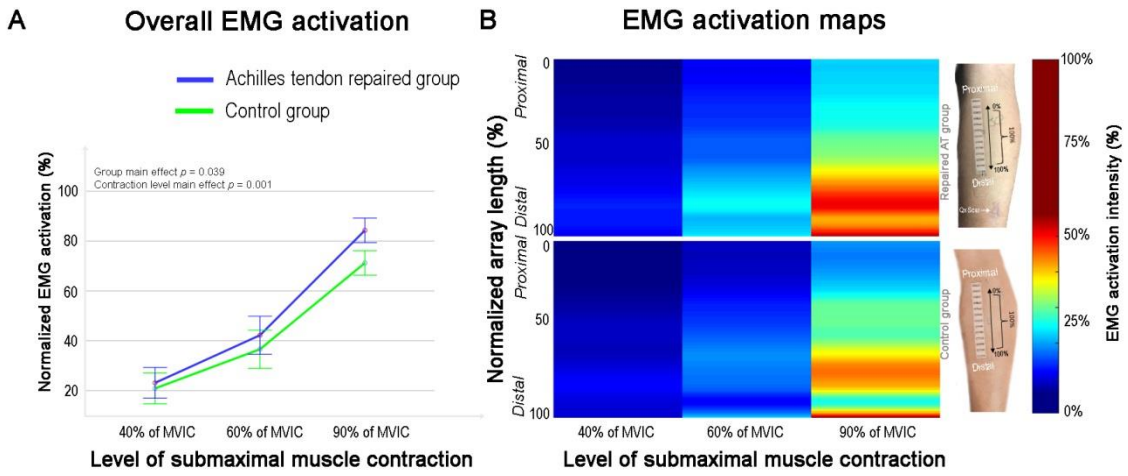

Figure 17. sEMG activation outcomes. A. Differences in overall sEMG activation (averaged channels) between 40%, 60%, and 90% of MVIC intensities of controls (green color) and patients (blue color). For a better interpretation of data, the y-axis normalization was substracted by 100% (basal measurement). B. Regional sEMG activation patterns of both groups. The figure shows three activation maps by the intensity of MVIC and describes the intensity of activation using a color bar (0% in dark blue to 100% in dark red). The maps also show the sEMG activation distribution across the normalized length (0% to 100%) of the GM. AT = Achilles tendon. Qx = surgery.

Figure 18 shows GM clustered regional maps of the differentiated map (AT group map minus control maps) show higher distal activation in the AT repair group. The distal cluster (colored region) was located between 79% and 97% of the electrode array length, between 75% and 97% of the array length, and between 85% and 99% of the array length for 90%, 60%, and 40% of MVIC, respectively (Figure 18). The Silhouette coefficient (0.89) was higher for 2 cluster intensities. Table 9 summarizes the distal and proximal clustering centroids for contractions at 40%, 60%, and 90% of MVIC and their p-values.

Table 9. Comparison of the different identified clusters.

	Cluster 1 (Distal)	Cluster 2 (Proximal)	Δ	*p*-value
sEMG activation at:				
40% of MVIC, median [min - max], %	2.27 [1.54 – 2.93]	0.92 [0.46 – 1.80]	1.35	<0.001
60% of MVIC, median [min - max], %	8.23 [5.26 – 9.38]	2.41 [-0.23 – 4.83]	5.82	<0.001
90% of MVIC, median [min - max], %	12.18 [6.93 – 16.08]	1.84 [-3.88 – 5.68]	10.34†	<0.001

†*Clinical importance estimated from the minimal detectable change of 8.6-9.6 % according to Sanchez-Gomez et al. (2020).*(Sánchez-Gómez et al. 2020) *MVIC: maximal isometric voluntary contraction.*

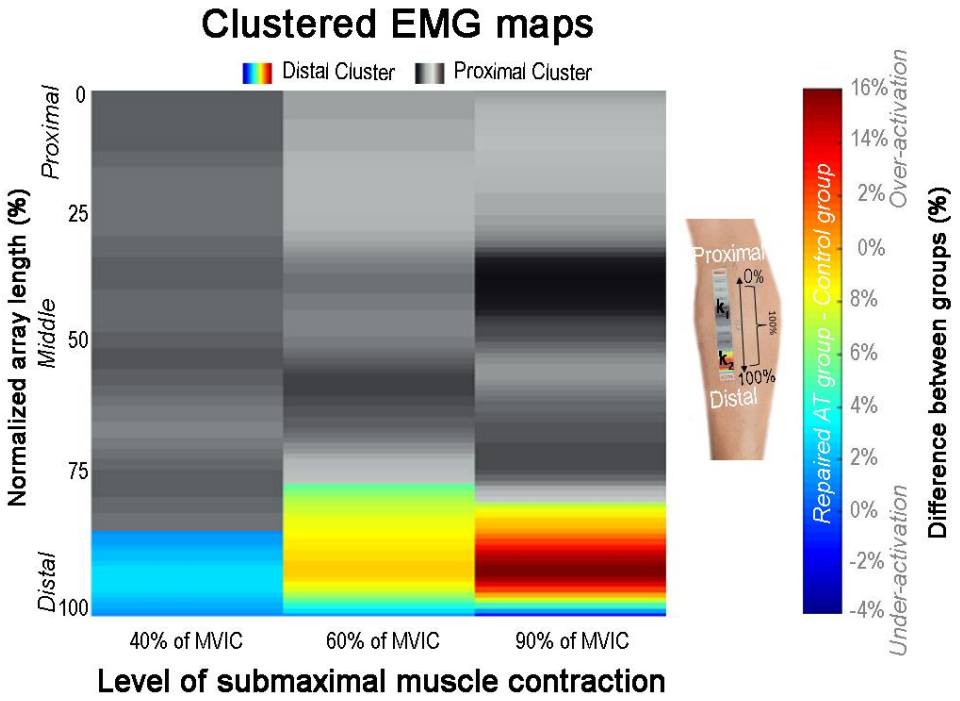

Figure 18. Clustered sEMG maps. The image illustrates the more prominent distal region activation of the gastrocnemius medialis when performing the isometric plantar flexion at three different levels of submaximal muscle contraction obtained using K-means clustering. The topographic limits obtained from the three differentiated regional sEMG intensity maps indicate that patients persist with increased distal activation between 75% and 99% of the array length used. AT = Achilles tendon. K1 = cluster one (proximal). K2 = cluster two (distal).

5.4 Discussion

Our main findings are a) overall sEMG activation (averaged channels) increase when the muscle contraction levels increased for both groups, and b) a distal overactivation of GM in repaired AT patients. GM adapts its activation probably to compensate for injury-induced changes in AT structural/mechanical properties. Muscle weakness is common in AT patients, but the literature reports heterogeneous results (Wenning et al., 2021; Zellers et al., 2019; Suydam et al., 2015; Wang et al., 2013; Peng et al., 2019; Oda et al., 2017) and little is known about its neurophysiological mechanisms. The higher sEMG activation agrees with the altered sEMG activation during functional tasks found for repaired AT patients (Wenning et al., 2021; Oda et al., 2017). In this sense, the higher activation could represent the response to AT lengthening (Suydam et al., 2015), higher distal recruitment to increase the force transmission to the tendon (Geremia et al., 2015), and/or an altered sensorimotor adaptation of the repaired AT (Avancini et al., 2015).

The increased activation may indicate a compensatory neural response to the impaired force-length relationship of the triceps surae (Suydam et al., 2015; McHugh et al., 2019) that shortens more the GM fibers than the soleus in patients with persistent plantarflexion weakness (McHugh et al., 2019). However, a more complacent AT (Geremia et al., 2015) also suggests an increased sEMG activation as a compensatory neural response to lower force transmission. It could be explained as an electromechanical delay (lower temporal efficiency), as found in Achilles tendinopathy, in which the central nervous system adapts to the impaired temporal efficiency of the muscle-tendon unit (Chang et al, 2015).

The Ehlers-Danlos mice model demonstrates that lower active force and higher intensity of electrical stimulation may be required at longer GM lengths (Huijing et al., 2010). However, a better understanding of the human force transmission mechanisms between the tendon, aponeurosis, and subtendons (Magnusson et al., 2003; Finni et al., 2018) needs to be clarified in patients with AT repair. It is also important to note that altered sensorimotor adaptation due to impaired afferent input could alter the sEMG activity of individuals with AT rupture (Avancini et al., 2015; Bressel et al., 2004). Nevertheless, this hypothesis still requires investigation.

We suggest the distal overactivation found in AT patients is a regional adaptation within the GM aiming to increase the plantarflexion strength. The sEMG topographical maps

allowed us to estimate the location of the predominantly activated muscle fibers (Mesin et al, 2011). This capacity is supported by the relationship ($R2 > 0.80$) between the high-density sEMG outcomes and the plantar flexion moment described in simulation studies (Sartori et al, 2017). The estimations of the GM contributing to about half of the total plantarflexion moment (Avancini et al., 2015; Cresswell et al, 1995) support the relevance of the distal redistribution of muscle activity as a possible compensatory strategy to increase the plantarflexion moment to produce plantar flexion at the desired level.

The distal spatial distribution of sEMG amplitude in GM suggests an increased muscle fiber shortening close to the myotendinous junction. Previous studies found altered pennation angle and shortened muscle fibers due to an elongated AT (Hullfish et al, 2019; Suydam et al., 2015; Hullfish et al, 2018), which may have implications in the muscle force transmission to the AT (Geremia et al., 2015). In healthy individuals, a similar mechanism was observed when the GM contractions elicited different regional activations triggered by tendon slackness (Avancini et al., 2015). Thus, a compensated regional sEMG activation may be expected when the AT is more compliant (Suydam et al., 2015). The dysfunction of the Golgi tendon organ (Avancini et al., 2015), which can suffer fibrosis following a tenotomy (Jamali et al., 2000), may also help to explain these results. AT patients are more susceptible to distributing their activity by anatomical factors such as tendon lengthening (Suydam et al., 2015; Baxter et al, 2019). The AT lengthening also can cause tendon slackness (Baxter et al, 2019), influencing the neural activity of the Golgi tendon organ, even in fibrotic conditions (Avancini et al., 2015; Baxter et al., 2019). Further studies should elucidate the adaptations induced by Golgi tendon organ dysfunction in repaired AT patients.

In our study, the distal overactivation of GM increased with higher plantar flexion requirements, which could reveal pathological adaptations in motor unit recruitment and/or firing rate. Unfortunately, the interference sEMG signal cannot assess these strategies (Del Vecchio et al., 2017). Therefore, the changes we observed claim confirmation in future studies, including motor unit decomposition techniques (Martinez-Valdes et al., 2021). Lastly, distal overactivation could result from altered muscle fatigability (Falla a et al., 2007). If that is the case, lower frequency manifestations of muscle fatigue would have been expected when patients were compared to healthy controls (McHugh et al., 2019), which was not the case here.

Our study has limitations. We were unable to perform ultrasound measurements across the whole testing. We have used only one linear array of electrodes for economic reasons, and multiple arrays would have given us more detailed neurophysiological information (Cudicio

et al., 2022). Due to the pandemic condition, the recruitment of patients was very difficult. Lastly, the measurement of other calf muscles contributing to the plantar flexion torque could help to understand the influence or not of crosstalk in our results.

5.5 Conclusion

In conclusion, distal GM overactivation and persistent plantar flexion weakness were observed in patients with AT repair one-year post-surgery performing voluntary plantar flexion isometric contractions at maximal and submaximal intensities. We interpret that tendon slackness changed AT mechanical properties, possibly resulting in a muscle activation redistribution, thereby leading to distal overactivation of GM while the plantar flexion strength demands increased.

6 CHAPTER SEVEN – ACUTE MOTOR UNIT RESPONSES TO LOW-INTENSITY NEUROMUSCULAR BIOFEEDBACK ONLY 12 DAYS AFTER SURGICAL REPAIR OF ACHILLES TENDON: A UNIQUE CASE STUDY

Published as:

De la Fuente, C., Silvestre, R., Botello, J., Neira, A., Soldan, M., & Carpes, F. P. (2023). Unique Case Study: Impact of Single-Session Neuromuscular Biofeedback on Motor Unit Properties Following 12 Days of Achilles Tendon Surgical Repair. Physiological Reports,e15868. Doi: 10.14814/phy2.15868

Abstract

In this unique case study, we explored the impact of a single-session of neuromuscular biofeedback on motor unit properties, neuromuscular electrical activation, and the Achilles tendon (AT) length only 12 days after undergoing AT surgical repair. We hypothesized that an immediate intervention after the surgical repair enhances motor unit properties and activation without causing AT lengthening. A 58-year-old male was included in the study after undergoing AT surgical repair 12 days prior. Motor unit decomposition of the Medial Gastrocnemius (MG) was performed before and after a neuromuscular biofeedback intervention, while plantar flexion contractions without any external resistance were performed, which involved the use of sEMG and ultrasonography. The analysis included motor unit population properties, sEMG amplitude, force paradigm, and AT length. After the intervention, more MG motor units were recruited, along with elevated peak and average firing rates. The coefficient of variation, sEMG amplitude, and recruitment threshold all showed significant increases, while the derecruitment threshold decreased. The non-injured limb exhibited a lower coefficient of variation, peak and average motor unit action potential amplitude, inter-pulse interval, derecruitment threshold, and sEMG amplitude. Moreover, the AT length experienced changes of -0.4 cm in the repaired AT limb and 0.3 cm in the non-injured limb. A single-session neuromuscular biofeedback of plantar flexion exercise without loading performed 12 days after AT surgery enhanced MG neuromuscular electrical activation in the repaired AT limb, without causing any signs of AT lengthening. Meanwhile, the non-repaired AT limb showed lower demands on motor unit properties.

Keywords: Neurophysiology; Decomposition; Neuromuscular Biofeedback; Rehabilitation; Surgery.

6.1 Introduction

Immediately after an Achilles tendon (AT) rupture surgical repair, the ankle is usually immobilized at a shortened length for 4 to 6 weeks aiming to underload the tendon and prevent an early lengthening or re-rupture by active movement (e.g., voluntary torque production) (De la Fuente et al., 2016). Unfortunately, immobilization reduces triceps sural strength by decreasing motor unit discharge rate and recruitment (Enoka and Duchateau 2017). These functional effects are acutely observed. For example, only 72 h of immobilization reduces motor excitability and recruitment, resulting in ~22% reduction of the maximal muscle strength (Enoka et al., 2017). A longer immobilization, for 4 to 6 weeks, leads to persistent impaired muscle activation up to one year after rehabilitation (De la Fuente et al., 2023). Thus, interventions focused on immediate action following surgical repair are expected to enhance the impairments caused by immobilization. However, due to the high risk of Achilles tendon (AT) lengthening, recent expert panels have not recommended the application of mechanical stimuli during the very early phase of tendon healing (Saxena et al., 2022).

Despite the high risk of Achilles tendon (AT) lengthening (Saxena et al., 2022), neuromuscular feedback strategies using real-time ultrasonography (US) and surface electromyography (sEMG) are potentially beneficial in early rehabilitation, if administrated under controlled mechanical stimuli over the AT during healing. To this end, neuromuscular biofeedback could be implemented considering low-intensity contractions to avoid tendon lengthening since repetitive loading has been tested in the past without generating clinical failure (De la Fuente et al., 2017; De la Fuente et al., 2017) during the early stage of tendon healing (Freedman et al., 2017). This approach can increase the firing rate of active populations of motor units and the number of recruited motor units (Stein et al., 1990). These last neurophysiological stimuli would be relevant for improving immobilization impairments like muscle inhibition and persistent weakness (De la Fuente et al., 2023). However, whether motor unit properties can be enhanced during a single session of neuromuscular biofeedback without AT lengthening during the early AT healing phase following a surgical repair remains unknown. Understanding these responses should be the first step before planning more extensive interventions aiming at physiological adaptations.

Here, we investigated whether a single-session of neuromuscular biofeedback intervention can influence Medial Gastrocnemius (MG) motor unit properties, neuromuscular activation, and the AT length only 12 days after AT surgical repair. We hypothesized that a

single-session of neuromuscular biofeedback intervention improves the MG motor unit properties and neuromuscular activation without increasing the AT length 12 days after AT surgical repair.

6.2 Methods

6.2.1 Case description and design

In this case report, we compared medial gastrocnemius (MG) motor unit population properties (number of recruited motor units, peak and average firing rate, coefficient of variation, decomposition accuracy, peak and average motor unit action potentials (MUAP), inter-pulse interval, and motor unit recruitment and derecruitment thresholds), sEMG amplitude, force paradigm, and AT length before and after a single-session of neuromuscular biofeedback (combined US and sEMG biofeedback). The intervention included submaximal muscle contractions (30% of maximal voluntary contraction of the non-injured limb) in the repaired AT and non-injured limb of a patient on day 12 after the AT repair surgery. The institutional ethics committee approved the research protocol, but allowed the inclusion of only one patient. The patient agreed to participate and provided informed consent. He was a male recreational soccer player (age 58 years old, body mass 94 kg, height 1.86 m, and body mass index 27.2 $kg.m^{-2}$), an office worker without comorbidities, and who suffered a non-contact AT rupture during a recreational soccer match. The rupture (acute, unilateral, and mid-substance) was repaired with the triple Dresden technique (De la Fuente et al., 2017; De la Fuente et al., 2017) by two senior foot and ankle surgeons with more than 15 years of experience.

6.2.2 Basal Measurements

Basal measurements were obtained prior to the intervention (Table 10). The AT resting angle was measured with the patient lying prone with the knee flexed at 90º (Carmont et al., 2015). The MG pennation angle and thickness were quantified with the patient resting in a prone position with 0º of knee extension and 20º of plantar flexion and using ultrasonography at the level where the sEMG sensor (Anvanti, Trigno, Delsys Inc., USA) was attached to the skin (Hermens et al., 2000). The superficial and deep aponeurosis were the

anatomical references (Cho et al., 2014). A maximal voluntary isometric plantar flexion contraction (MVIC) was measured in the non-injured AT limb using a wireless load cell sensor (S-beam load cell, Delsys Inc., USA) with the patient seated with hip, knee, and ankle at 90º. The AT rupture score (ATRS) and the verbal response to a numerical rating pain scale of the patient were obtained 30 min prior to the intervention session start.

Table 10. Basal measurements.

Measurements	**Non-injured**	**Repaired AT**	**Δ**
Achilles tendon resting angle (º)*	14.0	12.0	-2.0 (-14%)
MG resting pennation angle (º)	18.0	20.0	2.0 (11%)
MG resting thickness (mm)	17.4	16.3	1.1 (6%)
Maximal voluntary isometric contraction (N)	171	-	-
Clinical Scores	**Obtained points / maximal points**		
Achilles tendon rupture score (pts)	87/100		
Verbal numerical rate pain scale (pts)			
- Prior to the intervention	0/10		
- Maximal value during the intervention	3/10		

MG: medial gastrocnemius; cm: centimeters; º: sexagesimal degrees; mm: millimeters; N: Newton; pts: points.

6.2.3 Neuromuscular biofeedback protocols

The neuromuscular (US and sEMG) biofeedback was delivered with the patient in a prone posture performing 20 dynamic plantar flexion contractions without external resistance. The patient developed 20 s in total for each ankle plantar flexion, 5 s were used to move from the rest position to full plantarflexion, 10 s were used to maintain the full plantarflexion, and 5 s were used to move from full plantarflexion to the rest position. The participant repeated 5 series with 30 s of rest between series. Due to protective reasons, we used low-speed ankle movement because high-speed joint movement required higher stiffness material properties, which contradicts the early healing tendon stage. The protective range of motion was defined from rest plantarflexion to full plantarflexion range of motion, in coherence with past recommendations for the early stage following the Dresden surgical design, which also was tested at low-speed traction (De la Fuente et al., 2017). A 'beep' sound metronome was set.

The patient was instructed not to talk during the execution of the exercise. The verbal instructions at the beginning of the exercise were: "Please move your [big toe/little toes/ankle in plantar flexion] in sync with the metronome's rhythm. If you experience any pain while performing the exercise, you must stop immediately and inform me to halt the assessment."

Both US and sEMG signals were projected on a screen in front of the participant, providing neuromuscular biofeedback for both the evaluator and the participant (Figure 19). Before testing, the patient had around 5 minutes of familiarization guided by the evaluator. The US feedback was delivered in real-time (immediately visually projected) with the transducer positioned perpendicular over the third lateral portion and the third medial portion of the leg to identify the hallucis flexor longus (De la Cruz-Torres et al., 2020) and flexor digitorum longus muscles (Mickle et al., 2013), respectively. A good quality acquisition was considered when the displacement of the hallucis flexor longus and flexor digitorum longus muscles were distinguishable by both the evaluator and the patient during metatarsophalangeal flexion. The patient was requested to focus on the muscle displacement (aponeurosis movement represented by white pixel displacement) on the screen as an indicator of muscle activation while moving their big toe or little toes to elicit the targeted muscles (Figure 19).

The sEMG feedback was provided through the use of two superficial sEMG sensors (Avanti, Trigno, Delsys Inc., Boston, USA), which were attached to the MG and soleus muscle bellies (Figure 19). A good quality acquisition was ensured by the signal-to-noise ratio of MG and soleus activation clearly identified as at least double the width of the resting signal. The patient was instructed to focus on the increase in signal amplitude compared to the basal signal on the screen, which served as an indicator of muscle activation (Figure 19).

Figure 19. Biofeedback setup. A. Achilles Tendon (AT) angle at rest. B. AT length measured from calcaneus reference (Calc. Ref.) to the myotendinous junction (MTJ) of Medial Gastrocnemius. C. sEMG sensor on Medial Gastrocnemius to acquire firing rate during prolonged periods. D. Measurement setup. E. Ultrasonography feedback. F. sEMG sensors for feedback. G. Force and sEMG signals projected on the screen. H. Ultrasonographic measurement of muscle thickness. I. Resting pennation angle measurement. J. sEMG decomposition.

6.2.4 Data Acquisition and Processing

The AT length was measured using musculoskeletal ultrasonography with a 12 MHz linear transducer (Lumify S4-1, Philips, The Netherlands) and a 50 mm graded metric tape

(Seca 201, Germany). The measurement was taken from the tip of the calcaneus to the myotendinous junction of the MG.

For sEMG decomposition assumptions, the patient was positioned prone with 30º knee flexion and 20º plantar flexion to unload the AT during the testing (De la Fuente et al., 2017). Considering a randomized order, a plantar flexion contraction was performed by each limb to elicit 30% of the maximal voluntary isometric contraction (MVIC) measured in the non-injured limb. This submaximal intensity was defined to protect the surgical repair from failure (De la Fuente et al., 2016). In addition, low-intensity muscle contractions reduce the superposition of motor unit action potentials, providing better decomposition outputs (LeFever et al., 1982) and minimizing silent deformation at tendon-suture, a lengthening mechanism for the Dresden technique (De la Fuente et al., 2016). A uniaxial load cell (Delsys Inc., Boston, USA) was attached perpendicular at the metatarsal level of both limbs to register the force signals during the contractions to allow the control of a trapezoidal plantar flexion contraction at the target intensity, which was sustained for 20 s (isometric assessment) before and after the intervention session (Figure 19).

Two decomposition sEMG sensors (Galileo sensor, Delsys Inc., Boston, USA) recorded sEMG data from the repaired AT and non-injured limbs. We used 4-dry-electrodes for decomposition (four cylindroid probes of 0.5 mm diameter (De Luca et al., 2006)) and 4-dry-rectangular electrodes for references, which were positioned after the skin cleaning and shaving. The electrodes were 99.9% of Ag. The inter-electrode distance was 2.5 mm. The sEMG signals for decomposition were acquired with an sEMG Trigno amplifier (Delsys Inc., Boston, USA). An analog-digital converter of 16-bit sampled the sEMG signals at 2222 Hz. Simple differential capture with dual stabilizing reference was used (De Luca et al. 2006). The common-mode rejection ratio was lower than -80 dB. The total noise was lower than 750 nV, and an analog band-pass filtered with a 20-250 Hz cut-off frequency. A reference electrode was located at the lateral side of the most prominent bulk of the MG (Figure 19). The quality of the signals (electric interferences and contact problems) was visually inspected before data acquisition.

After sEMG signal acquisition, the data were decomposed into motor unit action potential trains basis. The threshold accuracy was set at > 80% (Jeon et al., 2020). The decomposition algorithm was based on a template-matching approach enhanced by maximum a posteriori probability methods (LeFever et al., 1982). The maximum a posteriori probability

(Bayesian inference) allowed to estimate the occurrence of motor unit firing and waveforms (LeFever et al., 1982). The firing rate time series were obtained by convoluting the impulse of firing trains with a 1-s Hanning window (Jeon et al., 2020). All estimations were made using the NeuroMap 1.0 software (Delsys Inc., Boston, USA).

6.2.5 Data analysis

Data distribution was checked using the Shapiro-Wilk and Levene tests ($\alpha = 5\%$). The motor unit properties, sEMG amplitude (mean root square from the 5-second plateau during the trapezoid contraction), force paradigm, and tendon length were described as the obtained values, and the absolute and percentage differences (Δ = without – with feedback intervention) prior to and after the intervention, were described for both in the AT repaired and non-injured limbs. The raster plot also was created. The space generated by the recruitment threshold and the peak firing rate was clustered (density-based spatial clustering of application with noise - DBSCAN) to understand the acquired motor unit strategies. The Epsilon neighborhood was 4. The epsilon parameter defines the searching radius around a core containing at least the minimum defined neighbors. The minimal number of neighbors in our study was 3. All descriptive statistics were conducted using Matlab software (Mathwork Inc., Natick, USA).

6.3 Results

The main changes observed following the neuromuscular biofeedback in the repaired AT limb were an increased number of motor units ($\Delta = 325\%$), peak firing rate ($\Delta = 74\%$), average firing rate ($\Delta = 40\%$), coefficient of variation ($\Delta = 40\%$), and sEMG amplitude ($\Delta =$ 52%, 43%, 26%, and 33% for each channel, respectively). In contrast, decreased derecruitment ($\Delta = -72\%$) and recruitment ($\Delta = -35\%$) thresholds were found in the repaired AT limb (Table 11 and Figure 20). Decomposition accuracy, peak and average MUAP amplitude, and AT length showed changes lower than 10%.

Regarding the non-injured limb, the neuromuscular biofeedback increased the number of motor units ($\Delta = 26\%$) and recruitment threshold ($\Delta = 233\%$). In contrast, there was a

decreased derecruitment threshold (Δ = -96%), sEMG amplitude (Δ = -65%, -78%, -28%, and -42% for each channel, respectively), coefficient of variation (Δ = -55%), inter-pulse interval (Δ = -49%), peak (Δ = 74%), and average (Δ = 40%) MUAP amplitude in the non-injured limb (Table 11 and Figure 20). Decomposition accuracy, peak and average firing rate, and AT length showed changes lower than 10%.

In total, we identified 5 different clusters of motor units based on peak firing rate and recruitment threshold space for both limbs (Table 11). In the repaired AT limb, the motor units recruitment previous to the neuromuscular biofeedback (4 clusters) characterized by the peak firing rate and recruitment threshold space were 7.4 ± 3.4 pps and 4.4 N ± 2.0 N (n = 1), 15.9 ± 3.5 pps and 10.1 N ± 6.8 N (n = 1), 9.0 ± 0.3 pps and 22.0 N ± 0.9 N (n = 3), and 6.4 ± 1.2 pps and 30.6 N ± 1.1 N (n = 3), while following the neuromuscular biofeedback (3 clusters) were characterized by 7.4 N ± 3.4 pps and 4.4 N ± 2.0 N (n = 2), by 12.9 N ± 1.7 pps and 12.8 N ± 1.7 N (n = 14), and by 15.9 N ± 3.5 pps and 10.1 N ± 6.8 N (n = 18), see Table 11. In the non-injured limb, the motor units recruitment before the neuromuscular biofeedback (2 clusters) were characterized by 15.9 ± 3.5 pps and 10.1 N ± 6.8 N (n = 2) and by 14.6 ± 5.3 pps and 1.5 N ± 0.2 N (n = 17), while after the neuromuscular biofeedback (3 clusters) were characterized by 7.4 N ± 3.4 pps and 4.4 N ± 2.0 N (n = 1), by 14.6 N ± 5.3 pps and 1.5 N ± 0.2 N (n = 1), and by 15.9 N ± 3.5 pps and 10.1 N ± 6.8 N (n = 22), see Table 11.

Finally, the AT length changed to 0.3 cm and -0.4 cm for the non-injured and repaired AT limbs, respectively.

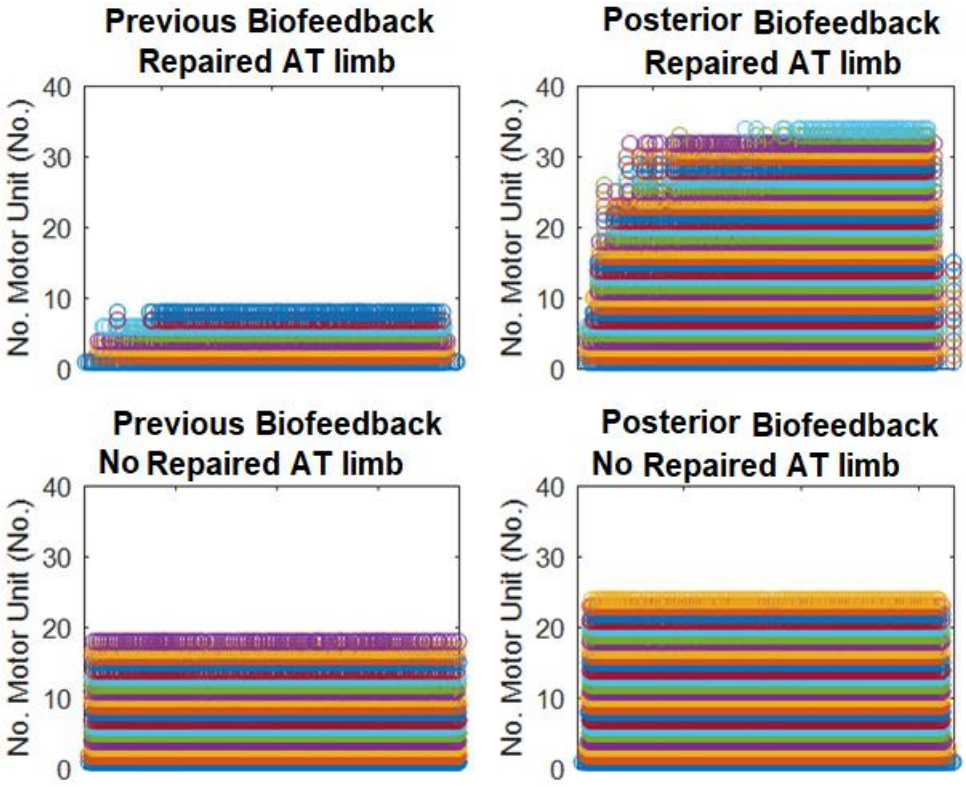

Figure 20. Raster plot of medial gastrocnemius motor unit recruitment before and after the neuromuscular biofeedback intervention. A. Repaired AT limb before intervention. B. Repaired AT limb after intervention. C. Non-injured AT limb before intervention. D. Non-injured AT limb after intervention.

Table 11. Motor unit and sEMG descriptive statistics, and cluster firing rate-recruitment threshold.

Measurements	**Non-injured**			**Repaired AT**		
	Pre-BF	**Post-BF**	**Δ**	**Pre-BF**	**Post-BF**	**Δ**
Recruited MU number (No.)	19	24	5 (26%)	8	34	26 (325%)
Coefficient of Variation (%)	4.2	1.9	-2.3 (-55%)	3.0	4.2	1.2 (40%)
Paradigm force (N)	31.0 ± 1.3	26.1 ± 0.5	-4.9 (-16%)	30.2 ± 0.9	24.0 ± 1.0	-6.2 (21%)
Decomposition accuracy (%)	92.8 ± 20.9	92.6 ± 18.8	-0.2 (< -1%)	90.5 ± 28.8	86.5 ± 15.9	-4.0 (-5%)
Peak MUAP amplitude (10^{-5} V)	20.62 ± 22.66	10.70 ± 5.18	-9.92 (-48%)	3.59 ± 1.50	3.67 ± 2.53	0.08 (2%)
Average MUAP Amplitude (10^{-5} V)	13.33 ± 12.07	7.70 ± 3.43	-5.60 (-42%)	2.95 ± 1.18	3.03 ± 2.32	0.08 (3%)
Peak Firing Rate (pps)	14.62 ± 5.96	14.57 ± 5.25	-0.05 (< -1%)	8.05 ± 3.05	13.99 ± 4.10	5.94 (74%)
Average Firing Rate (pps)	3.48 ± 1.99	4.57 ± 2.01	-0.05(< -1%)	2.30 ± 1.32	3.22 ± 1.39	0.92 (40%)
Inter-pulse interval (ms)	298.6± 147.2	153.4± 42.7	-145.2 (-49%)	201.1 ± 76.2	194.5 ± 68.0	-6.6 (-3%)
Recruitment Threshold (N)	1.5 ± 0.4	5.0 ± 1.2	3.5 (233%)	22.0 ± 11.0	14.4 ± 10.3	-7.6 (-35%)
Derecruitment Threshold (N)	26.8 ± 8.3	1.2 ± 0.3	-25.6 (-96%)	5.3 ± 2.8	3.1 ± 5.8	-2.2 (-72%)
sEMG amplitude:						
rms electrode 1 (10^{-5} V)	1.0954	0.3803	-0.7151 (-65%)	0.9367	1.4247	0.4880 (52%)
rms electrode 2 (10^{-5} V)	1.0206	0.2295	-0.7911 (-78%)	0.8923	1.2774	0.3851 (43%)
rms electrode 3 (10^{-5} V)	1.2884	0.9226	-0.3658 (-28%)	1.1973	1.5074	0.3101 (26%)
rms electrode 4 (10^{-5} V)	1.1339	0.6543	-0.4796 (-42%)	1.0254	1.3636	0.3382 (33%)
Length of the Achilles tendon (cm)	21.0	21.3	0.3 (1.4%)	22.5	22.1	-0.4 (-2%)

Clusters	**Without biofeedback**		**With biofeedback**		**Peak firing rate (pps)**	**Recruitment threshold (N)**	**Number of motor units (No.)**
	Pre	Post	Pre	Post			
Cluster 0	1	2	0	1	7.4 ± 3.4	4.4 ± 2.0	4
Cluster 1	3	0	0	0	9.0 ± 0.3	22.0 ± 0.9	3
Cluster 2	1	18	2	22	15.9 ± 3.5	10.1 ± 6.8	43
Cluster 3	3	0	0	0	6.4 ± 1.2	30.6 ± 1.1	3
Cluster 4	0	14	0	0	12.9 ± 1.7	12.8 ± 1.7	14
Cluster 5	0	0	17	1	14.6 ± 5.3	1.5 ± 0.2	18

MU = Motor units; N = Newton; V = Volt; MUAP = Motor unit action potential; Pps = pulses per second; ms = millisecond; sEMG = surface electromyography; No. = number; and rms = Root mean square.

6.4 Discussion

In this study, we provide insights into the transitory enhancement of muscle activation of a repaired AT patient after a single-session of neuromuscular biofeedback only 12 days following AT surgical repair, which means during the very early stage of AT healing. Our intervention included a unique case study conducted in a typically restricted phase for research due to the high risk of adverse events (re-rupture and tendon lengthening). To the best of our knowledge, this is the only study to date in which impaired motor unit properties are shown to acutely enhance after low-intensity contractions and neuromuscular biofeedback without observation of tendon lengthening during the healing phase of a surgically repaired AT. The repaired AT limb exhibited several changes, including the recruitment of newly low-threshold motor units, an increase in firing rate and sEMG amplitude, a decrease in derecruitment and recruitment motor unit threshold, and an increase in force fluctuations (higher variation coefficient). In contrast, the non-injured limb showed reduced demands on motor unit properties to perform the task after the neuromuscular biofeedback. Therefore, we hypothesized that these strategies might have been influenced by improvements in: i) spindle afference excitability, ii) the net descending excitability input, iii) motor unit synchronization, and/or iv) short-term potentiation on α-motor units.

The improvements in motor unit properties indicate that the gamma loop of the plantar flexors was actively involved in force production. This assumption relies on the fact that low-intensity muscle contractions strain the intrafusal muscle fibers (Richardson et al., 2006), increasing the availability of proprioceptive information, at least to the spinal cord level (Proske et al., 2012). This mechanism can likely explain the increased activation of the MG α-motor units through the up-regulation of motor unit recruitment and firing rate, as well as decreased recruitment and derecruitment thresholds. Other neurophysiological factors might impact the changes observed. For example, persistent inward currents in motor unit threshold modulation have a relevant role in regulating the thresholding of motor units (Heckman et al., 2008). Further experiments are needed to understand their modulating role during a single neuromuscular biofeedback session. Another strategy to enhance proprioceptive availability could involve building upon past research on acquiring novel visuomotor skills that activate the gamma loop (Ia afferents) for modulating sensory inputs (Perez et al., 2005). Additionally, increasing the net descending input in our setup may further support this goal. The visual

information delivered could allow visuomotor integration (Unell et al., 2021) using the cerebellum's action as a comparator (Flament and Ebner 1996), amplifying the proprioceptive information and net descending excitability.

Short-term potentiation (Hennig 2013) is a relevant peripheral condition that may also have played a role in our study. Our setup induced repetitive muscle contractions that may increase presynaptic calcium concentration. This, in turn, leads to the opening of AMPA and NMDA receptors to increase the postsynaptic ionic conductance at the peripherical level (Hennig 2013). Another intriguing finding was the increased force coefficient of variance during the plateau stage of the trapezoidal plantar flexion contraction to assess the intervention effect in the repaired AT limb. This coefficient exhibited contrasting behavior between the limbs. This finding implies that our intervention stimulated motor unit synchronization (Semmler 2002). However, force signal tracking showed worse synchronization in the injured limb compared to the non-injured limb, leading to a decrease in their force coefficient of variance. It suggests a quick impairment of motor unit synchronization in the repaired AT limb. This synchronization is useful for situations demanding rapid force development, highlighting the negative impact on low-frequency components of motor unit discharge (Semmler 2002).

Finally, we have not found evidence of tendon lengthening. This is in accordance with the *principle* of *no tendon lengthening* during a critical mechanical phase, specifically the early stage of AT healing. To set up our load conditions, we relied on our previous *in vitro* estimations to ensure that there was no excessive stress at the suture-tendon interface, which could potentially lead to silent lengthening (De la Fuente et al., 2017). Consequently, this case report presents novel evidence regarding an alternative intervention that can enhance muscle activation properties. These properties are significantly affected during the first weeks of immobilization and can be responsible for chronic pathological muscle adaptation, which often leads to a low rate of sports return after experiencing an Achilles tendon rupture.

The absence of measurements for H-reflex and M-response prevented the exploration of presynaptic and postsynaptic aspects during the patient's response to the intervention and, therefore, characterizes a limitation in our study.

6.5 Conclusion

A single-session of unloaded exercise within a protective range of motion, incorporating neuromuscular biofeedback, performed only 12 days after surgery in a patient with an AT repair, enhances MG neuromuscular electrical activation. This improvement was achieved by enhancement of motor unit properties in the repaired AT limb without indications of AT lengthening. Meanwhile, the non-repaired AT limb requires lower demands of motor unit properties. These promising outcomes warrant further testing during the early phases of AT ruptures.

7 CHAPTER EIGHT – MOTOR UNITS RECRUITMENT, FIRING RATE, AND PAIN SENSATION AFTER CUMULATIVE FATIGUE IN HEALTHY UNTRAINED MEN

ABSTRACT

Cumulative muscle fatigue results from repeated consecutive bouts of exercise. The expected force impairment and limited motor control following fatigue are discussed as the altered capacity of muscle recruitment and control. However, there is limited knowledge about the motor unit responses to cumulative fatigue, and most of the current research relies on discussing overall muscle activation. In this study, we aimed to describe the motor unit recruitment and firing rate when cumulative fatigue is induced by repeated bouts of exercise in the biceps brachialis of healthy untrained young men. Twenty-one participants (11 intervention and 10 matched controls; age of 22.1± 1.5 years old, height of 1.74± 0.08 m, body mass of 70.8± 6.8 kg, body mass index of 23.5± 1.5 kg m^{-2}, maximal elbow flexion isometric voluntary contraction of 44.7± 9.2 N) were recruited in a randomized, single-blind, prospective, and case-control study. Three groups were measured (cumulative fatigue until exhaustion, placebo, and control). The cumulative fatigue lasted three consecutive days, and the control group did not perform exercises. Placebo dose was a set of exercise not leading to exhaustion nor fatigue. sEMG signals were decomposed to obtain motor unit wave basis and firing rate time series. After the sEMG recordings, the same researcher applied a load of 1 kg at the upper, middle, and lower regions of the arm with an algometer to quantify pain sensation. Recruited motor unit, firing rate differences, and pain sensation were described and compared between groups (α = 5%). The motor unit recruitment for the cumulative fatigue and placebo dose was higher than the control (p =0.026). The firing rate for the cumulative fatigue dose did not differ from the placebo dose (p=0.088) but was higher than the control (p=0.039). Pain sensation was higher in the intervention group; the lower region was higher than the upper and lower regions, p=0.002; middle and lower regions, p=0.021. Following three bouts of exhaustion leading to cumulative fatigue in the biceps brachialis of healthy untrained men there was increased motor unit recruitment, firing rate, and distal muscle pain sensation.

Keywords: Muscle; Fatigue; Cumulative Fatigue; Surface electromyography; Decomposition.

7.1 Introduction

Cumulative fatigue results from repeated consecutive bouts of fatiguing muscle contractions (Machado et al., 2018). However, the expected reduction of the maximal voluntary contraction appears not to be an intrinsic characteristic of cumulative fatigue (Machado et al., 2018), as observed in acute fatigue (Powers et al., 2008). While the effects of fatigue can last from hours to days (Jones et al., 2017; Machado et al., 2018; Priego-Quesada et al., 2019), impairing daily life routine (Sjøgaard et al., 1998; Søgaard et al., 2017), the capacity to produce similar levels of force regardless of the condition of cumulative fatigue is intriguing. In this regard, a better understanding of motor unit decomposition after repetitive bouts of exhaustion fatigue could help to better understand the changes in force output in response to cumulative fatigue.

Muscles under cumulative fatigue may suffer from fiber damage, inflammation, and oxidative stress (Powers et al., 2008; Twist et al., 2005). For example, two consecutive bouts of fatiguing until exhaustion exercise in biceps brachialis increase plasma creatine kinase (a marker of muscle damage), reactive oxygen species production, and malondialdehyde concentration (a marker of oxidative stress) (Machado et al., 2018). At the same time, there is a lower content of reduced glutathione (a marker of anti-oxidative stress) (Machado et al., 2018). Similarly, increased pain is observed 48 hours after calf raise exercises until exhaustion (da Silva et al., 2018). The damage, inflammation, and oxidative stress would involve muscle fiber disruption where the membrane and sarcomeres are mainly damaged, releasing Ca^{++} from the retinaculum (Proske et al., 2001). But also, a higher intracellular Ca^{++} via stretch-activated channels occurs due to increased permeability (Kano et al., 2012). The loss of Ca^{++} homeostasis and the presence of reactive oxygen species, together with oxidative stress, leads to irreversible injury and cellular apoptosis (Farber 1990; Schanne et al., 1979; Horn et al., 2018; Kano et al., 2012).

The search for a better understanding of motor control under cumulative fatigue may benefit from using sEMG to monitor muscle recruitment. Additionally, the linear combination between motor unit wave basis and firing rate time series allows the decomposition of sEMG signals from array electrodes in the skin (De Luca et al., 2006). For example, sEMG has been identified as poor neuromuscular activation after strenuous exercises (Mendez-Villanueva et al., 2012; Machado et al., 2018). Also, findings of left shifting in the frequency spectrum,

increased ratio of the medium-low frequencies, and lower Shannon entropy on root mean square values (Machado et al., 2022) are in coherence with the electrical modulation of fatigued muscle contractions (Cashaback et al., 2013). Although nowadays we know more biochemical characteristics of cumulative fatigue (Machado et al., 2022; Powers et al., 2008; Sarker et al., 2020), there is limited knowledge about how firing rate and motor unit recruitment behave under conditions of cumulative fatigue.

Here, we aimed to describe the motor unit recruitment and firing rate when cumulative fatigue is induced by repeated dynamic bouts of exercise in the biceps brachialis of healthy untrained young men.

7.2 Methods

7.2.1 Study design

In this randomized, single-blind, prospective, and case-control study, there were three groups (intervention, placebo, and control groups). One group underwent cumulative fatigue protocol (three consecutive days of unilateral cumulative exercise until exhaustion), the second group (contralateral arm) underwent a placebo dose (non-fatiguing unilateral cumulative dose of exercise), and the third group was the control (without intervention). The groups were allocated with the block randomization technique (Kang, Ragan, and Park 2008). The allocation reason was 1:1 to obtain balanced independent groups (intervented groups and control). The protocol to induce cumulative fatigue lasted three consecutive days, and the control groups did not perform exercises during the three days. During the first and third days, sEMG signals were acquired and decomposed to obtain motor unit wave basis and firing rate time series.

This study was approved by the ethical committee of the local institution, the Pontificia Universidad Catolica de Chile (Santiago, Chile). All participants gave their signed informed consent to be part of the study.

7.2.2 Participants

Twenty-one untrained healthy men participants (11 intervention and 10 controls; age of 22.1± 1.5 years old, height of 1.74± 0.08 m, body mass of 70.8± 6.8 kg, body mass index of 23.5± 1.5 kg m^{-2}, maximal elbow flexion isometric voluntary contraction of 44.7± 9.2 N) were recruited. One participant voluntarily abandoned the study on the second day (after the first session of the fatigue protocol) due to an exacerbated pain sensation at the third distal region of the biceps brachialis muscle. The sample size (n = 20) was estimated from the effect size of d = 1.35 found for a similar setup in sEMG (Machado et al. 2022). We set an alpha error of 5%, allocation ratio of 1:1, and statistical power of 80% (around four twice, according to Cohen's recommendations) for two independent mean differences with two tails. The estimation was made using G*Power software 3.1.9.2 (Universtät Kiel, Germany).

The inclusion criteria were i) male sex, ii) untrained participants (less than 30 minutes of physical activity during the week), iii) body mass between 18.5 and 25.9 kg m^{-2}, and iii) age between 20 and 25 years. The exclusion criteria were i) any cardiovascular, neurology, metabolic, or orthopedic condition, ii) upper limb injuries, iii) pain reported before the experiment ended, iv) anxiety syndromes, v) skin allergy and conditions, vi) any medication, vii) sleep deprivation, and viii) any stressful situation that can alter our results.

7.2.3 Intervention

Before the intervention, the participants performed a warm-up of 5 minutes, performing active flexion and extension of the shoulder and elbow with sagittal plane movements against gravity force in a comfortable range of motion.

In the participants intervented with cumulative fatigue, one of the two arms started the protocol to induce fatigue by performing exercises until exhaustion on the first, second, and third day. Meanwhile, the contralateral arm received a placebo dose of the exercise without exhaustion each day. The placebo dose performed the same movement and condition of the exhaustion protocol, but the participant ended their exercises when they achieved 4 points of effort sensation (non-fatiguing dose) from a modified 10-point effort scale.

According to previous studies, a dumbbell with a mass close to 7% of the individual body mass was used to perform flexion-extension elbow exercises to induce cumulative fatigue through concentric and eccentric components (Priego-Quesada et al., 2020). The movement involved the full elbow range of motion while standing, with the trunk aligned to the vertical. The frequency was set at audible 30 pulses per minute. Each beat of the metronome indicates the start of elbow flexion from the full elbow extension. Exhaustion was defined as i) the incapacity to perform the full range of motion, ii) the complete loss of the rhythm coordination between the metronome and the participant's movement during three consecutive series, iii) postural compensation needed to complete the task, and iv) participant movement detention. Participants performed the exercise always at the same time of the day and therefore with 24 hours of interval between the sessions. They were instructed to maintain their routines in the days of the experiment, avoiding ingestion of alcohol or other stimulant beverages as well as not taking any medication that could interfere with the neuromuscular function and pain perception.

7.2.4 Measurements

Height, body mass, body mass index, and maximal voluntary isometric contraction (MVIC, mean of three tentatives of 5 seconds) were obtained 30 min prior to the start of the fatigue protocol. Height and body mass were obtained using a metric tape and a digital scale. For the assessment of the MVIC each participant was seated with the trunk upright in an adjustable seat to obtain 90º of the elbow and supinated forearm with flexion hip, knee at 90º, and ankle in a neutral position (Figure 19). A wireless S-beam load cell (Delsys Inc., USA) was positioned at the wrist, in the middle distance between the styloid process, to measure the compressive force generated against a rigid horizontal table by elbow flexion (Figure 21). The repetitions lasting 5 seconds were requested to obtain the repetition eliciting the MVIC.

From the MVIC result, a trapezoidal submaximal contraction set at 40% of the MVIC with an ascent and decent ramp of 5 seconds and a plateau of 20 seconds was performed to obtain surface electromyography signals at the basal, immediately after the first session of exercise on day 1 of the fatigue protocol, and after the third session of exercise on day 3 of the fatigue protocol. sEMG measurements were performed in both intervention and control groups.

To assess the pain perception, after the sEMG recordings, the same researcher applied a load of 1 kg at the upper, middle, and lower regions of the biceps brachii from both arms with an algometer (NOD, OTbioeletronica, Italy), considering fiber muscle damage would not homogenous. The participant should report the pain perception using a numerical scale from 0 to 10, in which 0 corresponds to the perception of “no pain” and 10 corresponds to the sensation of “extreme pain”.

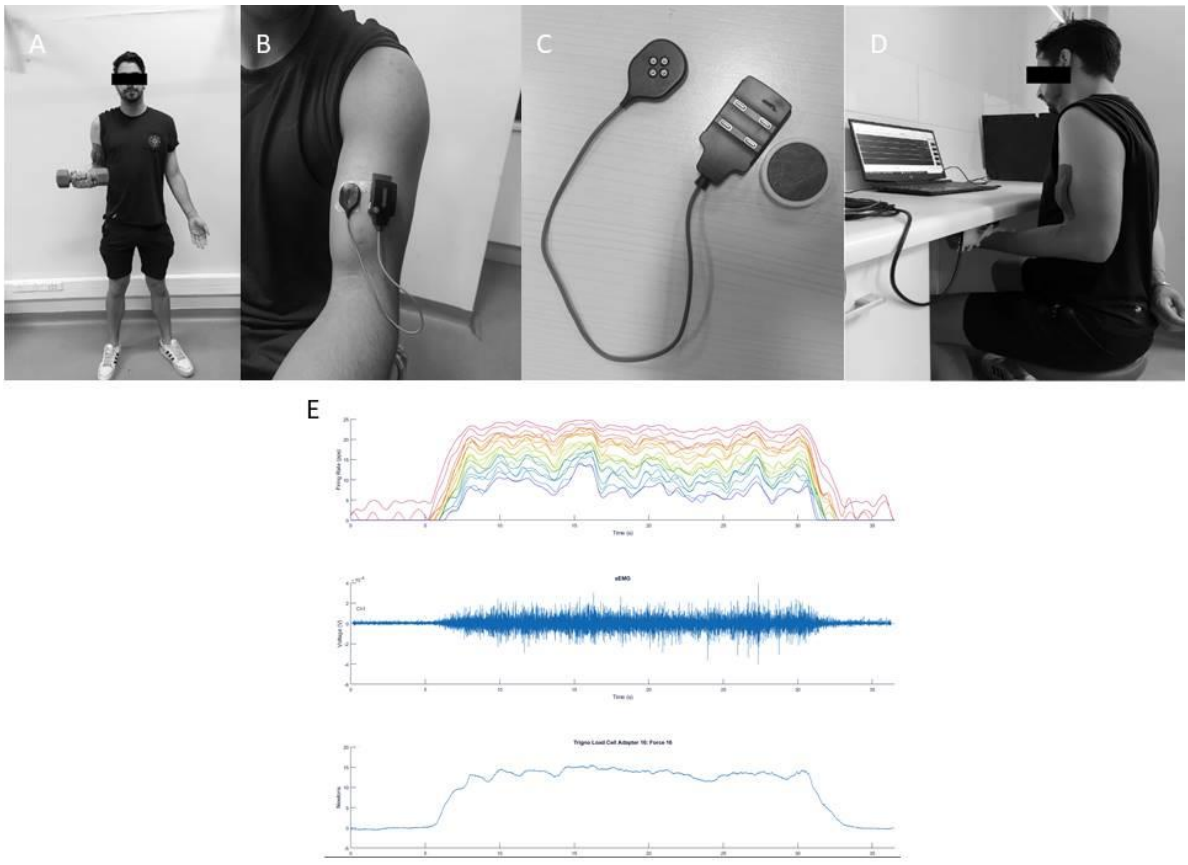

Figure 21. Study setup. A = Posture for the exercise. B = Electrode positioning. C = Details of the quadrifilar electrode and references. D = Position of the participant for the assessment of the maximal voluntary isometric contraction. E = Illustration of a typically decomposed electromyography (top), signal from electromyography channel (middle), and signal from the load cell (bottom).

7.2.5 Data collection and processing

We used a 4-dry-electrodes for decomposition (four cylindroid probes of 0.5 mm diameter (De Luca et al., 2006) and 4-dry-rectangular electrodes for references (Delsys Inc., USA) positioned on the muscle belly of the biceps brachialis after careful skin shave and cleaning. The electrodes were 99.9% of Ag. The inter-electrode distance was 2.5 mm, and the sEMG signals were acquired by a sEMG Trigno amplifier (Delsys Inc., USA) being analog-digital converted at 16-bit and sampled at 2222 Hz. Simple differential capture with dual stabilizing reference was used (De Luca et al., 2006). The common-mode rejection ratio was lower than -80 dB. The total noise was lower than 750 nV, and the analog band-pass filter was set with a cut-off frequency between 20 and 250 Hz. The reference electrode was located on the biceps brachialis according to SENIAM guidelines (Hermens et al., 2000). The quality of the signals (electric interferences and contact problems) was visually inspected before data acquisition.

After the acquisition of the sEMG signal, the data were decomposed into motor unit action potential trains basis. The threshold accuracy was set at > 80% (Jeon et al., 2020). The decomposition algorithm was based on a template-matching approach enhanced by maximum a posteriori probability methods (De Luca et al., 2006; Nawab et al., 2010). This maximum a posteriori probability (Bayesian inference) is used to estimate the occurrence of motor unit firing and waveforms (LeFever et al., 1982). The firing rate time series were obtained by convoluting the impulse of firing trains with a 1-s Hanning window (Jeon et al., 2020). All estimations were made using a demo version of the NeuroMap 1.0 software (Delsys Inc., USA). The motor unit recruitment corresponded to the active motor unit with an accuracy higher than 80% measured in number units (No.). The firing rate corresponded to the mean firing rate of the identified active population of motor units measured as pulse per second (pps).

7.2.6 Data Analysis

Raw recruited motor unit and firing rate data were described as median and interquartile range as they were not distributed normally after applying the Shapiro-Wilk test

(p>0.05). Recruited motor unit, firing rate differences, and pain sensation were described as their mean and standard deviation because they showed a normal distribution after applying the Shapiro-Wilk test. The comparison between the control, cumulative fatigue and placebo dose was performed on the difference between the last time point (day 3) and basal measurement (day 1) using one-way ANOVA with Bonferroni's multiple comparisons (p>0.05) when a main effect was found.

The time course comparison between fatigue and placebo dose was determined through the 2-way Friedman test. The factor time had three levels (basal, acute, and cumulative response), and the factor dose had two levels (fatigue and placebo dose). Multiple comparisons with Wilcoxon signed-rank tests and Bonferroni's adjustment were performed when a main effect was found.

The pain sensation was studied through a 3-way ANOVA test. The factor time had three levels (basal, acute, and cumulative response), the factor dose had two levels (fatigue, placebo dose and control), and the factor region had three levels (upper, middle, and lower region of the biceps brachialis muscle belly). The multiple comparisons were performed with Wilcoxon signed-rank tests and Bonferroni's adjustment when a main effect was found.

All comparisons were set with alpha equal to 5% through the SPSS software (IBM corp., USA).

7.3 Results

Regarding the difference between the last exercise bout and basal measurement, there was a main effect for motor unit recruitment ($F = 4.361$, p<0.023) and firing rate ($F = 4.163$, p<0.027). The motor unit recruitment for the exhaustion fatigue dose (8.7 ± 2.4 No.) did not differ from the placebo dose (6.3 ± 2.4 No.; $\Delta = 2.4 \pm 3.4$; $p = 0.867$), but was higher than the control (-1.0 ± 2.4 No.; $\Delta = 9.7 \pm 3.4$; $p = 0.026$). The firing rate for the exhaustion fatigue dose (2.46 ± 1.73 pps) did not differ from the placebo dose (0.25 ± 2.97 pps; $\Delta = 2.21 \pm 0.963$; $p = 0.088$) but was higher than the control (-0.10 ± 1.45 pps; $\Delta = 2.56 \pm 0.963$; $p = 0.039$). Motor unit and firing rate difference between doses are summarized in Figure 22 and Table 12.

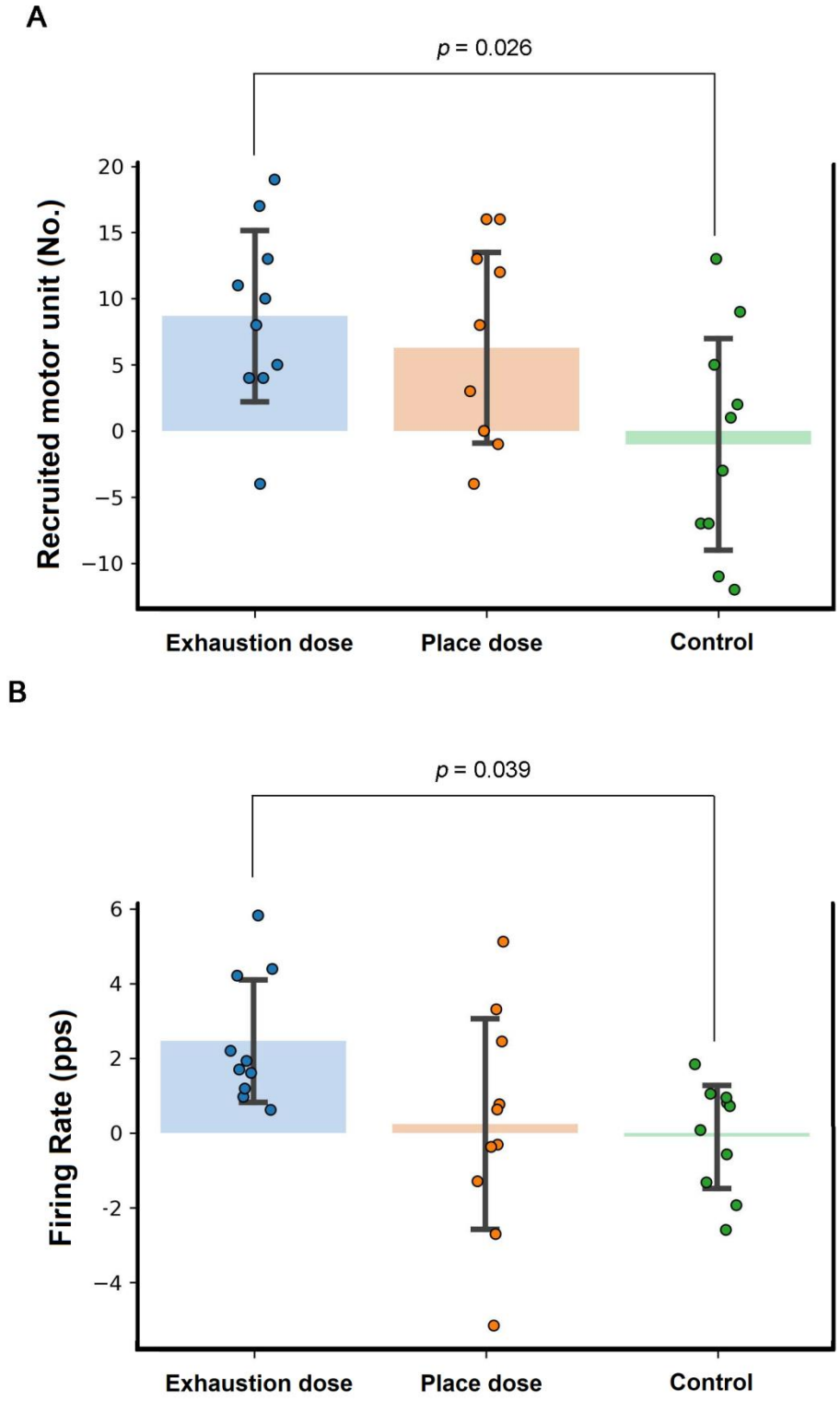

Figure 22. Cumulative fatiguing exercise comparison between experimental doses. Differences between the last bout of fatiguing exercise and basal measure are described.

Regarding the raw comparisons there was no group effect; the firing rate differed between three bouts of exercise (χ^2 = 15.8; p=0.08). The firing rate for the exhaustion fatigue dose was higher immediately after the first bout of exercise (10.4 [2.1] pps; Δ = 2.1 pps; p = 0.019) and after the last bout of exercise (10.6 [2.8] pps; Δ = 2.3 pps; p = 0.028) compared to the basal measurement (8.3 [2.3] pps). The motor unit recruitment was not different between the three bouts of exercise (χ^2 = 7.8; p=0.711). Motor unit and firing rate changes between doses are summarized in Figure 23 and Table 12.

Regarding pain perception, there was a main effect of time, region, and group (p<0.001), with interactions between time and group (p=0.012) and region and group (p<0.001). Pain perception increased from the basal to the first bout of exercise (p<0.001) and from the first to the last the third bout of exercise (p<0.001). The exhaustion fatigue dose caused pain with a significant difference between the groups (p<0.001), with pain perception higher for the lower regions of the muscle ($p < 0.01$). Table 12 includes the results of pain perception.

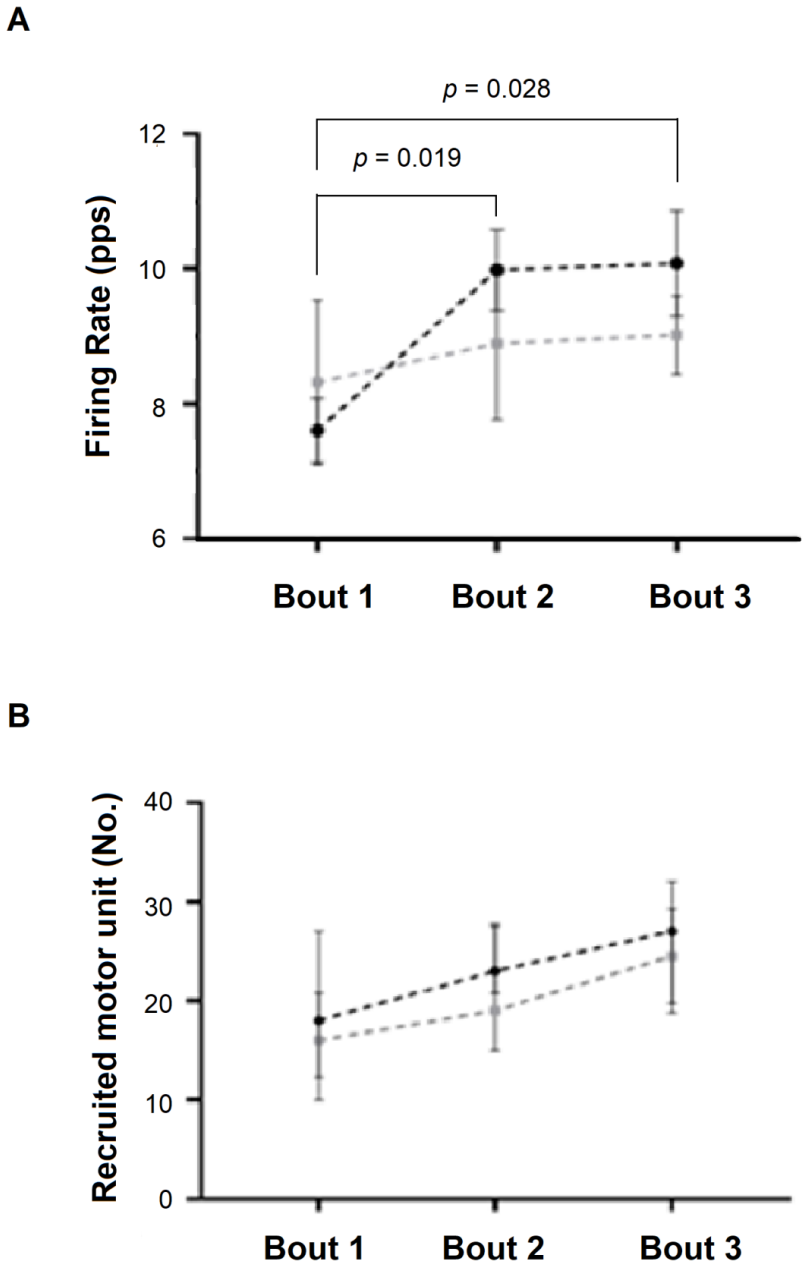

Figure 23. Time course comparison between exhaustion cumulative fatigue and placebo doses. A. Firing rate. B. Recruited motor unit.

Table 12. Recruited Motor units, firing rate, and pain perception after exhaustion fatigue dose.

Variables	Exhaution Fatigue dose			Placebo dose			Control	
	Basal	First	Last	Basal	First	Last	Basal	Last
Recruited MU number (No.)	18 [6.0]	22 [5.3]	27 [11.8]	16 [15.0]	19 [6.5]	24.5 [5.5]	17 [9.0]	17 [8.0]
Firing Rate (pps)	8.3 [2.3]	10.4 [2.1]	10.6 [2.8]	7.2 [3.6]	8.4 [4.4]	9.2 [2.4]	10.6 [4.2]	10.3 [1.2]
Pain perception								
Upper region (mm)	0.0 ± 0.0	0.3 ± 0.7	2.9 ± 1.6	0.0 ± 0.0	0.1 ± 0.3	0.6 ± 1.1	0.0 ± 0.0	0.0 ± 0.0
Middle region (mm)	0.0 ± 0.0	0.5 ± 0.8	4.2 ± 1.1	0.0 ± 0.0	0.0 ± 0.0	0.3 ± 0.7	0.0 ± 0.0	0.0 ± 0.0
Lower region (mm)	0.0 ± 0.0	1.2 ± 1.4	5.0 ± 1.6	0.0 ± 0.0	0.4 ± 0.5	1.1 ± 1.2	0.0 ± 0.0	0.0 ± 0.0

	Exhaution Fatigue dose	Placebo dose	Control
	Last – Basal measurement	Last – Basal measurement	Last – Basal measurement
Recruited MU number (No.)	8.7 ± 6.8	6.3 ± 7.3	-1.0 ± 8.5
Firing Rate (pps)	2.46 ± 1.73	0.25 ± 2.97	-0.10 ± 1.45

MU = Motor Unit. ; No. = Number; pps = Pulse per second

7.4 Discussion

In our study, the most important findings were i) a higher motor unit recruitment and firing rate under cumulative fatigue compared to controls (without muscle fatigue), ii) the firing rate remained increased under acute (one bout of fatiguing exercise in a single session) and cumulative fatigue (three bouts of fatiguing exercise in different days), and iii) cumulative fatigue condition caused an increased distal muscle pain sensation on biceps brachialis. Here, we provide insights into the main neurophysiology strategies of force generation and control after dynamic cumulative fatigue with eccentric component and distal pain sensation in the biceps brachialis in untrained young men. Our findings allow a better understanding of how the nervous system would control submaximal contractions through motor unit recruitment and firing rate. Well-established knowledge about peripheral biochemical and mechanical impairments similar to our setup (Machado et al., 2022; Powers et al., 2008; Sarker et al., 2020) may have the triggered neural adjustments for motor unit force increase under eccentric bouts of exercise. In particular, a maintained increased firing rate across the days is in coherence with findings of increased firing rate in acute isometric repeated muscle contractions (Contessa et al., 2016). This neural adjustment may serve as a mechanism of submaximal force control in the remaining active pool of motor units (Mettler et al., 2016). In our experiment, the higher motor unit recruitment and firing rate under cumulative fatigue would have obeyed a neural adjustment for muscle force control against repetitive lengthened and damaged muscle fibers. Apparently, the first dynamic exercises with an eccentric component triggered our observed neural adjustment, agreeing with previous reports (Clarkson et al., 2002).

The newly recruited motor units for cumulative and placebo doses suggest having aimed to control submaximal isometric muscle force caused by dynamic exercise with eccentric components. This is in accordance both with higher muscle activation previously summarized by literature (Dartnall et al., 2009) and with muscle activation redistribution following eccentric exercise bouts (Pincheira et al., 2021). In our setup, the higher distal fiber muscle damage factor (higher distal pain sensation (Tenberg et al., 2022) caused by cumulative fatigue dose compared to placebo dose has not affected the motor unit recruitment differently in our study (See Figure 22-B). But, both doses showed an increased motor unit recruitment compared to the control condition, which agrees with eccentric bouts of exercise

immediately and after 24h (Stožer et al., 2020; Dartnall et al., 2009). Thus, eccentric muscle contractions potentially can influence the recruitment of motor units threshold¸ likely by modification of muscle fiber length (Stožer et al., 2020) due to elastic tissue adaptation (Pincheira et al., 2018) and sarcomeres disruption (Stožer et al., 2020; Clarkson et al., 2002). According to the Equilibrium-Point hypothesis, the central nervous system controls motor unit recruitment by subthreshold depolarization of the alpha-motoneurons (Latash 2010) based on the tonic stretch reflex (λ) threshold, which directly involves the fiber muscle length (Latash 2010). Hence, the increased motor unit recruitment under repetitive dynamic exercise with eccentric component bouts suggests a neural adjustment for muscle force generation deficits.

Importantly, our findings agree with motoneuron pool excitation changes under cumulative fatigue dose, which showed an increased firing rate compared to the basal measurements (see Figure 23A) in contrast to the placebo and control conditions. The central nervous system in voluntary contractions develops a hierarchical inverse relation between firing rate and recruitment threshold (De Luca et al., 2012). Thus, our results suggest that the central nervous system adjusted the firing rate to compensate for muscle force twitch impairments, which agrees with repetitive isometric fatigue experiments (Contessa et al., 2018; Contessa et al., 2016). Consequently, cumulative fatigue dose may trigger neural adjustment to supply muscle force generation deficits, resulting in increased firing rates, newly recruited motor units, and decreased motor unit recruitment thresholds (Conwit et al., 2000). On the other hand, the increased firing rate across days in our experiment or repetitive dynamic exercise with an eccentric component suggests that the first 48h after cumulative fatigue dose with an eccentric component is not enough to recover a normal muscle activation pattern (Stožer et al., 2020). Regarding the opposed firing rate findings of literature (Rubinstein et al., 2005; Conwit et al., 2000; Fuglevand 1996), our setup targeted 40% of the MVC may have prevented the recruitment of motor units with lower firing rates of motor units with higher thresholds that can distort the group firing rate average (Contessa et al., 2016).

As a research limitation, we can mention the absence of measurements for H-reflex and M-response due to time assumptions, sEMG maps due to HD-sEMG equipment limitation, and medical image registers like ultrasonography due to monetary limitations.

7.5 Conclusion

Cumulative fatigue induced by exercising the biceps of healthy untrained men during three consecutive days increased motor unit recruitment and firing rate during the production of submaximal force. The cumulative fatigue also led to higher pain perception in the exercised region, especially at the distal portion.

This neural adjustment serves as a mechanism of submaximal force control in the remaining active pool of motor units following fatigue and muscle fiber damage after the first bout of eccentric fiber fatigue.

8 CHAPTER EIGHT – DISCUSSION

This thesis aimed to determine the electromyographical patterns in response to cumulative muscle fatigue, where we studied physiological and non-physiological factors able to change muscle activation. Specifically, we 1) identified methodological bias (windowing, slope, and parameters) in the analysis of electrical manifestations to estimate muscle fatigue and muscle activation maps, 2) determined the applicability of sEMG maps and motor unit decomposition patterns in acute and chronic adaptations, and 3) determined the Motor Unit behavior in cumulative fatigue resultant from dynamic muscle contractions. Here, our main findings were that 1) signal processing methods to estimate fatigue and activation maps are able to introduce biased electrical manifestations, 2) sEMG maps and motor unit decomposition are sensible to identify patterns in acute and chronic adaptations, and 3) increased firing rate and motor unit recruitment are the most relevant change during a three-day bout of cumulative fatigue. These findings have a deep impact on how to care for signal processing procedures during fatigue, introduce the relevance of visualization techniques in regional muscle activation (sEMG maps) for regional activation distribution, and introduce the increased firing rate as the most relevant marker of fatigue in motor unit decomposition under cumulative fatigue which can affect several daily, recreational, and physical and occupational activities.

Signal processing methods to estimate fatigue and activation maps can introduce biased electrical manifestations. On the one hand, the STFT window length and overlap selection in this thesis distort the frequency slope of myoelectrical manifestations of fatigue estimated from the median, mean, and peak frequencies, affecting the muscle fatigue estimation sensitivity. But also, the STFT parameters change the relationship between slope frequency and task failure, creating different time-series patterns when only one fatigue until exhaustion has occurred in physiological terms. On the other hand, sEMG segmentation parameters (overlap and window length) are needed to create sEMG maps. This also can distort regional muscle activation. Unfortunately, traditional signal segmentation compromises the sEMG map activation inferences and can conduct physiological misconceptions. Clinical and sport science studies did not fully consider it in the past, and nowadays, it must be important that researchers control the high-risk bias caused by sEMG signal processing.

Motor unit decomposition and sEMG maps are sensible for identifying patterns in acute and chronic adaptations. In this thesis, we were able to provide insight into the immediate enhancement of neuromuscular biofeedback during a typically restricted acute phase for research. This observational study was made after 12 days of a repaired Achilles tendon. Here, using advanced Bayesian motor unit decomposition methods, we observed how impaired motor unit properties enhanced with low-intensity contraction, which is not possible to obtain from low-resolution methods. The most relevant findings were newly recruited low-threshold motor units, increased firing rate and sEMG amplitude, and decreased recruitment motor unit threshold. On the other hand, in this thesis, we also were able to study neuromuscular adaptation under chronic conditions by sEMG. In patients with persistent plantar flexion weakness after one year of evolution, we could detect that overall sEMG activation increased when the muscle contraction levels increased and that there was a distal overactivation during plantar flexion in AT-repaired patients. After adopting bias caution over our signal processing procedures, these data analysis techniques allow us to detect altered sensorimotor adaptation under acute and chronic adaptation.

Finally, in this thesis, we were able to determine that increased firing rate and motor unit recruitment are the most relevant changes during a three-day bout of cumulative fatigue with an eccentric component. This neural adjustment may serve as a mechanism of submaximal force control in the remaining active pool of motor units. Our experiment clarifies unrevealed neural adjustment for muscle force control against repetitive lengthened and damaged muscle fibers using the Bayesian decomposition technique. These findings open an interesting issue of how the central nervous system in voluntary contractions resolves the hierarchical inverse relation between firing rate and recruitment threshold to supply muscle force generation deficits caused by cumulative fatigue and muscle damage needing new experimental setup and modeling under causal design studies.

9 CHAPTER NINE – CONCLUSION

This thesis allows us to understand better sEMG interpretations on electrical manifestations of topographical maps, motor unit decomposition, and acute and cumulative fatigue responses. Here, we conclude that i) windowing and overlap bias affect the electrical manifestations to estimate muscle fatigue and muscle activation maps, ii) sEMG maps and motor unit decomposition identify changes sEMG maps and motor unit decomposition for conditions similar to fatigue (inhibition and persistent weakness), and iii) three bouts of fatiguing exercise (cumulative muscle fatigue) trigger neurophysiological adaptations (firing rate and motor unit recruitment) to control submaximal isometric contractions.

10 CHAPTER TEN – LIMITATION OF THE THESIS

The limitations of each study were discussed at the end of each study discussion. However, regarding the thesis limitation, I recognized the CORONAVIRUS pandemic's was the main thesis limitation. Due to country border restrictions for foreigners, I was unable to visit my supervisor and the laboratory between March 2020 and September 2022. The other main limitation was the restriction and population fear to be measured due to the high risk of virus contamination between participants and researchers after August 2021. It resulted in a very restricted time frame to conduct the procedures to collect data for a significant part of our project (from August 2021 and December 2022). From January 2023 to August 2023, all thesis data were analyzed and written. My last limitation was being forced to finalize three jobs (Universidad de los Andes, Clinica Santa Maria, and Pontificia Universidad Catolica de Chile) during the all P.hD program because of their limited vision of studying and researching in an undeveloped country.

REFERENCES

Afsharipour, B., S. Soedirdjo, and R. Merletti. 2019. “Two-Dimensional Surface EMG: The Effects of Electrode Size, Interelectrode Distance and Image Truncation.” *Biomedical Signal Processing and Control* 49 (March): 298–307. https://doi.org/10.1016/j.bspc.2018.12.001.

Akobeng, Anthony K. 2016. “Understanding Type I and Type II Errors, Statistical Power and Sample Size.” *Acta Paediatrica (Oslo, Norway: 1992)* 105 (6): 605–9. https://doi.org/10.1111/apa.13384.

Alghannam, Gonzalez, and Betts. 2018. “Restoration of Muscle Glycogen and Functional Capacity: Role of Post-Exercise Carbohydrate and Protein Co-Ingestion.” *Nutrients* 10 (2). https://doi.org/10.3390/nu10020253.

Ali, Mohammed, Mark W. Jones, Xianghua Xie, and Mark Williams. 2019. “TimeCluster: Dimension Reduction Applied to Temporal Data for Visual Analytics.” *The Visual Computer* 35 (6): 1013–26. https://doi.org/10.1007/s00371-019-01673-y.

Allen, Jones, Tsay, Morgan, and Proske. 2018. “Muscle Damage Produced by Isometric Contractions in Human Elbow Flexors.” *Journal of Applied Physiology (Bethesda, Md.: 1985)* 124 (2): 388–99. https://doi.org/10.1152/japplphysiol.00535.2017.

Allman, and Rice. 2001. “Incomplete Recovery of Voluntary Isometric Force after Fatigue Is Not Affected by Old Age.” *Muscle & Nerve* 24 (9): 1156–67. https://doi.org/10.1002/mus.1127.

Al-Urzi, Muntadhir, Seth O’Neil, Paul Watson, and Charlotte Kelly. n.d. “Reliability of Isokinetic Dynamometry of the Plantarflexors in Knee Flexion and Extension,” Physiotherapy Practice and Research, 38 (1): 49–57.

Ament, W., G. J. Bonga, A. L. Hof, and G. J. Verkerke. 1993. “EMG Median Power Frequency in an Exhausting Exercise.” *Journal of Electromyography and Kinesiology: Official Journal of the International Society of Electrophysiological Kinesiology* 3 (4): 214–20. https://doi.org/10.1016/1050-6411(93)90010-T.

Andrews, Almeida, and Corrotte. 2014. “Damage Control: Cellular Mechanisms of Plasma Membrane Repair.” *Trends in Cell Biology* 24 (12): 734–42. https://doi.org/10.1016/j.tcb.2014.07.008.

Angelova, Silvija, Simeon Ribagin, Rositsa Raikova, and Ivanka Veneva. 2018. “Power Frequency Spectrum Analysis of Surface EMG Signals of Upper Limb Muscles during Elbow Flexion - A Comparison between Healthy Subjects and Stroke Survivors.” *Journal of Electromyography and Kinesiology: Official Journal of the International Society of Electrophysiological Kinesiology* 38 (February): 7–16. https://doi.org/10.1016/j.jelekin.2017.10.013.

Avancini, Carolina, Liliam F. de Oliveira, Luciano L. Menegaldo, and Taian M. Vieira. 2015. “Variations in the Spatial Distribution of the Amplitude of Surface Electromyograms Are Unlikely Explained by Changes in the Length of Medial Gastrocnemius Fibres with Knee Joint Angle.” *PloS One* 10 (5): e0126888. https://doi.org/10.1371/journal.pone.0126888.

Basmajian, john, and Carlo de Luca. 1985. *Muscles Alive: Their Functions Revealed by Electromyography*. 5th ed. Baltimore: Williams & Wilkins.

Baxter, Josh R., Daniel C. Farber, and Michael W. Hast. 2019. “Plantarflexor Fiber and Tendon Slack Length Are Strong Determinates of Simulated Single-Leg Heel Raise Height.” *Journal of Biomechanics* 86 (March): 27–33. https://doi.org/10.1016/j.jbiomech.2019.01.035.

Beniczky, Sándor, and Donald L. Schomer. 2020. “Electroencephalography: Basic Biophysical and Technological Aspects Important for Clinical Applications.” *Epileptic Disorders: International Epilepsy Journal with Videotape* 22 (6): 697–715. https://doi.org/10.1684/epd.2020.1217.

Botter, Alberto, and Taian M. Vieira. 2015. “Filtered Virtual Reference: A New Method for the Reduction of Power Line Interference With Minimal Distortion of Monopolar Surface EMG.” *IEEE Transactions on Bio-Medical Engineering* 62 (11): 2638–47. https://doi.org/10.1109/TBME.2015.2438335.

Bressel, Eadric, Brian T. Larsen, Peter J. McNair, and John Cronin. 2004. “Ankle Joint Proprioception and Passive Mechanical Properties of the Calf Muscles after an Achilles Tendon Rupture: A Comparison with Matched Controls.” *Clinical Biomechanics (Bristol, Avon)* 19 (3): 284–91. https://doi.org/10.1016/j.clinbiomech.2003.12.008.

Brorsson, Annelie, Richard W. Willy, Roy Tranberg, and Karin Grävare Silbernagel. 2017. “Heel-Rise Height Deficit 1 Year After Achilles Tendon Rupture Relates to Changes in Ankle Biomechanics 6 Years After Injury.” *The American Journal of Sports Medicine* 45 (13): 3060–68. https://doi.org/10.1177/0363546517717698.

Brown, Matthew, and Matthew Godman. 2011. “Simple Pattern Recognition via Image Moments.” *2011*, 7.

Calderón, Bolaños, and Caputo. 2014. “The Excitation–Contraction Coupling Mechanism in Skeletal Muscle.” *Biophysical Reviews* 6 (1): 133–60. https://doi.org/10.1007/s12551-013-0135-x.

Campanini, Isabella, Catherine Disselhorst-Klug, William Z. Rymer, and Roberto Merletti. 2020. “Surface EMG in Clinical Assessment and Neurorehabilitation: Barriers Limiting Its Use.” *Frontiers in Neurology* 11: 934. https://doi.org/10.3389/fneur.2020.00934.

Campanini, Merlo, Disselhorst-Klug, Mesin, Muceli, and Merletti. 2022. “Fundamental Concepts of Bipolar and High-Density Surface EMG Understanding and Teaching for Clinical, Occupational, and Sport Applications: Origin, Detection, and Main Errors.” *Sensors (Basel, Switzerland)* 22 (11): 4150. https://doi.org/10.3390/s22114150.

Carmont, Michael R., Karin Grävare Silbernagel, Annelie Brorsson, Nicklas Olsson, Nicola Maffulli, and Jon Karlsson. 2015. “The Achilles Tendon Resting Angle as an Indirect Measure of Achilles Tendon Length Following Rupture, Repair, and Rehabilitation.” *Asia-Pacific Journal of Sports Medicine, Arthroscopy, Rehabilitation and Technology* 2 (2): 49–55. https://doi.org/10.1016/j.asmart.2014.12.002.

Carpentier, Duchateau, and Hainaut. 2001. “Motor Unit Behaviour and Contractile Changes during Fatigue in the Human First Dorsal Interosseus.” *The Journal of Physiology* 534 (Pt 3): 903–12. https://doi.org/10.1111/j.1469-7793.2001.00903.x.

Carroll, Taylor, and Gandevia. 2017. “Recovery of Central and Peripheral Neuromuscular Fatigue after Exercise.” *Journal of Applied Physiology (Bethesda, Md.: 1985)* 122 (5): 1068–76. https://doi.org/10.1152/japplphysiol.00775.2016.

Cashaback, Joshua G. A., Tyler Cluff, and Jim R. Potvin. 2013. “Muscle Fatigue and Contraction Intensity Modulates the Complexity of Surface Electromyography.” *Journal of Electromyography and Kinesiology: Official Journal of the International Society of Electrophysiological Kinesiology* 23 (1): 78–83. https://doi.org/10.1016/j.jelekin.2012.08.004.

Chang, Yu-Jen, and Kornelia Kulig. 2015. “The Neuromechanical Adaptations to Achilles Tendinosis.” *The Journal of Physiology* 593 (15): 3373–87. https://doi.org/10.1113/JP270220.

Cheng, Jude, and Lanner. 2020. “Intramuscular Mechanisms of Overtraining.” *Redox Biology* 35 (August): 101480. https://doi.org/10.1016/j.redox.2020.101480.

Cho, Ki Hun, Hwang Jae Lee, and Wan Hee Lee. 2014. “Reliability of Rehabilitative Ultrasound Imaging for the Medial Gastrocnemius Muscle in Poststroke Patients.” *Clinical Physiology and Functional Imaging* 34 (1): 26–31. https://doi.org/10.1111/cpf.12060.

Cifrek, Mario, Vladimir Medved, Stanko Tonković, and Sasa Ostojić. 2009. “Surface EMG Based Muscle Fatigue Evaluation in Biomechanics.” *Clinical Biomechanics (Bristol, Avon)* 24 (4): 327–40. https://doi.org/10.1016/j.clinbiomech.2009.01.010.

Cifrek, Mario, Stanko Tonković, and Vladimir Medved. 2000. “Measurement and Analysis of Surface Myoelectric Signals during Fatigued Cyclic Dynamic Contractions.” *Measurement* 27 (2): 85–92. https://doi.org/10.1016/S0263-2241(99)00059-7.

Clarkson, and Hubal. 2002. “Exercise-Induced Muscle Damage in Humans.” *American Journal of Physical Medicine & Rehabilitation* 81 (11 Suppl): S52-69. https://doi.org/10.1097/00002060-200211001-00007.

Contessa, Adam, and De Luca. 2009. “Motor Unit Control and Force Fluctuation during Fatigue.” *Journal of Applied Physiology* 107 (1): 235–43. https://doi.org/10.1152/japplphysiol.00035.2009.

Contessa, De Luca, and Kline. 2016. “The Compensatory Interaction between Motor Unit Firing Behavior and Muscle Force during Fatigue.” *Journal of Neurophysiology* 116 (4): 1579–85. https://doi.org/10.1152/jn.00347.2016.

Contessa, Letizi, De Luca, and Kline. 2018. “Contribution from Motor Unit Firing Adaptations and Muscle Coactivation during Fatigue.” *Journal of Neurophysiology* 119 (6): 2186–93. https://doi.org/10.1152/jn.00766.2017.

Conwit, Stashuk, Suzuki, Lynch, Schrager, and Metter. 2000. “Fatigue Effects on Motor Unit Activity during Submaximal Contractions.” *Archives of Physical Medicine and Rehabilitation* 81 (9): 1211–16. https://doi.org/10.1053/apmr.2000.6975.

Costa, Marcelo V., Lucas A. Pereira, Ricardo S. Oliveira, Rafael E. Pedro, Thiago V. Camata, Taufik Abrao, Maria A. C. Brunetto, and Leandro R. Altimari. 2010. “Fourier and Wavelet Spectral Analysis of EMG Signals in Maximal Constant Load Dynamic Exercise.” *Annual International Conference of the IEEE Engineering in Medicine and Biology Society. IEEE Engineering in Medicine and Biology Society. Annual International Conference* 2010: 4622–25. https://doi.org/10.1109/IEMBS.2010.5626474.

Cowley, Dingwell, and Gates. 2014. “Effects of Local and Widespread Muscle Fatigue on Movement Timing.” *Experimental Brain Research* 232 (12): 3939–48. https://doi.org/10.1007/s00221-014-4020-z.

Cresswell, A. G., W. N. Löscher, and A. Thorstensson. 1995. “Influence of Gastrocnemius Muscle Length on Triceps Surae Torque Development and Electromyographic Activity in Man.” *Experimental Brain Research* 105 (2): 283–90. https://doi.org/10.1007/BF00240964.

Cronin, N. J., S. Kumpulainen, T. Joutjärvi, T. Finni, and H. Piitulainen. 2015. “Spatial Variability of Muscle Activity during Human Walking: The Effects of Different EMG Normalization Approaches.” *Neuroscience* 300 (August): 19–28. https://doi.org/10.1016/j.neuroscience.2015.05.003.

Cudicio, Alessandro, Eduardo Martinez-Valdes, Marta Cogliati, Claudio Orizio, and Francesco Negro. 2022. “The Force-Generation Capacity of the Tibialis Anterior Muscle at Different Muscle-Tendon Lengths Depends on Its Motor Unit Contractile Properties.” *European Journal of Applied Physiology* 122 (2): 317–30. https://doi.org/10.1007/s00421-021-04829-8.

Dartnall, Rogasch, Nordstrom, and Semmler. 2009. “Eccentric Muscle Damage Has Variable Effects on Motor Unit Recruitment Thresholds and Discharge Patterns in Elbow Flexor Muscles.” *Journal of Neurophysiology* 102 (1): 413–23. https://doi.org/10.1152/jn.91285.2008.

De la Fuente, C., C. Cruz-Montecinos, CJ De la Fuente, R Peña y Lillo, C. Chamorro, and H. Henriquez. 2018. “Early Short-Term Recovery of Single-Leg Heel Rise and ATRS after Achilles Tenorrhaphy: Cluster Analysis.” *Asian Journal of Sports Medicine* 9 (1): e67661. https://doi.org/10.5812/asjsm.67661.

De la Fuente, Carlos, Gabriel Carreño, Miguel Soto, Hugo Marambio, and Hugo Henríquez. 2017. “Clinical Failure after Dresden Repair of Mid-Substance Achilles Tendon Rupture: Human Cadaveric Testing.” *Knee Surgery, Sports Traumatology, Arthroscopy* 25 (6): 1849–56. https://doi.org/10.1007/s00167-016-4182-2.

De la Fuente, Carlos De, Carlos Cruz-Montecinos, Helen L. Schimidt, Hugo Henríquez, Sebastián Ruidiaz, and Felipe P. Carpes. 2017. “Biomechanical Properties of Different Techniques Used in Vitro for Suturing Mid-Substance Achilles Tendon Ruptures.” *Clinical Biomechanics (Bristol, Avon)* 50 (December): 78–83. https://doi.org/10.1016/j.clinbiomech.2017.10.008.

De la Fuente, Carlos, Hugo Henriquez, Michael R. Carmont, Javiera Huincahue, Tamara Paredes, María Tapia, Juan Pablo Araya, Nicolás Díaz, and Felipe P. Carpes. 2021. “Do the Heel-Rise Test and Isometric Strength Improve after Achilles Tendon Repair Using Dresden Technique?” *Foot and Ankle Surgery: Official Journal of the European Society of Foot and Ankle Surgeons*, January. https://doi.org/10.1016/j.fas.2021.01.007.

De la Fuente, Carlos I., Roberto Peña Y. Lillo, Rodrigo Ramirez-Campillo, Pablo Ortega-Auriol, Mauricio Delgado, Joel Alvarez-Ruf, and Gabriel Carreño. 2016. “Medial Gastrocnemius Myotendinous Junction Displacement and Plantar-Flexion Strength in Patients Treated With Immediate Rehabilitation After Achilles Tendon Repair.” *Journal of Athletic Training* 51 (12): 1013–21. https://doi.org/10.4085/1062-6050-51.12.23.

De la Fuente, Carlos, Eduardo Martinez-Valdes, Carlos Cruz-Montecinos, Rodrigo Guzman-Venegas, David Arriagada, Roberto Peña Y Lillo, Hugo Henríquez, and Felipe P. Carpes. 2018. “Changes in the Ankle Muscles Co-Activation Pattern after 5 Years Following Total Ankle Joint Replacement.” *Clinical Biomechanics (Bristol, Avon)* 59 (November): 130–35. https://doi.org/10.1016/j.clinbiomech.2018.09.019.

De la Fuente, Carlos, Eduardo Martinez-Valdes, Jose Ignacio Priego-Quesada, Alejandro Weinstein, Oscar Valencia, Marcos R. Kunzler, Joel Alvarez-Ruf, and Felipe P. Carpes. 2021. “Understanding the Effect of Window Length and Overlap for Assessing SEMG in Dynamic Fatiguing Contractions: A Non-Linear Dimensionality Reduction and Clustering.” *Journal of Biomechanics* 125 (August): 110598. https://doi.org/10.1016/j.jbiomech.2021.110598.

De la Fuente, Carlos, Eduardo Martinez-Valdes, Emmanuel S. da Rocha, Jeam M. Geremia, Marco A. Vaz, and Felipe P. Carpes. 2023. “Distal Overactivation of Gastrocnemius Medialis in Persistent Plantarflexion Weakness Following Achilles Tendon Repair.” *Journal of Biomechanics* 148 (February): 111459. https://doi.org/10.1016/j.jbiomech.2023.111459.

De la Fuente, Carlos, Roberto Peña y Lillo, Gabriel Carreño, and Hugo Marambio. 2016. “Prospective Randomized Clinical Trial of Aggressive Rehabilitation after Acute Achilles Tendon Ruptures Repaired with Dresden Technique.” *Foot (Edinburgh, Scotland)* 26 (March): 15–22. https://doi.org/10.1016/j.foot.2015.10.003.

De Luca. 1979. “Physiology and Mathematics of Myoelectric Signals.” *IEEE Transactions on Biomedical Engineering* BME-26 (6): 313–25. https://doi.org/10.1109/TBME.1979.326534.

De Luca, Carlo J., Alexander Adam, Robert Wotiz, L. Donald Gilmore, and S. Hamid Nawab. 2006. “Decomposition of Surface EMG Signals.” *Journal of Neurophysiology* 96 (3): 1646–57. https://doi.org/10.1152/jn.00009.2006.

De Luca, Carlo J., Mikhail Kuznetsov, L. Donald Gilmore, and Serge H. Roy. 2012. “Inter-Electrode Spacing of Surface EMG Sensors: Reduction of Crosstalk Contamination during Voluntary Contractions.” *Journal of Biomechanics* 45 (3): 555–61. https://doi.org/10.1016/j.jbiomech.2011.11.010.

De Luca, and Contessa. 2012. “Hierarchical Control of Motor Units in Voluntary Contractions.” *Journal of Neurophysiology* 107 (1): 178–95. https://doi.org/10.1152/jn.00961.2010.

Del Vecchio, Alessandro, Francesco Negro, Francesco Felici, and Dario Farina. 2017. “Associations between Motor Unit Action Potential Parameters and Surface EMG Features.” *Journal of Applied Physiology (Bethesda, Md.: 1985)* 123 (4): 835–43. https://doi.org/10.1152/japplphysiol.00482.2017.

De-la-Cruz-Torres, Blanca, Irene Barrera-García-Martín, Mónica De la Cueva-Reguera, María Bravo-Aguilar, María Blanco-Morales, Emmanuel Navarro-Flores, Carlos Romero-Morales, and Vanesa Abuín-Porras. 2020. “Does Function Determine the Structure? Changes in Flexor Hallucis Longus Muscle and the Associated Performance Related to Dance Modality: A Cross-Sectional Study.” *Medicina (Kaunas, Lithuania)* 56 (4): 186. https://doi.org/10.3390/medicina56040186.

Dorrity, Michael W., Lauren M. Saunders, Christine Queitsch, Stanley Fields, and Cole Trapnell. 2020. “Dimensionality Reduction by UMAP to Visualize Physical and Genetic Interactions.” *Nature Communications* 11 (March). https://doi.org/10.1038/s41467-020-15351-4.

Drazan, John F., Todd J. Hullfish, and Josh R. Baxter. 2019. “Muscle Structure Governs Joint Function: Linking Natural Variation in Medial Gastrocnemius Structure with Isokinetic Plantar Flexor Function.” *Biology Open* 8 (12). https://doi.org/10.1242/bio.048520.

Eken, Maaike M., Siri M. Braendvik, Ellen Marie Bardal, Han Houdijk, Annet J. Dallmeijer, and Karin Roeleveld. 2019. “Lower Limb Muscle Fatigue during Walking in Children with Cerebral Palsy.” *Developmental Medicine and Child Neurology* 61 (2): 212–18. https://doi.org/10.1111/dmcn.14002.

Enoka, Roger M, and Jacques Duchateau. 2008. “Muscle Fatigue: What, Why and How It Influences Muscle Function.” *The Journal of Physiology* 586 (Pt 1): 11–23. https://doi.org/10.1113/jphysiol.2007.139477.

Enoka, Roger M., and Jacques Duchateau. 2017. “Rate Coding and the Control of Muscle Force.” *Cold Spring Harbor Perspectives in Medicine* 7 (10): a029702. https://doi.org/10.1101/cshperspect.a029702.

Espírito Santo, Rafaela Cavalheiro do, Marcelo Gava Pompermayer, Rodrigo Rico Bini, Vanessa Olszewski, Elton Gonçalves Teixeira, Rafael Chakr, Ricardo Machado Xavier, and Claiton Viegas Brenol. 2018. “Neuromuscular Fatigue Is Weakly Associated with Perception of Fatigue and Function in Patients with Rheumatoid Arthritis.” *Rheumatology International* 38 (3): 415–23. https://doi.org/10.1007/s00296-017-3894-z.

Falla, Deborah, Corrado Cescon, Rene Lindstroem, and Marco Barbero. 2017. “Muscle Pain Induces a Shift of the Spatial Distribution of Upper Trapezius Muscle Activity During a Repetitive Task: A Mechanism for Perpetuation of Pain With Repetitive Activity?”

The Clinical Journal of Pain 33 (11): 1006–13. https://doi.org/10.1097/AJP.0000000000000513.

Falla, Deborah, and Dario Farina. 2007. "Periodic Increases in Force during Sustained Contraction Reduce Fatigue and Facilitate Spatial Redistribution of Trapezius Muscle Activity." *Experimental Brain Research* 182 (1): 99–107. https://doi.org/10.1007/s00221-007-0974-4.

Farber. 1990. "The Role of Calcium Ions in Toxic Cell Injury." *Environmental Health Perspectives* 84 (March): 107–11.

Farina, Dario, Frédéric Leclerc, Lars Arendt-Nielsen, Olivier Buttelli, and Pascal Madeleine. 2008. "The Change in Spatial Distribution of Upper Trapezius Muscle Activity Is Correlated to Contraction Duration." *Journal of Electromyography and Kinesiology: Official Journal of the International Society of Electrophysiological Kinesiology* 18 (1): 16–25. https://doi.org/10.1016/j.jelekin.2006.08.005.

Farina, Merletti, and Enoka. 2014. "The Extraction of Neural Strategies from the Surface EMG: An Update." *Journal of Applied Physiology (Bethesda, Md.: 1985)* 117 (11): 1215–30. https://doi.org/10.1152/japplphysiol.00162.2014.

Farina, and Negro. 2015. "Common Synaptic Input to Motor Neurons, Motor Unit Synchronization, and Force Control." *Exercise and Sport Sciences Reviews* 43 (1): 23–33. https://doi.org/10.1249/JES.0000000000000032.

Farina, Schulte, Merletti, Rau, and Disselhorst-Klug. 2003. "Single Motor Unit Analysis from Spatially Filtered Surface Electromyogram Signals. Part I: Spatial Selectivity." *Medical & Biological Engineering & Computing* 41 (3): 330–37. https://doi.org/10.1007/BF02348439.

Ferguson, Christopher J. 2009. "An Effect Size Primer: A Guide for Clinicians and Researchers." *Professional Psychology: Research and Practice* 40 (5): 532–38. https://doi.org/10.1037/a0015808.

Finni, T., M. Bernabei, G. C. Baan, W. Noort, C. Tijs, and H. Maas. 2018. "Non-Uniform Displacement and Strain between the Soleus and Gastrocnemius Subtendons of Rat Achilles Tendon." *Scandinavian Journal of Medicine & Science in Sports* 28 (3): 1009–17. https://doi.org/10.1111/sms.13001.

Finni, Taija, John A. Hodgson, Alex M. Lai, V. Reggie Edgerton, and Shantanu Sinha. 2006. "Muscle Synergism during Isometric Plantarflexion in Achilles Tendon Rupture Patients and in Normal Subjects Revealed by Velocity-Encoded Cine Phase-Contrast MRI." *Clinical Biomechanics (Bristol, Avon)* 21 (1): 67–74. https://doi.org/10.1016/j.clinbiomech.2005.08.007.

Flament, D, and T Ebner. 1996. "The Cerebellum as Comparator: Increases in Cerebellar Activity during Motor Learning May Reflect Its Role as Part of an Error Detection/Correction Mechanism." *Behavioral and Brain Sciences*, 1996.

Fong, Tsorng-Harn, Chin-Ho Wong, Jeng-Yee Lin, Chuh-Kai Liao, Li-Yung Ho, and Feng-Chou Tsai. 2010. "Correction of Asymmetric Calf Hypertrophy with Differential Selective Neurectomy." *Aesthetic Plastic Surgery* 34 (3): 335–39. https://doi.org/10.1007/s00266-009-9445-6.

Franch, Gabriele, Giuseppe Jurman, Luca Coviello, Marta Pendesini, and Cesare Furlanello. 2019. "MASS-UMAP: Fast and Accurate Analog Ensemble Search in Weather Radar Archives." *Remote Sensing* 11 (24): 2922. https://doi.org/10.3390/rs11242922.

Freedman, Benjamin R., Nabeel S. Salka, Tyler R. Morris, Pankti R. Bhatt, Adam M. Pardes, Joshua A. Gordon, Courtney A. Nuss, et al. 2017. "Temporal Healing of Achilles Tendons After Injury in Rodents Depends on Surgical Treatment and Activity." *The Journal of the American Academy of Orthopaedic Surgeons* 25 (9): 635–47. https://doi.org/10.5435/JAAOS-D-16-00620.

Fuente, C. de la, G. Carreño-Zillmann, H. Marambio, and H. Henríquez. 2016. “Is the Dresden Technique a Mechanical Design of Choice Suitable for the Repair of Middle Third Achilles Tendon Ruptures? A Biomechanical Study.” *Revista Espanola De Cirugia Ortopedica Y Traumatologia* 60 (5): 279–85. https://doi.org/10.1016/j.recot.2016.06.004.

Fuglevand. 1996. “Neural Aspects of Fatigue.” *Neuroscientist* 2 (July): 203–6. https://doi.org/10.1177/107385849600200407.

Fujisawa, Tamaki, Yamada, and Matsuoka. 2017. “Influence of Gender on Muscle Fatigue during Dynamic Knee Contractions.” *Physical Therapy Research* 20 (1): 1–8. https://doi.org/10.1298/ptr.E9889.

Gallina, Alessio, S. Jayne Garland, and James M. Wakeling. 2018. “Identification of Regional Activation by Factorization of High-Density Surface EMG Signals: A Comparison of Principal Component Analysis and Non-Negative Matrix Factorization.” *Journal of Electromyography and Kinesiology: Official Journal of the International Society of Electrophysiological Kinesiology* 41 (August): 116–23. https://doi.org/10.1016/j.jelekin.2018.05.002.

Gandevia. 2001. “Spinal and Supraspinal Factors in Human Muscle Fatigue.” *Physiological Reviews* 81 (4): 1725–89. https://doi.org/10.1152/physrev.2001.81.4.1725.

Geremia, Jeam Marcel, Maarten Frank Bobbert, Mayra Casa Nova, Rafael Duvelius Ott, Fernando de Aguiar Lemos, Raquel de Oliveira Lupion, Viviane Bortoluzzi Frasson, and Marco Aurélio Vaz. 2015. “The Structural and Mechanical Properties of the Achilles Tendon 2 Years after Surgical Repair.” *Clinical Biomechanics (Bristol, Avon)* 30 (5): 485–92. https://doi.org/10.1016/j.clinbiomech.2015.03.005.

Géron, Aurélien. 2019. *Hands-On Machine Learning with Scikit-Learn, Keras, and TensorFlow.* 2nd Edition. O’Reilly Media, Inc.

Ghaderi, Parviz, and Hamid R. Marateb. 2017. “Muscle Activity Map Reconstruction from High Density Surface EMG Signals With Missing Channels Using Image Inpainting and Surface Reconstruction Methods.” *IEEE Transactions on Bio-Medical Engineering* 64 (7): 1513–23. https://doi.org/10.1109/TBME.2016.2603463.

González-Izal, M., A. Malanda, I. Navarro-Amézqueta, E. M. Gorostiaga, F. Mallor, J. Ibañez, and M. Izquierdo. 2010. “EMG Spectral Indices and Muscle Power Fatigue during Dynamic Contractions.” *Journal of Electromyography and Kinesiology: Official Journal of the International Society of Electrophysiological Kinesiology* 20 (2): 233–40. https://doi.org/10.1016/j.jelekin.2009.03.011.

Guzmán-Venegas, Rodrigo A., Jorge L. Biotti Picand, and Francisco J. Berral de la Rosa. 2015. “Functional Compartmentalization of the Human Superficial Masseter Muscle.” *PloS One* 10 (2): e0116923. https://doi.org/10.1371/journal.pone.0116923.

Hamrick, Mark W., Meghan E. McGee-Lawrence, and Danielle M. Frechette. 2016. “Fatty Infiltration of Skeletal Muscle: Mechanisms and Comparisons with Bone Marrow Adiposity.” *Frontiers in Endocrinology* 7. https://doi.org/10.3389/fendo.2016.00069.

Hart, Joseph M., Brian Pietrosimone, Jay Hertel, and Christopher D. Ingersoll. 2010. “Quadriceps Activation Following Knee Injuries: A Systematic Review.” *Journal of Athletic Training* 45 (1): 87–97. https://doi.org/10.4085/1062-6050-45.1.87.

Hawkes, David, Michael Grant, Jessica McMahon, Ian Horsley, and Omid Khaiyat. 2018. “Can Grip Strength Be Used as a Surrogate Marker to Monitor Recovery from Shoulder Fatigue?” *Journal of Electromyography and Kinesiology: Official Journal of the International Society of Electrophysiological Kinesiology* 41 (August): 139–46. https://doi.org/10.1016/j.jelekin.2018.06.002.

Heckman, C. J., Michael Johnson, Carol Mottram, and Jenna Schuster. 2008. “Persistent Inward Currents in Spinal Motoneurons and Their Influence on Human Motoneuron

Firing Patterns." *The Neuroscientist: A Review Journal Bringing Neurobiology, Neurology and Psychiatry* 14 (3): 264–75. https://doi.org/10.1177/1073858408314986.

Hegyi, András, Dániel Csala, Annamária Péter, Taija Finni, and Neil J. Cronin. 2019. "High-Density Electromyography Activity in Various Hamstring Exercises." *Scandinavian Journal of Medicine & Science in Sports* 29 (1): 34–43. https://doi.org/10.1111/sms.13303.

Heikkinen, Juuso, Iikka Lantto, Tapio Flinkkila, Pasi Ohtonen, Jaakko Niinimaki, Pertti Siira, Vesa Laine, and Juhana Leppilahti. 2017. "Soleus Atrophy Is Common After the Nonsurgical Treatment of Acute Achilles Tendon Ruptures: A Randomized Clinical Trial Comparing Surgical and Nonsurgical Functional Treatments." *The American Journal of Sports Medicine* 45 (6): 1395–1404. https://doi.org/10.1177/0363546517694610.

Hennig, Matthias H. 2013. "Theoretical Models of Synaptic Short Term Plasticity." *Frontiers in Computational Neuroscience* 7 (April): 45. https://doi.org/10.3389/fncom.2013.00045.

Hermens, H. J., B. Freriks, C. Disselhorst-Klug, and G. Rau. 2000. "Development of Recommendations for SEMG Sensors and Sensor Placement Procedures." *Journal of Electromyography and Kinesiology: Official Journal of the International Society of Electrophysiological Kinesiology* 10 (5): 361–74. https://doi.org/10.1016/s1050-6411(00)00027-4.

Hill, Ethan C., Terry J. Housh, Cory M. Smith, Joshua L. Keller, Richard J. Schmidt, and Glen O. Johnson. 2018. "Sex- and Mode-Specific Responses to Eccentric Muscle Fatigue." *International Journal of Sports Medicine* 39 (12): 893–901. https://doi.org/10.1055/a-0664-0733.

Hody, Croisier, Bury, Rogister, and Leprince. 2019. "Eccentric Muscle Contractions: Risks and Benefits." *Frontiers in Physiology* 10 (May). https://doi.org/10.3389/fphys.2019.00536.

Horita, T., and T. Ishiko. 1987. "Relationships between Muscle Lactate Accumulation and Surface EMG Activities during Isokinetic Contractions in Man." *European Journal of Applied Physiology and Occupational Physiology* 56 (1): 18–23. https://doi.org/10.1007/BF00696370.

Horn, and Jaiswal. 2018. "Cellular Mechanisms and Signals That Coordinate Plasma Membrane Repair." *Cellular and Molecular Life Sciences: CMLS* 75 (20): 3751–70. https://doi.org/10.1007/s00018-018-2888-7.

Huang, Xuan, Lei Wu, and Yinsong Ye. 2019. "A Review on Dimensionality Reduction Techniques." *International Journal of Pattern Recognition and Artificial Intelligence* 33 (10): 1950017. https://doi.org/10.1142/S0218001419500174.

Huijing, Peter A., Nicol C. Voermans, Guus C. Baan, Tinelies E. Busé, Baziel G. M. van Engelen, and Arnold de Haan. 2010. "Muscle Characteristics and Altered Myofascial Force Transmission in Tenascin-X-Deficient Mice, a Mouse Model of Ehlers-Danlos Syndrome." *Journal of Applied Physiology (Bethesda, Md.: 1985)* 109 (4): 986–95. https://doi.org/10.1152/japplphysiol.00723.2009.

Hullfish, Todd J., Kathryn M. O'Connor, and Josh R. Baxter. 2018. "Gastrocnemius Fascicles Are Shorter and More Pennate Immediately Following Acute Achilles Tendon Rupture." *BioRxiv*, October, 445569. https://doi.org/10.1101/445569.

Hullfish, Todd J., Kathryn M. O'Connor, and Josh R. Baxter. 2019. "Medial Gastrocnemius Muscle Remodeling Correlates with Reduced Plantarflexor Kinetics 14 Weeks Following Achilles Tendon Rupture." *Journal of Applied Physiology (Bethesda, Md.: 1985)* 127 (4): 1005–11. https://doi.org/10.1152/japplphysiol.00255.2019.

Jamali, A. A., P. Afshar, R. A. Abrams, and R. L. Lieber. 2000. “Skeletal Muscle Response to Tenotomy.” *Muscle & Nerve* 23 (6): 851–62. https://doi.org/10.1002/(sici)1097-4598(200006)23:6<851::aid-mus3>3.0.co;2-a.

Jandacka, Daniel, Julia Freedman Silvernail, Jaroslav Uchytil, David Zahradnik, Roman Farana, and Joseph Hamill. 2017. “Do Athletes Alter Their Running Mechanics after an Achilles Tendon Rupture?” *Journal of Foot and Ankle Research* 10: 53. https://doi.org/10.1186/s13047-017-0235-0.

Jeon, Hohyub, Yongchul Jung, Seongjoo Lee, and Yunho Jung. 2020. “Area-Efficient Short-Time Fourier Transform Processor for Time–Frequency Analysis of Non-Stationary Signals.” *Applied Sciences* 10 (20): 7208. https://doi.org/10.3390/app10207208.

Jeon, Sunggun, William M. Miller, and Xin Ye. 2020. “A Comparison of Motor Unit Control Strategies between Two Different Isometric Tasks.” *International Journal of Environmental Research and Public Health* 17 (8): 2799. https://doi.org/10.3390/ijerph17082799.

Jones, Griffiths, and Mellalieu. 2017. “Training Load and Fatigue Marker Associations with Injury and Illness: A Systematic Review of Longitudinal Studies.” *Sports Medicine (Auckland, N.Z.)* 47 (5): 943–74. https://doi.org/10.1007/s40279-016-0619-5.

Jordanic, Mislav, Mónica Rojas-Martínez, Miguel Angel Mañanas, and Joan Francesc Alonso. 2016. “Spatial Distribution of HD-EMG Improves Identification of Task and Force in Patients with Incomplete Spinal Cord Injury.” *Journal of Neuroengineering and Rehabilitation* 13 (1): 41. https://doi.org/10.1186/s12984-016-0151-8.

Jordanić, Mislav, Mónica Rojas-Martínez, Miguel Angel Mañanas, Joan Francesc Alonso, and Hamid Reza Marateb. 2017. “A Novel Spatial Feature for the Identification of Motor Tasks Using High-Density Electromyography.” *Sensors (Basel, Switzerland)* 17 (7). https://doi.org/10.3390/s17071597.

Kang, Minsoo, Brian G. Ragan, and Jae-Hyeon Park. 2008. “Issues in Outcomes Research: An Overview of Randomization Techniques for Clinical Trials.” *Journal of Athletic Training* 43 (2): 215–21. https://doi.org/10.4085/1062-6050-43.2.215.

Kano, Sonobe, Inagaki, Sudo, and Poole. 2012. “Mechanisms of Exercise-Induced Muscle Damage and Fatigue: Intracellular Calcium Accumulation.” *The Journal of Physical Fitness and Sports Medicine* 1 (3): 505–12. https://doi.org/10.7600/jpfsm.1.505.

Karthick, P. A., M. Navaneethakrishna, N. Punitha, A. R. Jac Fredo, and S. Ramakrishnan. 2016. “Analysis of Muscle Fatigue Conditions Using Time-Frequency Images and GLCM Features.” *Current Directions in Biomedical Engineering* 2 (1): 483–87. https://doi.org/10.1515/cdbme-2016-0107.

Kinugasa, Ryuta, Yasuo Kawakami, and Tetsuo Fukunaga. 2005. “Muscle Activation and Its Distribution within Human Triceps Surae Muscles.” *Journal of Applied Physiology (Bethesda, Md.: 1985)* 99 (3): 1149–56. https://doi.org/10.1152/japplphysiol.01160.2004.

Krzywinski, Martin, and Naomi Altman. 2013. “Power and Sample Size.” *Nature Methods* 10 (12): 1139–40. https://doi.org/10.1038/nmeth.2738.

Lacome, Carling, Hager, Dine, and Piscione. 2018. “Workload, Fatigue, and Muscle Damage in an Under-20 Rugby Union Team Over an Intensified International Tournament.” *International Journal of Sports Physiology and Performance* 13 (8): 1059–66. https://doi.org/10.1123/ijspp.2017-0464.

Ladegaard, Jørn. 2002. “Story of Electromyography Equipment.” *Muscle & Nerve. Supplement* 11: S128-133. https://doi.org/10.1002/mus.10176.

Lark, Sally D., James A. Dickie, James A. Faulkner, and Matthew J. Barnes. 2019. “Muscle Activation and Local Muscular Fatigue during a 12-Minute Rotational Bridge.” *Sports Biomechanics* 18 (4): 402–13. https://doi.org/10.1080/14763141.2018.1433870.

Larson, and Brown. 2018. “The Effects of Trunk Extensor and Abdominal Muscle Fatigue on Postural Control and Trunk Proprioception in Young, Healthy Individuals.” *Human Movement Science* 57 (February): 13–20. https://doi.org/10.1016/j.humov.2017.10.019.

Latash. 2010. “Motor Synergies and the Equilibrium-Point Hypothesis.” *Motor Control* 14 (3): 294–322. https://doi.org/10.1123/mcj.14.3.294.

LeFever, R. S., and C. J. De Luca. 1982. “A Procedure for Decomposing the Myoelectric Signal into Its Constituent Action Potentials--Part I: Technique, Theory, and Implementation.” *IEEE Transactions on Bio-Medical Engineering* 29 (3): 149–57. https://doi.org/10.1109/tbme.1982.324881.

Lepley, Adam S., and Lindsey K. Lepley. 2021. “Mechanisms of Arthrogenic Muscle Inhibition.” *Journal of Sport Rehabilitation*, September, 1–10. https://doi.org/10.1123/jsr.2020-0479.

Machado, A. S., W. da Silva, C. F. de Andrade, C. I. De la Fuente, M. A. de Souza, and F. P. Carpes. 2022. “Green Tea Supplementation Favors Exercise Volume in Untrained Men under Cumulative Fatigue.” *Science & Sports*, December. https://doi.org/10.1016/j.scispo.2022.02.006.

Machado, da Silva, Souza, and Carpes. 2018. “Green Tea Extract Preserves Neuromuscular Activation and Muscle Damage Markers in Athletes Under Cumulative Fatigue.” *Frontiers in Physiology* 9 (August). https://doi.org/10.3389/fphys.2018.01137.

MacIntosh, Holash, and Renaud. 2012. “Skeletal Muscle Fatigue--Regulation of Excitation-Contraction Coupling to Avoid Metabolic Catastrophe.” *Journal of Cell Science* 125 (Pt 9): 2105–14. https://doi.org/10.1242/jcs.093674.

Magnusson, S. P., P. Hansen, P. Aagaard, J. Brønd, P. Dyhre-Poulsen, J. Bojsen-Moller, and M. Kjaer. 2003. “Differential Strain Patterns of the Human Gastrocnemius Aponeurosis and Free Tendon, in Vivo.” *Acta Physiologica Scandinavica* 177 (2): 185–95. https://doi.org/10.1046/j.1365-201X.2003.01048.x.

Marco, Alberto, and Taian. 2017. “Surface EMG and Muscle Fatigue: Multi-Channel Approaches to the Study of Myoelectric Manifestations of Muscle Fatigue.” *Physiological Measurement* 38 (5): R27–60. https://doi.org/10.1088/1361-6579/aa60b9.

Martinez-Valdes, E., R. A. Guzman-Venegas, R. A. Silvestre, J. H. Macdonald, D. Falla, O. F. Araneda, and D. Haichelis. 2016. “Electromyographic Adjustments during Continuous and Intermittent Incremental Fatiguing Cycling.” *Scandinavian Journal of Medicine & Science in Sports* 26 (11): 1273–82. https://doi.org/10.1111/sms.12578.

Martinez-Valdes, Eduardo, Francesco Negro, Michail Arvanitidis, Dario Farina, and Deborah Falla. 2021. “Pain-Induced Changes in Motor Unit Discharge Depend on Recruitment Threshold and Contraction Speed.” *Journal of Applied Physiology (Bethesda, Md.: 1985)* 131 (4): 1260–71. https://doi.org/10.1152/japplphysiol.01011.2020.

Martinez-Valdes, Eduardo, Francesco Negro, Deborah Falla, Alessandro Marco De Nunzio, and Dario Farina. 2018. “Surface Electromyographic Amplitude Does Not Identify Differences in Neural Drive to Synergistic Muscles.” *Journal of Applied Physiology (Bethesda, Md.: 1985)* 124 (4): 1071–79. https://doi.org/10.1152/japplphysiol.01115.2017.

Martinez-Valdes, Eduardo, Francesco Negro, Deborah Falla, Jakob Lund Dideriksen, C. J. Heckman, and Dario Farina. 2020. “Inability to Increase the Neural Drive to Muscle Is Associated with Task Failure during Submaximal Contractions.” *Journal of Neurophysiology* 124 (4): 1110–21. https://doi.org/10.1152/jn.00447.2020.

McHugh. 2003. “Recent Advances in the Understanding of the Repeated Bout Effect: The Protective Effect against Muscle Damage from a Single Bout of Eccentric Exercise.”

Scandinavian Journal of Medicine & Science in Sports 13 (2): 88–97. https://doi.org/10.1034/j.1600-0838.2003.02477.x.

McHugh, Malachy P., Karl F. Orishimo, Ian J. Kremenic, Julia Adelman, and Stephen J. Nicholas. 2019. "Electromyographic Evidence of Excessive Achilles Tendon Elongation During Isometric Contractions After Achilles Tendon Repair." *Orthopaedic Journal of Sports Medicine* 7 (11): 2325967119883357. https://doi.org/10.1177/2325967119883357.

McInnes, Leland. 2018. "Scientific Computing with Python. UMAP: Uniform Manifold Aproximation and Projection for Dimensional Reduction." Presented at the Scientific Computing with python., Texas (Austin), USA, September 15. https://www.youtube.com/watch?v=nq6iPZVUxZU.

McInnes, Leland, John Healy, and James Melville. 2018. "UMAP: Uniform Manifold Approximation and Projection for Dimension Reduction." *ArXiv:1802.03426 [Cs, Stat]*, December. http://arxiv.org/abs/1802.03426.

McPherson, Schilaty, Anderson, Nagai, and Bates. 2023. "Arthrogenic Muscle Inhibition after Anterior Cruciate Ligament Injury: Injured and Uninjured Limb Recovery over Time." *Frontiers in Sports and Active Living* 5: 1143376. https://doi.org/10.3389/fspor.2023.1143376.

Meehan, Connor, Stephen Meehan, and Wayne Moore. 2020. "Uniform Manifold Approximation and Projection (UMAP)." MATLAB Central File Exchange. 2020. https://www.mathworks.com/matlabcentral/fileexchange/71902.

Mendez-Villanueva, Alberto, Johann Edge, Rob Suriano, Peter Hamer, and David Bishop. 2012. "The Recovery of Repeated-Sprint Exercise Is Associated with PCr Resynthesis, While Muscle PH and EMG Amplitude Remain Depressed." *PloS One* 7 (12): e51977. https://doi.org/10.1371/journal.pone.0051977.

Merletti, R., and G. L. Cerone. 2020. "Tutorial. Surface EMG Detection, Conditioning and Pre-Processing: Best Practices." *Journal of Electromyography and Kinesiology* 54 (October): 102440. https://doi.org/10.1016/j.jelekin.2020.102440.

Merletti, R., M. Knaflitz, and C. J. De Luca. 1990. "Myoelectric Manifestations of Fatigue in Voluntary and Electrically Elicited Contractions." *Journal of Applied Physiology (Bethesda, Md.: 1985)* 69 (5): 1810–20. https://doi.org/10.1152/jappl.1990.69.5.1810.

Merletti, R., and S. Muceli. 2019. "Tutorial. Surface EMG Detection in Space and Time: Best Practices." *Journal of Electromyography and Kinesiology: Official Journal of the International Society of Electrophysiological Kinesiology* 49 (December): 102363. https://doi.org/10.1016/j.jelekin.2019.102363.

Mesin, Luca, Roberto Merletti, and Taian M. M. Vieira. 2011. "Insights Gained into the Interpretation of Surface Electromyograms from the Gastrocnemius Muscles: A Simulation Study." *Journal of Biomechanics* 44 (6): 1096–1103. https://doi.org/10.1016/j.jbiomech.2011.01.031.

Mettler, Joni A., and Lisa Griffin. 2016. "Muscular Endurance Training and Motor Unit Firing Patterns during Fatigue." *Experimental Brain Research* 234 (1): 267–76. https://doi.org/10.1007/s00221-015-4455-x.

Mickle, Karen J., Christopher J. Nester, Gillian Crofts, and Julie R. Steele. 2013. "Reliability of Ultrasound to Measure Morphology of the Toe Flexor Muscles." *Journal of Foot and Ankle Research* 6 (1): 12. https://doi.org/10.1186/1757-1146-6-12.

Moritani, T., L. Oddsson, and A. Thorstensson. 1991. "Activation Patterns of the Soleus and Gastrocnemius Muscles during Different Motor Tasks." *Journal of Electromyography and Kinesiology: Official Journal of the International Society of Electrophysiological Kinesiology* 1 (2): 81–88. https://doi.org/10.1016/1050-6411(91)90001-L.

Nawab, S. Hamid, Shey-Sheen Chang, and Carlo J. De Luca. 2010. “High-Yield Decomposition of Surface EMG Signals.” *Clinical Neurophysiology: Official Journal of the International Federation of Clinical Neurophysiology* 121 (10): 1602–15. https://doi.org/10.1016/j.clinph.2009.11.092.

Negro, Muceli, Castronovo, Holobar, and Farina. 2016. “Multi-Channel Intramuscular and Surface EMG Decomposition by Convolutive Blind Source Separation.” *Journal of Neural Engineering* 13 (2): 026027. https://doi.org/10.1088/1741-2560/13/2/026027.

Nilsson-Helander, Katarina, Roland Thomeé, Karin Grävare Silbernagel, Karin Grävare-Silbernagel, Pia Thomeé, Eva Faxén, Bengt I. Eriksson, and Jon Karlsson. 2007. “The Achilles Tendon Total Rupture Score (ATRS): Development and Validation.” *The American Journal of Sports Medicine* 35 (3): 421–26. https://doi.org/10.1177/0363546506294856.

Oda, Hiroyuki, Kanae Sano, Yoko Kunimasa, Paavo V. Komi, and Masaki Ishikawa. 2017. “Neuromechanical Modulation of the Achilles Tendon During Bilateral Hopping in Patients with Unilateral Achilles Tendon Rupture, Over 1 Year After Surgical Repair.” *Sports Medicine (Auckland, N.Z.)* 47 (6): 1221–30. https://doi.org/10.1007/s40279-016-0629-3.

Oskolkov, Nikolay. 2019. “How Exactly UMAP Works.” Medium. November 6, 2019. https://towardsdatascience.com/how-exactly-umap-works-13e3040e1668.

Pandian, A. Pasumpon, Ram Palanisamy, and Klimis Ntalianis, eds. 2020. *Proceeding of the International Conference on Computer Networks, Big Data and IoT (ICCBI - 2019)*. Lecture Notes on Data Engineering and Communications Technologies. Springer International Publishing. https://doi.org/10.1007/978-3-030-43192-1.

Peng, Wei-Chen, Yuan-Hung Chao, Amy S. N. Fu, Shirley S. M. Fong, Christer Rolf, Hongsen Chiang, Shiyi Chen, and Hsing-Kuo Wang. 2019. “Muscular Morphomechanical Characteristics After an Achilles Repair.” *Foot & Ankle International* 40 (5): 568–77. https://doi.org/10.1177/1071100718822537.

Perez, Monica A., Bjarke K. S. Lungholt, and Jens B. Nielsen. 2005. “Presynaptic Control of Group Ia Afferents in Relation to Acquisition of a Visuo-Motor Skill in Healthy Humans.” *The Journal of Physiology* 568 (Pt 1): 343–54. https://doi.org/10.1113/jphysiol.2005.089904.

Pincheira, Hoffman, Cresswell, Carroll, Brown, and Lichtwark. 2018. “The Repeated Bout Effect Can Occur without Mechanical and Neuromuscular Changes after a Bout of Eccentric Exercise.” *Scandinavian Journal of Medicine & Science in Sports* 28 (10): 2123–34. https://doi.org/10.1111/sms.13222.

Pincheira, Patricio A., Eduardo Martinez-Valdes, Carlos De la Fuente, Felipe Palma, Oscar Valencia, Gunther Redenz, and Rodrigo Guzman-Venegas. 2020. “Quantifying Topographical Changes in Muscle Activation: A Statistical Parametric Mapping Approach.” *Proceedings* 49 (1): 71. https://doi.org/10.3390/proceedings2020049071.

Pincheira, Patricio A., Eduardo Martinez-Valdes, Rodrigo Guzman-Venegas, Deborah Falla, Marta I. Garrido, Andrew G. Cresswell, and Glen A. Lichtwark. 2021. “Regional Changes in Muscle Activity Do Not Underlie the Repeated Bout Effect in the Human Gastrocnemius Muscle.” *Scandinavian Journal of Medicine & Science in Sports* 31 (4): 799–812. https://doi.org/10.1111/sms.13912.

Powers, Scott K., and Malcolm J. Jackson. 2008. “Exercise-Induced Oxidative Stress: Cellular Mechanisms and Impact on Muscle Force Production.” *Physiological Reviews* 88 (4): 1243–76. https://doi.org/10.1152/physrev.00031.2007.

Priego-Quesada, Jose I., Carlos De la Fuente, Marcos R. Kunzler, Pedro Perez-Soriano, David Hervás-Marín, and Felipe P. Carpes. 2020. “Relationship between Skin Temperature, Electrical Manifestations of Muscle Fatigue, and Exercise-Induced Delayed Onset

Muscle Soreness for Dynamic Contractions: A Preliminary Study." *International Journal of Environmental Research and Public Health* 17 (18): 6817. https://doi.org/10.3390/ijerph17186817.

Priego-Quesada, Oficial-Casado, Gandia-Soriano, and FP Carpes. 2019. "A Preliminary Investigation about the Observation of Regional Skin Temperatures Following Cumulative Training Loads in Triathletes during Training Camp." *Journal of Thermal Biology* 84 (August): 431–38. https://doi.org/10.1016/j.jtherbio.2019.07.035.

Proske, and Morgan. 2001. "Muscle Damage from Eccentric Exercise: Mechanism, Mechanical Signs, Adaptation and Clinical Applications." *The Journal of Physiology* 537 (Pt 2): 333–45. https://doi.org/10.1111/j.1469-7793.2001.00333.x.

Proske, Uwe, and Simon C. Gandevia. 2012. "The Proprioceptive Senses: Their Roles in Signaling Body Shape, Body Position and Movement, and Muscle Force." *Physiological Reviews* 92 (4): 1651–97. https://doi.org/10.1152/physrev.00048.2011.

Raez, M. B. I., M. S. Hussain, and F. Mohd-Yasin. 2006. "Techniques of EMG Signal Analysis: Detection, Processing, Classification and Applications." *Biological Procedures Online* 8: 11–35. https://doi.org/10.1251/bpo115.

Rampichini, Susanna, Taian Martins Vieira, Paolo Castiglioni, and Giampiero Merati. 2020. "Complexity Analysis of Surface Electromyography for Assessing the Myoelectric Manifestation of Muscle Fatigue: A Review." *Entropy* 22 (5): 529. https://doi.org/10.3390/e22050529.

Rice, and McNair. 2010. "Quadriceps Arthrogenic Muscle Inhibition: Neural Mechanisms and Treatment Perspectives." *Seminars in Arthritis and Rheumatism* 40 (3): 250–66. https://doi.org/10.1016/j.semarthrit.2009.10.001.

Richardson, Michael S., Joel T. Cramer, Debra A. Bemben, Randa L. Shehab, John Glover, and Michael G. Bemben. 2006. "Effects of Age and ACL Reconstruction on Quadriceps Gamma Loop Function." *Journal of Geriatric Physical Therapy (2001)* 29 (1): 28–34.

Rubinstein, and Kamen. 2005. "Decreases in Motor Unit Firing Rate during Sustained Maximal-Effort Contractions in Young and Older Adults." *Journal of Electromyography and Kinesiology: Official Journal of the International Society of Electrophysiological Kinesiology* 15 (6): 536–43. https://doi.org/10.1016/j.jelekin.2005.04.001.

Sánchez-Gómez, Rubén, Ricardo Becerro-de-Bengoa-Vallejo, Carlos Romero Morales, Marta Elena Losa-Iglesias, Aitor Castrillo de la Fuente, Daniel López-López, Ignacio Díez Vega, and César Calvo-Lobo. 2020. "Muscle Activity of the Triceps Surae With Novel Propulsion Heel-Lift Orthotics in Recreational Runners." *Orthopaedic Journal of Sports Medicine* 8 (10): 2325967120956914. https://doi.org/10.1177/2325967120956914.

Sánchez-Rico, Marina, and Jesús M. Alvarado. 2019. "A Machine Learning Approach for Studying the Comorbidities of Complex Diagnoses." *Behavioral Sciences (Basel, Switzerland)* 9 (12). https://doi.org/10.3390/bs9120122.

Sarker, and Mirka. 2020. "The Effects of Repetitive Bouts of a Fatiguing Exertion (with Breaks) on the Slope of EMG Measures of Localized Muscle Fatigue." *Journal of Electromyography and Kinesiology: Official Journal of the International Society of Electrophysiological Kinesiology* 51 (April): 102382. https://doi.org/10.1016/j.jelekin.2019.102382.

Sartori, Massimo, Utku Ş Yavuz, and Dario Farina. 2017. "In Vivo Neuromechanics: Decoding Causal Motor Neuron Behavior with Resulting Musculoskeletal Function." *Scientific Reports* 7 (1): 13465. https://doi.org/10.1038/s41598-017-13766-6.

Saxena, Amol, Alessio Giai Via, Karin Grävare Silbernagel, Markus Walther, Robert Anderson, Ludger Gerdesmeyer, and Nicola Maffulli. 2022. “Current Consensus for Rehabilitation Protocols of the Surgically Repaired Acute Mid-Substance Achilles Rupture: A Systematic Review and Recommendations From the ‘GAIT’ Study Group.” *The Journal of Foot and Ankle Surgery: Official Publication of the American College of Foot and Ankle Surgeons* 61 (4): 855–61. https://doi.org/10.1053/j.jfas.2021.12.008.

Schanne, Kane, Young, and Farber. 1979. “Calcium Dependence of Toxic Cell Death: A Final Common Pathway.” *Science (New York, N.Y.)* 206 (4419): 700–702. https://doi.org/10.1126/science.386513.

Semmler. 2014. “Motor Unit Activity after Eccentric Exercise and Muscle Damage in Humans.” *Acta Physiologica (Oxford, England)* 210 (4): 754–67. https://doi.org/10.1111/apha.12232.

Semmler, John G. 2002. “Motor Unit Synchronization and Neuromuscular Performance.” *Exercise and Sport Sciences Reviews* 30 (1): 8–14. https://doi.org/10.1097/00003677-200201000-00003.

Shair, E. F., S. A. Ahmad, M. H. Marhaban, S. B. Mohd Tamrin, and A. R. Abdullah. 2017. “EMG Processing Based Measures of Fatigue Assessment during Manual Lifting.” Review Article. BioMed Research International. Hindawi. February 19, 2017. https://doi.org/10.1155/2017/3937254.

Silva, Willian da, Álvaro S. Machado, Mauren A. Souza, Pâmela B. Mello-Carpes, and Felipe P. Carpes. 2018. “Effect of Green Tea Extract Supplementation on Exercise-Induced Delayed Onset Muscle Soreness and Muscular Damage.” *Physiology & Behavior* 194 (October): 77–82. https://doi.org/10.1016/j.physbeh.2018.05.006.

Singh, Pushpendra, Shiv Dutt Joshi, Rakesh Kumar Patney, and Kaushik Saha. 2017. “The Fourier Decomposition Method for Nonlinear and Non-Stationary Time Series Analysis.” *Proceedings of the Royal Society A: Mathematical, Physical and Engineering Sciences* 473 (2199): 20160871. https://doi.org/10.1098/rspa.2016.0871.

Siva, Sivakar. 2020. “Dimensionality Reduction for Data Visualization: PCA vs TSNE vs UMAP vs LDA.” Medium. December 1, 2020. https://towardsdatascience.com/dimensionality-reduction-for-data-visualization-pca-vs-tsne-vs-umap-be4aa7b1cb29.

Sjøgaard, and Søgaard. 1998. “Muscle Injury in Repetitive Motion Disorders.” *Clinical Orthopaedics and Related Research*, no. 351 (June): 21–31.

Smith, Housh, Hill, Keller, Johnson, and Schmidt. 2017. “Effects of Fatigue and Recovery on Electromechanical Delay during Isokinetic Muscle Actions.” *Physiological Measurement* 38 (10): 1837–47. https://doi.org/10.1088/1361-6579/aa8983.

Snyder. 1998. “Overtraining and Glycogen Depletion Hypothesis.” *Medicine and Science in Sports and Exercise* 30 (7): 1146–50. https://doi.org/10.1097/00005768-199807000-00020.

Soderberg, and Cook. 1984. “Electromyography in Biomechanics.” *Physical Therapy* 64 (12): 1813–20. https://doi.org/10.1093/ptj/64.12.1813.

Søgaard, and Sjøgaard. 2017. “Physical Activity as Cause and Cure of Muscular Pain: Evidence of Underlying Mechanisms.” *Exercise and Sport Sciences Reviews* 45 (3): 136–45. https://doi.org/10.1249/JES.0000000000000112.

Solnik, Stanislaw, Patrick Rider, Ken Steinweg, Paul DeVita, and Tibor Hortobágyi. 2010. “Teager-Kaiser Energy Operator Signal Conditioning Improves EMG Onset Detection.” *European Journal of Applied Physiology* 110 (3): 489–98. https://doi.org/10.1007/s00421-010-1521-8.

Srhoj-Egekher, Vedran, Mario Cifrek, and Vladimir Medved. 2011. “The Application of Hilbert-Huang Transform in the Analysis of Muscle Fatigue during Cyclic Dynamic Contractions.” *Medical & Biological Engineering & Computing* 49 (6): 659–69. https://doi.org/10.1007/s11517-010-0718-7.

Stadler, Alfred, Wolfgang Schima, Ahmed Ba-Ssalamah, Joachim Kettenbach, and Edith Eisenhuber. 2007. “Artifacts in Body MR Imaging: Their Appearance and How to Eliminate Them.” *European Radiology* 17 (5): 1242–55. https://doi.org/10.1007/s00330-006-0470-4.

Stäudle, Benjamin, Olivier Seynnes, Guido Laps, Gert-Peter Brüggemann, and Kirsten Albracht. 2022. “Altered Gastrocnemius Contractile Behavior in Former Achilles Tendon Rupture Patients During Walking.” *Frontiers in Physiology* 13: 792576. https://doi.org/10.3389/fphys.2022.792576.

Stein, R. B., B. S. Brucker, and D. R. Ayyar. 1990. “Motor Units in Incomplete Spinal Cord Injury: Electrical Activity, Contractile Properties and the Effects of Biofeedback.” *Journal of Neurology, Neurosurgery, and Psychiatry* 53 (10): 880–85. https://doi.org/10.1136/jnnp.53.10.880.

Stock, Beck, and Defreitas. 2012. “Effects of Fatigue on Motor Unit Firing Rate versus Recruitment Threshold Relationships.” *Muscle & Nerve* 45 (1): 100–109. https://doi.org/10.1002/mus.22266.

Stožer, Vodopivc, and Križančić Bombek. 2020. “Pathophysiology of Exercise-Induced Muscle Damage and Its Structural, Functional, Metabolic, and Clinical Consequences.” *Physiological Research* 69 (4): 565–98. https://doi.org/10.33549/physiolres.934371.

Suydam, Stephen M., Thomas S. Buchanan, Kurt Manal, and Karin Gravare Silbernagel. 2015. “Compensatory Muscle Activation Caused by Tendon Lengthening Post-Achilles Tendon Rupture.” *Knee Surgery, Sports Traumatology, Arthroscopy: Official Journal of the ESSKA* 23 (3): 868–74. https://doi.org/10.1007/s00167-013-2512-1.

Tan, Lizhe, and Jean Jiang. 2019. “Chapter 4 - Discrete Fourier Transform and Signal Spectrum.” In *Digital Signal Processing (Third Edition)*, edited by Lizhe Tan and Jean Jiang, 91–142. Academic Press. https://doi.org/10.1016/B978-0-12-815071-9.00004-X.

Tenberg, Nosaka, and Wilke. 2022. “The Relationship Between Acute Exercise-Induced Changes in Extramuscular Connective Tissue Thickness and Delayed Onset Muscle Soreness in Healthy Participants: A Randomized Controlled Crossover Trial.” *Sports Medicine - Open* 8 (1): 57. https://doi.org/10.1186/s40798-022-00446-7.

Theisen, Daniel, Isabel Rada, Amélie Brau, Paul Gette, and Romain Seil. 2016. “Muscle Activity Onset Prior to Landing in Patients after Anterior Cruciate Ligament Injury: A Systematic Review and Meta-Analysis.” *PloS One* 11 (5): e0155277. https://doi.org/10.1371/journal.pone.0155277.

Twist, and Eston. 2005. “The Effects of Exercise-Induced Muscle Damage on Maximal Intensity Intermittent Exercise Performance.” *European Journal of Applied Physiology* 94 (5–6): 652–58. https://doi.org/10.1007/s00421-005-1357-9.

Unell, Alyssa, Zachary M. Eisenstat, Ainsley Braun, Abhinav Gandhi, Sharon Gilad-Gutnick, Shlomit Ben-Ami, and Pawan Sinha. 2021. “Influence of Visual Feedback Persistence on Visuo-Motor Skill Improvement.” *Scientific Reports* 11 (1): 17347. https://doi.org/10.1038/s41598-021-96876-6.

Vieira, Taian M. M., Ian D. Loram, Silvia Muceli, Roberto Merletti, and Dario Farina. 2011. “Postural Activation of the Human Medial Gastrocnemius Muscle: Are the Muscle Units Spatially Localised?” *The Journal of Physiology* 589 (Pt 2): 431–43. https://doi.org/10.1113/jphysiol.2010.201806.

Vigotsky, Andrew D., Israel Halperin, Gregory J. Lehman, Gabriel S. Trajano, and Taian M. Vieira. 2017. “Interpreting Signal Amplitudes in Surface Electromyography Studies in Sport and Rehabilitation Sciences.” *Frontiers in Physiology* 8: 985. https://doi.org/10.3389/fphys.2017.00985.

Vinti, Maria, Jean-Michel Gracies, Marco Gazzoni, and Taian Vieira. 2018. “Localised Sampling of Myoelectric Activity May Provide Biased Estimates of Cocontraction for Gastrocnemius Though Not for Soleus and Tibialis Anterior Muscles.” *Journal of Electromyography and Kinesiology: Official Journal of the International Society of Electrophysiological Kinesiology* 38 (February): 34–43. https://doi.org/10.1016/j.jelekin.2017.11.003.

Vøllestad, N. K. 1997. “Measurement of Human Muscle Fatigue.” *Journal of Neuroscience Methods* 74 (2): 219–27. https://doi.org/10.1016/s0165-0270(97)02251-6.

Walton, David M., Raul A. Kuchinad, Tanya D. Ivanova, and Jayne S. Garland. 2002. “Reflex Inhibition during Muscle Fatigue in Endurance-Trained and Sedentary Individuals.” *European Journal of Applied Physiology* 87 (4): 462–68. https://doi.org/10.1007/s00421-002-0670-9.

Waly, Sherif M., Shihab S. Asfour, and Tarek M. Khalil. 1996. “Effects of Time Windowing on the Estimated EMG Parameters.” *Computers and Industrial Engineering* 31 (1–2): 515–18. https://doi.org/10.1016/0360-8352(96)00188-x.

Wang, Hsing-Kuo, Hongsen Chiang, Wen-Shiang Chen, Tiffany Tingfang Shih, Yung-Cheng Huang, and Ching-Chuan Jiang. 2013. “Early Neuromechanical Outcomes of the Triceps Surae Muscle-Tendon after an Achilles’ Tendon Repair.” *Archives of Physical Medicine and Rehabilitation* 94 (8): 1590–98. https://doi.org/10.1016/j.apmr.2013.01.015.

Wang, Lejun, Yuting Wang, Aidi Ma, Guoqiang Ma, Yu Ye, Ruijie Li, and Tianfeng Lu. 2018. “A Comparative Study of EMG Indices in Muscle Fatigue Evaluation Based on Grey Relational Analysis during All-Out Cycling Exercise.” *BioMed Research International* 2018 (April). https://doi.org/10.1155/2018/9341215.

Wang, Zijian, Lei Cao, Zuo Zhang, Xiaoliang Gong, Yaoru Sun, and Haoran Wang. 2018. “Short Time Fourier Transformation and Deep Neural Networks for Motor Imagery Brain Computer Interface Recognition.” *Concurrency and Computation: Practice and Experience* 30 (January). https://doi.org/10.1002/cpe.4413.

Watanabe, Kohei, Motoki Kouzaki, Madoka Ogawa, Hiroshi Akima, and Toshio Moritani. 2018. “Relationships between Muscle Strength and Multi-Channel Surface EMG Parameters in Eighty-Eight Elderly.” *European Review of Aging and Physical Activity: Official Journal of the European Group for Research into Elderly and Physical Activity* 15: 3. https://doi.org/10.1186/s11556-018-0192-z.

Wenning, Markus, Marlene Mauch, Albrecht Heitner, Johannes Lienhard, Ramona Ritzmann, and Jochen Paul. 2021. “Neuromechanical Activation of Triceps Surae Muscle Remains Altered at 3.5 Years Following Open Surgical Repair of Acute Achilles Tendon Rupture.” *Knee Surgery, Sports Traumatology, Arthroscopy: Official Journal of the ESSKA*, March. https://doi.org/10.1007/s00167-021-06512-z.

Xie, Hongbo, and Zhizhong Wang. 2006. “Mean Frequency Derived via Hilbert-Huang Transform with Application to Fatigue EMG Signal Analysis.” *Computer Methods and Programs in Biomedicine* 82 (2): 114–20. https://doi.org/10.1016/j.cmpb.2006.02.009.

Xu, Yuhang, Haipeng Liu, Dongmei Hao, Michael Taggart, and Dingchang Zheng. 2022. “Uterus Modeling From Cell to Organ Level: Towards Better Understanding of Physiological Basis of Uterine Activity.” *IEEE Reviews in Biomedical Engineering* 15: 341–53. https://doi.org/10.1109/RBME.2020.3023535.

Yamaguchi, Suzuki, Kanda, Inami, and Okada. 2020. “Changes in Urinary Titin N-Terminal Fragments as a Biomarker of Exercise-Induced Muscle Damage in the Repeated Bout Effect.” *Journal of Science and Medicine in Sport* 23 (6): 536–40. https://doi.org/10.1016/j.jsams.2019.12.023.

Yip, Eugene, Jihyun Yun, Keith Wachowicz, Zsolt Gabos, Satyapal Rathee, and B. G. Fallone. 2017. “Sliding Window Prior Data Assisted Compressed Sensing for MRI Tracking of Lung Tumors.” *Medical Physics* 44 (1): 84–98. https://doi.org/10.1002/mp.12027.

Zellers, Jennifer A., Adam R. Marmon, Anahid Ebrahimi, and Karin Grävare Silbernagel. 2019. “Lower Extremity Work along with Triceps Surae Structure and Activation Is Altered with Jumping after Achilles Tendon Repair.” *Journal of Orthopaedic Research: Official Publication of the Orthopaedic Research Society* 37 (4): 933–41. https://doi.org/10.1002/jor.24260.

Zhang, Kai, Guanghua Xu, Zezhen Han, Kaiquan Ma, Xiaowei Zheng, Longting Chen, Nan Duan, and Sicong Zhang. 2020. “Data Augmentation for Motor Imagery Signal Classification Based on a Hybrid Neural Network.” *Sensors (Basel, Switzerland)* 20 (16). https://doi.org/10.3390/s20164485.

Zhang, Z. G., H. T. Liu, S. C. Chan, K. D. K. Luk, and Y. Hu. 2010. “Time-Dependent Power Spectral Density Estimation of Surface Electromyography during Isometric Muscle Contraction: Methods and Comparisons.” *Journal of Electromyography and Kinesiology: Official Journal of the International Society of Electrophysiological Kinesiology* 20 (1): 89–101. https://doi.org/10.1016/j.jelekin.2008.09.007.

Zhu, Mingxing, Bin Yu, Wanzhang Yang, Yanbing Jiang, Lin Lu, Zhen Huang, Shixiong Chen, and Guanglin Li. 2017. “Evaluation of Normal Swallowing Functions by Using Dynamic High-Density Surface Electromyography Maps.” *Biomedical Engineering Online* 16 (1): 133. https://doi.org/10.1186/s12938-017-0424-x.

ANNEX 1 – Ethical approvements

PONTIFICIA UNIVERSIDAD CATÓLICA DE CHILE

ACTA DE RESOLUCIÓN
COMITÉ ÉTICO CIENTÍFICO DE CIENCIAS DE LA SALUD UC
Re-acreditado por SEREMI de Salud
Resolución Exenta Nº 012793 del 27 de octubre de 2021

NUEVO ESTUDIO

Fecha y N° de Sesión: 07 de julio de 2022; Sesión Ordinaria N°12

Investigador Responsable: Carlos de la Fuente Cancino

ID Protocolo: 220514001

Título del Proyecto: Caracterización de movimientos funcionales

Facultad/Unidad Académica: Facultad de Medicina, Pontificia Universidad Católica de Chile

Académico Responsable: Carlos de la Fuente Cancino

Sitio de realización: Departamento de Ciencias de la Salud

Financiamiento: Fondos interdepartamentales: PRIMER CONCURSO DE CIENCIAS DE LA SALUD INTERDISCIPLINA

Miembros del Comité que participaron en la aprobación del estudio:

Mg. Ivonne Vargas Celis, Presidente subrogante

Mg. Mónica Vergara Quezada, Secretaria ejecutiva

Sr. Jorge Muñoz Castillo, Abogado miembro externo

Srta. Alyssa Garay Navea, Representante de la comunidad

PONTIFICIA UNIVERSIDAD CATÓLICA DE CHILE

Dr. Francisco Acevedo, Departamento de Hemato-Oncología

EU Mónica Cifuentes Soro, miembro externo

Dra. Colomba Cofré D., Departamento de Gastroenterología y Nutrición Pediátrica

EU Víctor Contreras, Departamento de Anestesiología

Dr. Juan Francisco Miquel, Departamento de Gastroenterología

Sra. Ximena Ortega Fuenzalida, Ingeniero Agrónomo

Dra. Marisa Torres Hidalgo, Departamento de Salud Pública

Dra. Claudia Uribe Torres, Escuela de Enfermería

Documentos recibidos por el Comité:

- Carta Presentación Investigador Responsable
- Carta Apoyo Jefe de Departamento
- Responsabilidad del Investigador
- Declaración Simple del Investigador Responsable

Documentos revisados y aprobados por el Comité:

- Consentimiento Informado_General_Adultos_2021
- Formulario Solicitud Revisión Ética CEC-Salud UC 2022.docx

PONTIFICIA UNIVERSIDAD CATÓLICA DE CHILE

Considerando que:

1- Los investigadores referidos cuentan con la experiencia necesaria para la conducción y el desarrollo de este tipo de estudio;

2- La metodología descrita es apropiada para el cumplimiento de los objetivos del estudio, de acuerdo con los estándares internacionales de rigor científico;

3- Durante la conducción del estudio se garantiza un balance riesgo/beneficio favorable para los participantes, por cuanto sólo se realizan procedimientos de bajo riesgo;

4- La población por estudiar no es considerada vulnerable y, el protocolo resguarda la seguridad y bienestar de los participantes;

5- Se ha contemplado el resguardo de la confidencialidad de la información sensible e identificable en la difusión de los resultados, por lo que no introduce un riesgo de menoscabo para la intimidad de los participantes; y

6- Los participantes ingresarán voluntariamente luego de ser adecuadamente informados sobre los aspectos esenciales del estudio, sus deberes y derechos, y los plazos estipulados para el cumplimiento de los objetivos de la investigación.

Constatado que el texto del documento de Consentimiento Informado,

PONTIFICIA UNIVERSIDAD CATÓLICA DE CHILE

contiene:

1- La descripción general de los objetivos de la investigación;

2- El detalle de los procedimientos que involucra la participación en este estudio;

3- Los antecedentes sobre el uso que se dará a la información obtenida a partir de cada procedimiento de la investigación;

4- El compromiso respecto a la utilización actual y futura de la información, la que sólo se realizará dentro de los marcos del presente estudio y para el logro de dichos objetivos;

5- El resguardo de la confidencialidad y el anonimato de la información recogida, según corresponde a cada procedimiento del estudio;

6- El detalle respecto del costo en tiempo que significa la participación en el estudio;

7- La información sobre los beneficios y derechos por la participación en la investigación; y

8- La voluntariedad de la participación y la garantía para cada participante de hacer abandono del estudio, sin repercusión alguna.

Resolución CEC-Salud UC:

Este proyecto cuenta con la opinión favorable del Comité con fecha **07 de julio de 2022**, en la **sesión ordinaria N°12**, la que tiene vigencia de un año.

PONTIFICIA UNIVERSIDAD CATÓLICA DE CHILE

El Investigador Responsable deberá solicitar **la renovación anual** de la presente aprobación ética con 30 días de anticipación al vencimiento de la fecha de aprobación original, si desea continuar con el estudio. Si no ha recibido la respuesta oficial a su solicitud, el investigador deberá detener las actividades del proyecto, no podrá enrolar a ningún nuevo participante y no podrá proceder con el análisis de los datos.

Para iniciar el proceso de consentimiento y de reclutamiento se debe disponer previamente de la última versión aprobada y timbrada del documento de Consentimiento Informado. De este modo, el Investigador Responsable velará por la realización de estos procedimientos, utilizando la copia de la versión original (timbrada, fechada y firmada por el CEC-Salud UC). Asimismo, debido a la contingencia actual de pandemia, y en virtud del resguardo del balance riesgo beneficio favorable a los participantes, el CEC-Salud UC indica al Investigador Responsable tomar los resguardos en el proceso y firma de acta del consentimiento informado para evitar posible contagio asociado a este procedimiento y a cualquier otra actividad del estudio

En la eventualidad de requerir cualquier modificación al estudio o a los documentos aprobados originalmente, el investigador deberá notificarlo al Comité por medio de una enmienda (a través de plataforma) para la evaluación y emisión de una nueva acta de

PONTIFICIA UNIVERSIDAD CATÓLICA DE CHILE

resolución ética. **(ID: 220514001)**

MG. Mónica Vergara Quezada.
Secretaria Ejecutiva
CEC-Salud UC

MG. Ivonne Vargas Celis
Presidenta (S)
CEC-Salud UC

Santiago, 18 de julio de 2022

EN CASO DE CUALQUIER DUDA SE LE SOLICITA CONTACTARSE CON EL CEC-Salud UC

Se certifica que la información comunida en el presente documento es correcta y que refleja el Acta del Comité Ético Científico de Ciencias de la Salud UC (CEC-Salud UC). Este Comité adhiere a los principios éticos de la Pontificia Universidad Católica de Chile, que considera como eje fundamental el respeto a la dignidad de la persona humana en cualquier condición. Este Comité cumple además con las Guías de buena práctica clínica definidas por la Conferencias Internacional de Armonización (GCP-ICH), y con las leyes chilenas 19.628; 20.120; 20.584 y 20.850 que modifica el Código Sanitario

COMITÉ ÉTICO CIENTÍFICO

Clínica Santa María

ACTA DE APROBACIÓN DE ESTUDIOS DE INVESTIGACIÓN CLÍNICA
COMITÉ ÉTICO CIENTÍFICO CLÍNICA SANTA MARÍA

FECHA 25 DE MARZO DE 2019

1. REFERENCIAS DEL ESTUDIO

TÍTULO DEL ESTUDIO:	Fatiga muscular durante contracciones dinámicas tras tenorrafias de Aquiles posterior a 1 año		
INVESTIGADOR RESPONSABLE:	Rigo, Carlos De la Fuente Cancino		
CORREO ELECTRÓNICO:	cdelafuente@clinicasantamaria.cl	TELÉFONO:	954265340
CENTRO DE INVESTIGACIÓN (UNIDAD/ DEPTO/ SERVICIO):	Servicio de Biomecánica Clínica Santa María		
FECHA INICIO DEL ESTUDIO:	1° abril 2019	FECHA TÉRMINO DEL ESTUDIO:	1° octubre 2020
PATROCINADOR			

TIPO DE ESTUDIO:

Unicéntrico		Multicéntrico		Internacional		Nacional	
Observacional		Descriptivo		Analítico		Experimental	■
Prospectivo		Retrospectivo					

Otros (especificar) _____

N° EUDRACT: (Si fuere el caso)			
CÓDIGO PROTOCOLO:			
VERSIÓN PROTOCOLO:		FECHA PROTOCOLO:	
VERSIÓN CONSENTIMIENTO INFORMADO:		FECHA CONSENTIMIENTO INFORMADO:	
INFORME PÓLIZA DE SEGURO:			

ACTA DE APROBACIÓN DE ESTUDIOS DE INVESTIGACIÓN CLÍNICA
COMITÉ ÉTICO CIENTÍFICO CLÍNICA SANTA MARÍA

Fatiga muscular durante contracciones dinámicas tras tenorrafias de Aquiles posterior a 1 año

2. CERTIFICACION DE APROBACION DEL ESTUDIO

Con fecha 25 DE MARZO DE 2019, habiendo dado cumplimiento a las observaciones hechas en reunión institucional del día 11 de marzo de 2019, el Comité Ético Científico de Clínica Santa María, ha resuelto **OTORGAR SU APROBACION** al estudio de la referencia considerando que cumple con los requisitos metodológicos, éticos y legales para su realización.

Esta aprobación tiene **vigencia por un año** al cabo del cual el CEC CSM solicitará un estado de avance del estudio y/o revisará un seguimiento a fin de confirmar su reaprobación o determinar su eventual suspensión.

3. DOCUMENTOS APROBADOS

- Documento de Consentimiento Informado

4. LA APROBACION DEL ESTUDIO IMPLICA LO SIGUIENTE:

EL COMITÉ ÉTICO CIENTÍFICO DE CLÍNICA SANTA MARÍA HA OTORGADO LA APROBACIÓN AL ESTUDIO DE LA REFERENCIA CONSIDERANDO QUE CUMPLE CON LOS SIGUIENTES REQUISITOS EXIGIDOS PARA SU REALIZACIÓN:

1. Idoneidad del investigador y sus colaboradores
2. Pertinencia y justificación del estudio teniendo en cuenta el conocimiento disponible
3. Rigor metodológico y calidad científica de la investigación
4. Justificación de los riesgos y molestias previsibles para los sujetos de investigación, así como los beneficios esperados.
5. El procedimiento para obtener el consentimiento informado, incluyendo la hoja de información para los sujetos con información clara, suficiente y comprensible.
6. Pertinencia del plan de reclutamiento de sujetos
7. Compensaciones previstas para los sujetos por eventuales daños derivados de su participación en el estudio.
8. El seguro o la garantía financiera prevista
9. El cumplimiento de las normas científicas, técnicas y éticas, nacionales e internacionales que rigen este tipo de investigaciones.

COMITE ETICO CIENTIFICO

Clínica Santa María

ACTA DE APROBACIÓN DE ESTUDIOS DE INVESTIGACIÓN CLÍNICA
COMITÉ ÉTICO CIENTÍFICO CLÍNICA SANTA MARÍA

Fatiga muscular durante contracciones dinámicas isocinéticas de Aquiles posterior a 1 año

5. COMPROMISOS QUE ASUME EL INVESTIGADOR DURANTE LA EJECUCION DEL ESTUDIO

AL APROBAR EL ESTUDIO DE LA REFERENCIA EL CEC CLÍNICA SANTA MARÍA DA POR SENTADO QUE DURANTE EL DESARROLLO DEL ESTUDIO EL INVESTIGADOR RESPONSABLE Y SU EQUIPO DEBERÁN CUMPLIR CON LAS SIGUIENTES NORMAS DE BUENAS PRÁCTICAS CLÍNICAS:

1. Mantener estricta confidencialidad de toda la información derivada de esta investigación, asegurando la anonimización de los datos de los sujetos participantes.
2. Garantizar que el acceso a los datos de la historia clínica de los sujetos estará restringido sólo a los miembros del equipo investigador autorizados por el CEC Clínica Santa María y será utilizada exclusivamente para el desarrollo de los objetivos del estudio.
3. Hacer uso de esta aprobación sólo en el Centro autorizado por este CEC: en Clínica Santa María
4. Informar estado de avance anual del estudio.
5. Disponibilidad para facilitar el seguimiento anual que el CEC hará del estudio.
6. Informar oportunamente de cualquier modificación o interrupción del protocolo
7. Comunicar toda modificación del equipo de investigadores
8. Comunicar oportunamente cualquier evento adverso grave que ocurra durante el desarrollo del estudio.
9. Una vez finalizado el estudio, enviar informe final al CEC Clínica Santa María.
10. Si el estudio se publica, enviar al CEC Clínica Santa María un ejemplar.
11. Cumplir con la las normas éticas, convenios y declaraciones aprobados internacionalmente en materia de investigación científico biomédica y con la normativa nacional vigente: leyes 20.120, 20.584, 19.628, 20.850.
12. Capacitación certificada y actualizada en BPC del IP y su equipo

COMITÉ ÉTICO CIENTÍFICO APROBADO 25 MAR 2016 CLÍNICA SANTA MARÍA

Dr. Agustín Espejo Saavedra
Presidente
Comité Ético Científico
Clínica Santa María

Clínica Santa María
Especialistas en ti

Paciente N°_____/

CONSENTIMIENTO INFORMADO ESTUDIO OBSERVACIONAL

Título del estudio: **Fatiga muscular durante contracciones dinámicas tras tenorrafias de Aquiles posterior a 1 año**
Nombre Investigador Responsable: Carlos De la Fuente Cancino
Unidad/Departamento/Servicio: Centro de Salud Deportivo
Teléfono: +56954261340
Correo electrónico: cdelafuente@clinicasantamaria.cl / delafuentte@gmail.com
Estudio patrocinado por (si fuere el caso): NA

A. Hoja de información al paciente

1. Invitación

El propósito de esta información es ayudarlo(a) a tomar la decisión de participar -o no- en un estudio de investigación médica.

Para que pueda tomar una decisión informada de si desea o no participar de la investigación, en este documento se describe el objetivo del estudio, sus derechos y obligaciones, los procedimientos necesarios para el estudio y los posibles beneficios y riesgos de participar en él.

Tome el tiempo que necesite para decidir, lea detenidamente la información que sigue y no dude en hacer las preguntas que desee al médico que se lo está explicando, a su familia o amigos.

2. Razones de la invitación

Usted es invitado a participar en este estudio porque *podrá aportar información para conocer el estatus de pacientes como usted. Este conocimiento (conclusiones) son relevantes para que los equipos médicos mejoren la calidad de sus tratamientos y tras analizar esta información, en el futuro pacientes como usted podrían verse beneficiados si conseguimos identificar las variables modificables de rehabilitación para optimizarlas en un tratamiento.*

3. Objetivo del estudio

El objetivo de este estudio es *Determinar el efecto de la fatiga muscular (consorcio) durante contracciones dinámicas (levantamiento sucesiva del talón como ya lo hizo a los 3,6 y 9 meses) tras tenorrafias de Aquiles (la cirugía que recibió) posterior a 1 año.*

COMITÉ ÉTICO CIENTÍFICO APROBADO 25 MAR 2019 CLÍNICA SANTA MARIA

Clínica Santa María

Paciente Nº_____/

CONSENTIMIENTO INFORMADO ESTUDIO OBSERVACIONAL

4. Procedimientos de la investigación

Si usted acepta participar en nuestra investigación, será sometido a los siguientes procedimientos:

1) *Se obtendrá el registro de su peso corporal, estatura, perímetros de piernas y tiempo en meses desde su cirugía.*
2) *Se le adosaran 3 sensores de electromiografía de superficie en cada pierna. Ello implica que se limpiara una zona de 3x2.5 cm^2 con alcohol en la piel y se posicionara el sensor con cinta adhesiva hipoalergenica (3M, Chile).*
3) *Se le solicitara realizar sucesivas elevaciones de talón a la máxima altura que sea posible y la prueba acabara cuando ya no pueda elevar más su talón. El ritmo de ejecución será supidó por un sonido (bip). Esta prueba corresponde a una prueba de fatigabilidad muscular habitual de nuestra unidad y disponible para solicitar en el centro.*

Todo el procedimiento se realizará en la Unidad de Biomecánica del centro de salud deportivo de clínica santa maría (Santiago, Chile), la cual requerirá de una sola sesión (un mismo día) por persona tomando aproximadamente un tiempo de 1 hora.

5. Beneficios posibles para los sujetos participantes

El principal beneficio es el bien común de futuros pacientes que atraviesen una etapa similar a la suya, no obstante, la información que se pueda extraer de la evaluación puede ser presentada a su médico tratante y potencialmente ser empleado para optimizar la etapa de reintegro deportivo.

6. Riesgos posibles para los sujetos participantes del estudio

Los riesgos relacionados con el procedimiento de este investigación son mínimos. El riesgo identificado por el equipo es el discomfort muscular tras el ejercicio que tiene un tiempo asociado alrededor de tres días y si usted posee piel sensible, la posible irritación del área donde serán posicionados los sensores. Es por esto que, para resguardar su seguridad, usted estará acompañado siempre durante todo el proceso del profesional kinesiólogo Carlos De la Fuente quien otorgara todas las instrucciones y tomara todos resguardos para realizar una prueba segura en todo momento para su salud. El kinesiólogo se compromete con el adecuado manejo del eventual dolor del tendón operado tras más de un año de intervención quirúrgica. Como medidas preventivas el kinesiólogo Carlos De la Fuente le aplicará hielo posterior al ejercicio, educación para disminuir el posible discomfort (elongaciones musculares) y además él, empleará materiales hipo alergénicos nuevos que son de uso médico habitual en Clínica Santa María.

7. Voluntariedad y revocación del consentimiento

Su participación en esta investigación es completamente voluntaria. Usted tiene el derecho a no aceptar participar o revocar su consentimiento y retirarse de esta investigación en el momento que lo estime conveniente. Al hacerlo, usted no pierde ningún derecho que se le entrega como paciente de esta institución y no se verá afectada la calidad de la atención médica que merece.

8. Confidencialidad

Toda la información derivada de esta investigación será mantenida en estricta confidencialidad. Sólo tendrán acceso a ella los miembros del equipo investigador autorizados por el Comité Ético Científico de Clínica Santa María y será utilizada exclusivamente para el desarrollo de los objetivos del estudio.

COMITÉ ÉTICO CIENTÍFICO APROBADO 25 MAR 2019 CLÍNICA SANTA MARÍA

Clínica Santa María
Especialistas en s

Paciente Nº_____/

CONSENTIMIENTO INFORMADO ESTUDIO OBSERVACIONAL

9. Publicación científica y confidencialidad

Es posible que los datos y resultados derivados de este estudio puedan ser publicados en revistas y conferencias médicas, si esto ocurre, y en conformidad en lo establecido en las leyes 20.584, 20.120 y 19.628, sus datos clínicos serán anonimizados a fin de que usted no pueda ser identificado(a).

10. Costos

La evaluación no tiene costo para usted.

11. Compensaciones

En caso de existir algún tipo de daño o complicación relacionado específicamente con la participación en esta investigación, los costos recaerán sobre equipo investigador Klgo. Carlos De la Fuente, Dr. Hugo Henríquez y Dr. Hugo Maramblo. No existirán compensaciones por complicaciones inherentes a la condición clínica del sujeto.

12. Derechos del paciente

Cualquier pregunta que usted desee hacer en relación a su participación en este estudio, será respondida por el Investigador Responsable cuyos datos de contacto se encuentran al inicio de este documento.

Cualquier pregunta que usted desee hacer en relación a sus derechos como participante del presente estudio de investigación puede comunicarse con el Presidente del Comité Ético Científico de Clínica Santa María Dr. Agustín Espejo García – comite.eticocientifico@clinicasantamaria.cl – tel 229132847.

El Comité Ético Científico está conformado por un grupo de personas independientes del investigador y del patrocinador, que evalúa y monitorea el estudio desde su inicio hasta su finalización, y cuya función es asegurar que su bienestar como participante sea preservado y sus derechos respetados.

COMITÉ ÉTICO CIENTÍFICO APROBADO 25 MAR 2019 CLÍNICA SANTA MARÍA

Clínica Santa María
Especialistas en ti

Paciente Nº_____/

CONSENTIMIENTO INFORMADO ESTUDIO OBSERVACIONAL

B. Consentimiento informado - Hoja de firmas

Al firmar el presente documento, declaro que:

1. Se me ha explicado el propósito de esta investigación médica, los procedimientos y riesgos, además de los beneficios y derechos que corresponden.
2. Firmo este documento voluntariamente, sin ser forzado(a) a hacerlo.
3. No estoy renunciando a ningún derecho que me corresponda.
4. Se me comunicará toda nueva información relacionada con este estudio médico y que surja durante éste y que pueda afectar de forma directa para mi condición de salud.
5. Se me ha explicado que tengo derecho a revocar mi consentimiento para participar en este estudio cuando lo desee, sin que ello genere para mi pérdida de ninguna especie.
6. Yo autorizo al Investigador Responsable y sus colaboradores a acceder y usar los datos contenidos en mi ficha clínica anonimizados para los propósitos de esta investigación médica.
7. Al momento de la firma, se me entrega una copia firmada de este documento.

Los espacios que siguen van escritos de puño y letra por los firmantes

Nombre del paciente	RUT	Firma	Fecha	Hora
Nombre del representante o testigo y relación con el paciente (si fuese pertinente)	RUT	Firma	Fecha	Hora
Nombre del investigador autorizado que explica el Consentimiento Informado	RUT	Firma	Fecha	Hora
Nombre director de la institución o delegado	RUT	Firma	Fecha	Hora

Este documento sólo es válido si cuenta con la autorización y timbre del Comité Ético Científico de Clínica Santa María.

Marzo 2018

COMITÉ ÉTICO CIENTÍFICO APROBADO 25 MAR 2019 CLÍNICA SANTA MARÍA

Clínica Santa María

Santiago, 26 de marzo de 2019
N°021/DM

Doctor
Agustín Espejo G.
Presidente
Comité de Ética Científico
Clínica Santa María
Presente

Estimado Dr. Espejo:

Mediante la presente tomo conocimiento que con fecha 25 de Marzo de 2019 fue aprobado por el Comité de Ética Científico el siguiente protocolo de investigación clínica titulado:

- **Efecto de la fatiga muscular durante contracciones dinámicas tras tenorrafias de Aquiles posterior a 1 año.**

Además, informo a usted que esta Dirección Médica autoriza que esta investigación se lleve a cabo en Clínica Santa María, bajo la conducción y responsabilidad del IR Kigo. Carlos de la Fuente Cancino.

Saluda Atentamente a usted.

SANTA MARÍA - DIRECTOR MÉDICO - SANTIAGO

Dr. Javier González García
Director Médico
Clínica Santa María

C.C: IR Kigo. Carlos de la Fuente Cancino.

Av. Santa María 0410, Providencia
Tel. 2 2913 0000
Fax. 2 2913 3513
E-mail: info@clinicasantamaria.cl
www.clinicasantamaria.cl

CARTA DE SOLICITUD DE EVALUACIÓN

Santiago, Junio 22, 2022

Dr. Ricardo Vacarezza
Presidente del Comité de Ética Científico Adulto
Servicio de Salud Metropolitano Oriente
Presente

Quien suscribe, presenta a ustedes para ser sometido al proceso de evaluación ético científico el presente estudio denominado "**Patrones cinemáticos, nivel de actividad física y funcionalidad** "

Declaro estar en conocimiento el procedimiento de evaluación del proyecto de investigación y aceptar la decisión que se tome por los miembros al interior del Comité de Ética Científico Adulto del Servicio de Salud Metropolitano Oriente perteneciente a la ciudad de Santiago, reservándome el derecho a solicitar información que me permita hacer las modificaciones correspondientes y necesarias para realizar el presente proyecto. Nosotros presentamos Carta de presentación, CV investigador principal, CV investigador Senior, Protocolo Original, Consentimiento Informado, Resumen ejecutivo, Carta de Compromiso y Carta de Autorizacion de Clinica MEDS (director medico).

SERVICIO DE SALUD METROPOLITANO ORIENTE
COMITE ETICO-CIENTIFICO
20/07/2022

ANNEX 2 – MATLAB GENERIC CODES

K-MEANS CODE

```
function [centroids, cluster_idx] = kMeans(data, k, max_iters)
    % data: NxD matrix, where N is the number of data points and D is
the dimensionality
    % k: number of clusters
    % max_iters: maximum number of iterations

    % Randomly initialize the centroids from the data points
    num_data_points = size(data, 1);
    idx = randperm(num_data_points, k);
    centroids = data(idx, :);

    % Initialize variables to store cluster assignments and previous
cluster assignments
    cluster_idx = zeros(num_data_points, 1);
    prev_cluster_idx = zeros(num_data_points, 1);

    % Main k-means loop
    for iter = 1:max_iters
        % Assign each data point to the nearest centroid
        for i = 1:num_data_points
            distances = sum((data(i, :) - centroids).^2, 2);
            [~, cluster_idx(i)] = min(distances);
        end

        % If cluster assignments have not changed, break the loop
        if isequal(cluster_idx, prev_cluster_idx)
            break;
        end

        % Update the centroids based on the current cluster assignments
        for j = 1:k
            cluster_points = data(cluster_idx == j, :);
            centroids(j, :) = mean(cluster_points);
        end

        % Store the current cluster assignments for comparison in the
next iteration
        prev_cluster_idx = cluster_idx;
    end
end
```

K-MEDIODS CODE

```
function [medoids, clusters, costs] = kMedoids(data, k, max_iters)
    % data: NxD matrix, where N is the number of data points and D is
the dimensionality
    % k: number of clusters
    % max_iters: maximum number of iterations

    N = size(data, 1);
    D = size(data, 2);

    % Initialize medoids randomly
    medoid_indices = randperm(N, k);
    medoids = data(medoid_indices, :);

    clusters = zeros(N, 1);
    costs = zeros(N, 1);

    for iter = 1:max_iters
        % Assign data points to the nearest medoids
        for i = 1:N
            distances = sum(abs(data(i, :) - medoids), 2);
            [min_dist, min_idx] = min(distances);
            clusters(i) = min_idx;
            costs(i) = min_dist;
        end

        % Update medoids
        for j = 1:k
            cluster_points = data(clusters == j, :);
            cluster_costs = sum(abs(cluster_points - medoids(j, :)),
2);
            [min_cost, min_idx] = min(cluster_costs);
            medoids(j, :) = cluster_points(min_idx, :);
        end
    end
end
```

TAEGER KEISER ENERGY OPERATOR CODE

```
Taeger Keiser Energy Operator Matlab

function energy = teager_kaiser_energy(signal)
    % signal: The input time series signal

    % Calculate the Teager-Kaiser Energy Operator
    teo = signal(2:end-1) .^ 2 - signal(1:end-2) .* signal(3:end);

    % Set the first and last samples of the energy to zero (to keep the
size consistent)
    energy = [0; teo; 0];
end
```

SHORT FAST FOURIER CODE

```
function [frequencies, magnitude] = shortFFT(signal, fs)
    % signal: input time-domain signal
    % fs: sampling frequency

    % Compute the FFT of the signal
    N = length(signal);
    Y = fft(signal);

    % Compute the frequency axis
    f = fs*(0:(N/2))/N;

    % Compute the magnitude of the FFT
    magnitude = abs(Y(1:N/2+1));

    % Return the frequencies and magnitude
    frequencies = f;
end
```

DBSCAN CODE

```
function [labels, clusters] = dbscan(X, epsilon, MinPts)
    % X: input data matrix (each row is a data point)
    % epsilon: maximum distance between points to be considered
neighbors
    % MinPts: minimum number of points required to form a dense region

    N = size(X, 1);  % Number of data points
    labels = zeros(N, 1);  % Cluster labels (-1 for noise)
    clusters = 0;  % Number of clusters

    for i = 1:N
        if labels(i) == 0
            % Find neighbors within epsilon distance
            neighbors = find(pdist2(X(i, :), X) <= epsilon);

            if length(neighbors) < MinPts
                labels(i) = -1;  % Mark as noise
            else
                clusters = clusters + 1;
                expandCluster(X, i, neighbors, clusters, labels,
epsilon, MinPts);
            end
        end
    end
end

function expandCluster(X, i, neighbors, clusterIdx, labels, epsilon,
MinPts)
    labels(i) = clusterIdx;

    while ~isempty(neighbors)
        currentPoint = neighbors(1);
        neighbors(1) = [];

        if labels(currentPoint) == 0
            labels(currentPoint) = clusterIdx;
            newNeighbors = find(pdist2(X(currentPoint, :), X) <=
epsilon);

            if length(newNeighbors) >= MinPts
                neighbors = [neighbors newNeighbors];
            end
        elseif labels(currentPoint) == -1
            labels(currentPoint) = clusterIdx;
        end
    end
end
```